Siberian Branch of Russian Academy of Science

BUDKER INSTITUTE OF NUCLEAR PHYSICS

R.R. Akhmetshin, G.A. Aksenov, E.V. Anashkin, M. Arpagaus,
V.M. Aulchenko, B.O. Baibusinov, V.Sh. Banzarov, L.M. Barkov,
S.E. Baru, N.S. Bashtovoy, A.E. Bondar, D.V. Bondarev,
A.V. Bragin, D.V. Chernyak, A.G. Chertovskikh, A.G. Dvoretsky,
S.I. Eidelman, G.V. Fedotovich, N.I. Gabyshev, A.A. Grebeniuk,
D.N. Grigoriev, V.W. Hughes, P.M. Ivanov, S.V. Karpov,
V.F. Kazanin, B.I. Khazin, I.A. Koop, M.S. Korostelev,
P.P. Krokovny, L.M. Kurdadze, A.S. Kuzmin, M. Lechner,
I.B. Logashenko, P.A. Lukin, A.P. Lysenko, Yu.I. Merzlyakov,
K.Yu. Mikhailov, A.I. Milstein, I.N. Nesterenko, V.S. Okhapkin,
A.V. Otboev, E.A. Perevedentsev, A.A. Polunin, A.S. Popov,
T.A. Purlatz, N.I. Root, A.A. Ruban, N.M. Ryskulov,
A.G. Shamov, Yu.M. Shatunov, A.I. Shekhtman, B.A. Shwartz,
V.A. Sidorov, A.N. Skrinsky, V.P. Smakhtin, I.G. Snopkov,
E.P. Solodov, P.Yu. Stepanov, A.I. Sukhanov, J.A. Thompson,
V.M. Titov, A.A. Valishev, Yu.V. Yudin, S.G. Zverev

RECENT RESULTS FROM CMD-2 DETECTOR AT VEPP-2M

Budker INP 99-11

http://www.inp.nsk.su/publications

Novosibirsk
1999

Siberian Branch of Russian Academy of Science
BUDKER INSTITUTE OF NUCLEAR PHYSICS

R.R. Akhmetshin, G.A. Aksenov, E.V. Anashkin, M. Arpagaus,
V.M. Aulchenko, B.O. Baibusinov, V.Sh. Banzarov,
L.M. Barkov, S.E. Baru, N.S. Bashtovoy, A.E. Bondar,
D.V. Bondarev, A.V. Bragin, D.V. Chernyak,
A.G. Chertovskikh, A.G. Dvoretsky, S.I. Eidelman,
G.V. Fedotovitch, N.I. Gabyshev, A.A. Grebeniuk,
D.N. Grigoriev, V.W. Hughes, P.M. Ivanov, S.V. Karpov,
V.F. Kazanin, B.I. Khazin, I.A. Koop, M.S. Korostelev,
P.P. Krokovny, L.M. Kurdadze, A.S. Kuzmin, M. Lechner,
I.B. Logashenko, P.A. Lukin, A.P. Lysenko, Yu.I. Merzlyakov,
K.Yu. Mikhailov, A.I. Milstein, I.N. Nesterenko, V.S. Okhapkin,
A.V. Otboev, E.A. Perevedentsev, A.A. Polunin, A.S. Popov,
T.A. Purlatz, N.I. Root, A.A. Ruban, N.M. Ryskulov,
A.G. Shamov, Yu.M. Shatunov, A.I. Shekhtman, B.A. Shwartz,
V.A. Sidorov, A.N. Skrinsky, V.P. Smakhtin, I.G. Snopkov,
E.P. Solodov, P.Yu. Stepanov, A.I. Sukhanov, J.A. Thompson,
V.M. Titov, A.A. Valishev, Yu.V. Yudin, S.G. Zverev

RECENT RESULTS FROM CMD-2 DETECTOR AT VEPP-2M

Budker INP 99-11
Novosibirsk
1999

Recent results from CMD-2 detector at VEPP-2M

R.R. Akhmetshin, G.A. Aksenov, E.V. Anashkin, M. Arpagaus, V.M. Aulchenko, B.O. Baibusinov, V.Sh. Banzarov, L.M. Barkov, S.E. Baru, N.S. Bashtovoy, A.E. Bondar, D.V. Bondarev, A.V. Bragin, D.V. Chernyak, A.G. Chertovskikh, A.G. Dvoretsky, S.I. Eidelman, G.V. Fedotovitch, N.I. Gabyshev, A.A. Grebeniuk, D.N. Grigoriev, V.W. Hughes, P.M. Ivanov, S.V. Karpov, V.F. Kazanin, B.I. Khazin, I.A. Koop, M.S. Korostelev, P.P. Krokovny, L.M. Kurdadze, A.S. Kuzmin, M. Lechner, I.B. Logashenko, P.A. Lukin, A.P. Lysenko, Yu.I. Merzlyakov, K.Yu. Mikhailov, A.I. Milstein, I.N. Nesterenko, V.S. Okhapkin, A.V. Otboev, E.A. Perevedentsev, A.A. Polunin, A.S. Popov, T.A. Purlatis, N.I. Root, A.A. Ruban, N.M. Ryskulov, A.G. Shamov, Yu.M. Shatunov, A.I. Shekhtman, B.A. Shwartz, V.A. Sidorov, A.N. Skrinsky, V.P. Smakhtin, I.G. Snopkov, E.P. Solodov, P.Yu. Stepanov, A.I. Sukhanov, J.A. Thompson, V.M. Titov, A.A. Valishev, Yu.V. Yudin, S.G. Zverev

Abstract

Preliminary results of the study of e^+e^- annihilation into hadrons by the CMD-2 collaboration at VEPP-2M are presented for the c.m. energy range from 0.61 to 1.39 GeV. The total integrated luminosity of about 25 pb^{-1} has been collected since 1992. New results are reported on the pion form factor around the ρ-meson, ω-meson parameters, measurements of various decay modes of the ϕ-meson as well as searches for its rare decay modes. The unique possibility to have tagged kaons and η-mesons in the ϕ-meson decays is used to study some decay modes of $K^0_S, K^\pm$ and η-mesons. Also discussed are the cross sections and production mechanisms for processes of the multipion production in the non-resonant energy ranges.

Contents

1 Introduction

Investigation of e^+e^- annihilation into hadrons at low energies has a long history, but despite thirty years of experimental studies, we are still rather far from complete understanding of the field. One needs more precise measurements of the ρ-, ω- and ϕ-meson parameters as well as properties of the continuum which will provide unique information about interactions of light quarks and spectroscopy of their bound states.

In addition, the knowledge of the total cross section of e^+e^- annihilation into hadrons (or $R = \sigma(e^+e^- \to hadrons)/\sigma(e^+e^- \to \mu^+\mu^-)$) at low energies as well as of the magnitude of the exclusive cross sections is necessary for precise calculations of various quantities. Among them are strong interaction contributions to vacuum polarization for $(g\text{-}2)_\mu$ and $\alpha(m_Z^2)$ [1], tests of Standard Model by the hypothesis of conserved vector current relating $e^+e^- \to$ hadrons to hadronic τ-lepton decays [2], determination of the QCD parameters based on QCD sum rules [3] etc.

In the energy range under study the energy behavior of the total hadronic cross section as well as that of the cross sections for exclusive channels is complicated. It is characteristic of various resonances (ρ, ω, ϕ plus their recurrences) as well as onsets of the separate hadronic channels. This makes the exclusive approach the only one possible. By exclusive approach we mean the procedure when one measures separate annihilation channels one by one. Another reason for such an approach is the lack of a theoretical model capable of successful quantitative description of the energy region close to threshold of hadron production.

Following this logics, to determine the value of R we need to measure with high precision the cross sections of $\pi^+\pi^-$ (the ρ-meson), various decay modes of the ω- and ϕ-mesons as well as the cross sections of multihadronic production in the continuum (beyond the resonances).

These physical tasks became the goal of the general-purpose detector CMD-2 [4, 5] which has been running at the VEPP-2M e^+e^- collider [6] in Novosibirsk since 1992 studying the c.m. energy range from threshold of hadron production to 1.4 GeV. The total integrated luminosity collected in 1992-1998 is about 25 pb^{-1}. This work reports on the recent results of the analysis for various channels of e^+e^- annihilation into hadrons from the CMD-2 detector.

Here we present results of the study of the pion form factor in the energy range from 0.61 to 0.96 GeV with a high data sample of about 150,000 events and a record systematic uncertainty of 1.4%. The fit of the energy dependence provides the information on the ρ-meson parameters as well as on the magnitude of $\rho - \omega$ interference. Various theoretical models are discussed.

Also studied are the parameters of the ω-meson and consistence of the measured mass and width with the world average values [7] are discussed.

Already the first run with the CMD-2 performed at the end of 1992 at the ϕ-meson energy showed a high potential of the detector for precise studies of the ϕ-meson parameters. Using a relatively small integrated luminosity of 290 nb^{-1} corresponding to about 400,000 ϕ-meson decays, CMD-2 measured for the first time the branching ratios of all four main decay modes with the accuracy comparable to the world average [8].

Since that time several more dedicated runs around the ϕ-meson have been performed with the total integrated luminosity of 15.8 nb^{-1} or about 2.1×10^7 ϕ-meson decays. A large data sample combined with the good energy and angular resolution of the detector allowed much more precise measurements of the main decay modes as well as by far higher sensitivity in searches for rare decay modes. Analysis of the part of this statistics for several decay modes has already been published [9, 10, 11, 12]. Here we report on the

recent development in the analysis:

- From a sample of 3.4 million ϕ-mesons the high precision measurement of the resonance mass and width as well as of the branching ratio for the decay mode $\phi \to K_S^0 K_L^0$ has been performed. Alternatively, one can use the value of $Br(\phi \to K_S^0 K_L^0)$ from [7] and obtain a high accuracy value of the leptonic width.

- Magnetic dipole transitions between low lying vector and pseudoscalar mesons are of big importance for the tests of the nonrelativistic quark model and understanding the SU(3) symmetry breaking [13, 14]. The probability of the decay $\phi \to \eta\gamma$ has been previously measured by different groups via the η-meson decays into neutral final states only ($\eta \to 2\gamma, \eta \to 3\pi^0$ [7, 15]). CMD-2 performed the first measurement of this decay mode using a data sample of about 3.3 million ϕ-meson decays and the mixed final state $\eta \to \pi^+\pi^-\pi^0$.

  New information has been obtained on the $\phi \to \eta'\gamma$ decay. Since the first observation of this decay mode at CMD-2 described in [10], a bigger data sample appeared due to using the endcap BGO calorimeter as well as a new decay mode $\eta \to \pi^+\pi^-\pi^0$ in addition to the previously used $\eta \to 2\gamma$. New analysis confirms the existence of this decay mode with the branching ratio at the 10^{-4} level.

- The decay $\phi \to f_0(980)\gamma$ is particularly interesting for two reasons:

  1. The 20% decay probability into a two kaon final state [7] seems puzzlingly high if $f_0(980)$ is a member of the strangeness-0 scalar meson nonet. Various explanations for this large coupling to kaons have been advanced including the idea that $f_0(980)$ is composed of four quarks, with a "hidden strangeness" component: ($f_0 = s\,\bar{s}(u\,\bar{u} + d\,\bar{d})/\sqrt{2}$), or that it may be a $K - \overline{K}$ molecule (see a list of references in [11]). The value of the branching ratio for the $\phi \to f_0(980)\gamma$ decay mode appears to be very sensitive to the model [16, 17].
  2. The presence in the final state of the $K_S^0 K_L^0$ from the ϕ-meson decay is of crucial importance for the planned measurements of the ϵ'/ϵ at ϕ-factories. The ϕ-meson decay into $f_0(980)\gamma$ accompanied with a low energy photon escaping detection leads to the C-even

final state of $K_S^0 K_S^0$ and can mimic the CP-violating decay. In accordance with [18, 19] this effect becomes important if the final state has a C-even component as large as 5×10^{-5}. Although theoretical predictions for such a decay give for the probability of this decay the values about 10^{-6} or even much less [16, 20, 21] the experimental measurement is needed for their confirmation.

The decay $\phi \to f_0(980)\gamma$ with $f_0(980)$ decaying to two kaons is expected to be too small to be observed before the ϕ-factories. But it can be probed through the $f_0(980)$ decay to two charged or two neutral pions. In [17] the branching ratio of the decay $\phi \to f_0(980)\gamma \to \pi\pi\gamma$ is predicted at the level of $(1-2) \times 10^{-5}$ in the $K - \bar{K}$ molecule model and 5×10^{-5} for the conventional two quark structure while it is 2.4×10^{-4} in the four-quark model [16]. Thus, observation or even an upper limit for this decay mode will help to distinguish between different possible structures of the $f_0(980)$ meson.

In this paper we present results of a search for the $\phi \to f_0(980)\gamma$ decay in the event sample where two charged pions and one photon were detected in the CMD-2 detector. The events in our sample arise primarily from the much larger background: the radiative processes $e^+e^- \to \pi^+\pi^-\gamma$ where the photon comes from initial electrons or from final pions. Therefore the signal from the $f_0(980)\gamma$ final state can be seen most effectively as an interference structure at $E_\gamma \approx 40$ MeV in the spectrum of radiative photons. Our previous result based on a smaller data sample has been published in [11]. As a by-product of our analysis of the $\pi^+\pi^-\gamma$ events, we place an upper limit for the C-parity violating decay $\phi \to \rho\gamma$ which is two orders of magnitude stronger than before [7].

Another possibility is to study the $\pi^0\pi^0\gamma$ final state which has much better background conditions and to look for the possible revelations of the decay $f_0(980) \to \pi^0\pi^0$. Observation of the $\phi \to f_0(980)\gamma$ using this decay mode of the $f_0(980)$-meson has been recently reported by SND [22]. CMD-2 is able to observe both decay modes. Here we present results of two measurements in the charged and neutral mode of the $f_0(980)$ decay separately as well as results of the combined analysis of both decay modes.

Similar arguments about the unknown meson structure as well as the background for CP studies at the ϕ-factories can be equally applied to the $a_0(980)$-meson. The mode whose observation is

currently feasible is that due to the $a_0(980) \to \eta\pi^0$ decay. First observation of the radiative decay $\phi \to a_0(980)\gamma$ has been recently reported by SND [23]. We present results of the independent study of this decay mode with CMD-2.

- Conversion decays of any vector meson are the natural consequence of the radiative decays when instead of a real photon the vector meson decays into a pseudoscalar meson and a virtual photon which internally converts into a lepton pair (electron or muon one). The values of the branching ratios are interesting as a test of different theoretical models as well as for the precise calculation of the background to a search for quark-gluon plasma in heavy ion collisions. Studies of the spectra of invariant masses for produced lepton pairs can provide important information on the transition form factors [24]. Until recently there existed a single measurement of the conversion decay $\phi \to \eta e^+e^-$ [25]. We report on the new determination of the branching ratio of this decay mode by two independent methods (using the decay modes $\eta \to \gamma\gamma$ and $\eta \to \pi^+\pi^-\pi^0$ respectively) as well as on the first observation of the decay mode $\phi \to \pi^0 e^+e^-$.

- Rare decays of the ϕ-meson to the final states with the even number of pions ($\pi^+\pi^-$, $2\pi^+2\pi^-$) are double suppressed by the G-parity and OZI rule and can provide important information on the mechanisms of the OZI rule breaking. We report on the new measurement of the decay mode $\phi \to \pi^+\pi^-$ and on the first observation of the four pion mode.

- As it was realized at the very early steps of the ϕ-meson studies at e^+e^- colliders, $K^0_SK^0_L$ pairs can be used for studying CP and CPT violation. These suggestions including studies of quantum mechanical correlations were discussed [26, 4] for experiments at VEPP-2M and carefully reviewed later in [21]. Some preliminary results on the study of $K^0_SK^0_L$ coupled decays with the CMD-2 detector based on a relatively small data sample have already been published [9].

  It should be emphasized that the ϕ decay into two neutral kaons provides a pure $K^0_SK^0_L$ state and the detection of one kaon at a long distance predetermines the presence of K^0_S decay within few millimetres from the beam, opening thereby a unique opportunity to study rare decays of pure K^0_S. We present the first direct measurement of the branching ratio for the semileptonic decay $K_S \to \pi^\pm e^\mp \nu$.

  The combination of the intensive decay of the ϕ into two slow charged

kaons and a good 4π detector gives a possibility to study charged kaon decays and their interactions using the recoil particle as a tag. All major decay modes are well detected in the CMD-2 detector and their relative rates could be measured with relatively low systematic errors. These branching ratios were measured in optical spark chamber experiments [7] in 70's and their agreement is poor. We present our first results on the determination of the relative branching ratios of two- and three-particle decay modes with the accuracy comparable to the best previous experiments.

- Because of the very high data sample of produced ϕ-mesons the radiative decay $\phi \to \eta\gamma$ which proceeds with the probability of about 1.3% is an intensive source of tagged η-mesons. Tagging is due to an exceptionally clear signature - presence of a hard monochromatic photon with the energy of about 360 MeV. This circumstance can be used to study various decay modes of the η-meson. Particularly, we report on a search for the P- and CP-parity violating decays $\eta \to \pi^+\pi^-$ and $\eta \to \pi^0\pi^0$ as well as on the measurements of the branching ratios $\eta \to e^+e^-\gamma$ and $\eta \to \pi^+\pi^-e^+e^-$ with an accuracy comparable or better than the world average.

Finally, we discuss e^+e^- annihilation into four pions (two possible channels $\pi^+\pi^-2\pi^0$ and $2\pi^+2\pi^-$ have been studied). We show the importance of taking into account the interference of various possible intermediate mechanisms as well as of the amplitudes differing by permutations of identical pions. The $\pi^+\pi^-2\pi^0$ final state is dominated by a mixture of $\omega\pi^0$ and $a_1(1260)\pi$ mechanisms whereas the latter seems to be the only one contributing to the $2\pi^+2\pi^-$ final state.

For the first time we measure energy dependence of the cross section of the process $e^+e^- \to 2\pi^+2\pi^-\pi^0$ and show that it is dominated by contributions from the $\eta\pi^+\pi^-$ and $\omega\pi^+\pi^-$ states.

The structure of the preprint is as follows. While composing the text, we did not follow strictly the physical motivations of the considered problems. Instead, we prefer to present our results according to the logics of the analysis, so that processes with similar final states and therefore similar selection criteria are being discussed in common. For example, observation of the decay mode $\phi \to \eta'\gamma$ via the η decay mode to $\pi^+\pi^-\pi^0$ is considered together with the production of four charged pions and similar processes. The feature combining these processes is similar selection criteria and principles of kinematical reconstruction.

In the second Section we briefly describe the CMD-2 detector and its performance during the experiments in 1992-1998. Section 3 presents main features of the data taking such as the date of each run, the energy range studied, the integrated luminosity etc. In Section 4 one describes the preliminary division of the whole data sample into different classes (neutral events or events without tracks, one track events, two track events from one vertex, Bhabha events and all others). Section 5 deals with the procedure of luminosity measurements while Section 6 describes the calculation of the radiative corrections. Sections 7 and 8 present the methods of c.m. energy determination around the ϕ-meson and in other energy ranges respectively. After that we describe the physical results presenting in Section 9 the measurement of the pion form factor and in Section 10 the determination of the ω-meson parameters. Sections 11 through 25 deal with various problems studied in the ϕ-meson energy range while Sections 26 through 30 describe measurements in the non-resonant energy ranges below the ϕ (Section 26) and above it (Sections 27 through 30). The work ends with brief conclusions and a summary of all results obtained at the CMD-2 detector since 1992.

2 CMD-2 detector

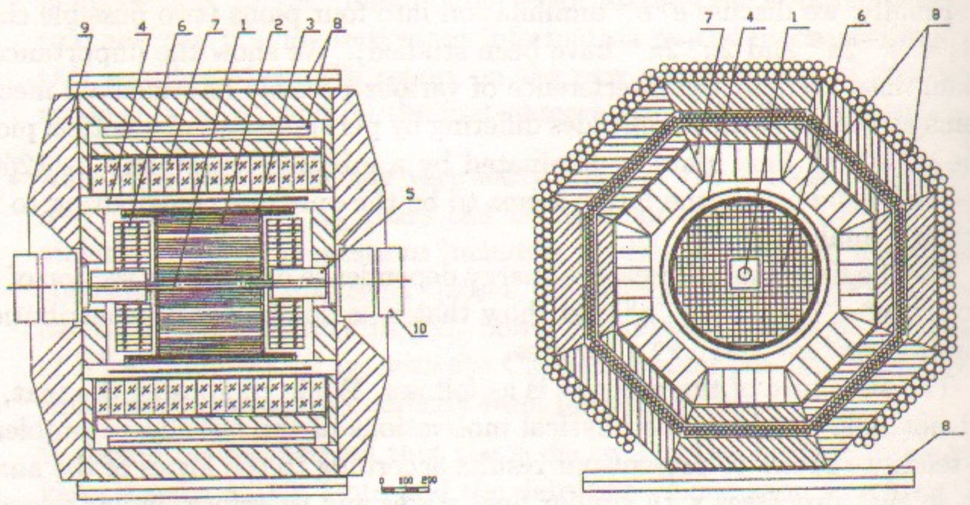

Figure 1: The layout of the CMD-2 detector: 1 - beam pipe; 2 - drift chamber; 3 - Z-chamber; 4 - superconductive solenoid; 5 - compensating magnet; 6 - endcap BGO calorimeter; 7 - barrel CsI(Tl)calorimeter; 8 - muon range system; 9 - yoke; 10 - quadrupole lenses

The layout of CMD-2 [5] is shown in Fig.1. The coordinate part of the detector consists of a cylindrical drift chamber (DC) and double-layer multiwire proportional chamber (Z-chamber) with an accurate measurement of the coordinate along the beam direction. Outside of the superconductive solenoid [27] with a 1 T magnetic field the CsI barrel calorimeter and muon range system are placed. To ensure a good energy resolution of the barrel calorimeter the construction of the solenoid has been optimized to have a reasonably small radiation length of 0.38 X_0. The endcap calorimeter is made of BGO crystals. Both barrel and endcap calorimeters cover a solid angle of $0.92\times4\pi$ steradians.

2.1 Drift chamber

The drift chamber [28, 29] consists of 80 jet-like cells arranged in 3 superlayers. The outer radius of the DC is 30 cm and the sensitive length of wires is 44 cm. A radially moving charged particle hits 19 sense wires. The drift coordinate in the plane transverse to the beam axis is measured with an accuracy of 250 μm. Coordinates along the wires (z-coordinates) are measured by charge division with an accuracy of 0.4 cm. The momentum resolution of the DC is equal to $\sigma_p/p = \sqrt{90 \cdot (p(GeV))^2 + 7\%}$. The accuracy in the measurement of polar and azimuthal angles is $\sigma_\theta = 1.5 \cdot 10^{-2}$ and $\sigma_\phi = 7 \cdot 10^{-3}$ radians respectively. Multiple sampling of the charged particle track allows to have 20% resolution in the measurement of the specific energy losses.

2.2 Z-chamber

Z-chamber [28] consists of two layers of MWPC, located between the radii of 30.6 and 32.3 cm. Having a total length of about 80 cm, ZC covers polar angles from 0.64 to $(\pi - 0.64)$ radians. The innermost and outermost cathodes of ZC are divided in strips with a pitch of 6.5 mm and provide the measurement of the track coordinate along the beam axis on the corresponding layer. A position along the beam axis is obtained with the center-of-gravity calculation for the charges induced on the cathode strips. The spatial resolution of ZC is $\sim$ 250 μm for tracks perpendicular to the beam axis and degrades to $\sim$ 1 mm for inclined tracks.

The small anode wire spacing ($\sim$ 3 mm) and fast gas mixture (CF_4 + 20% iC_4H_{10}) lead to the time resolution better than 5 ns (r.m.s.) for two track events. This allows to use ZC as a part of the first level charged trigger, consisting of a pretrigger and a special tracking processor (Track Finder) looking for tracks in the DC.

2.3 Barrel CsI calorimeter

The barrel electromagnetic calorimeter [30] with a thickness of 8.1 X_0 consists of 892 6x6x15 cm^3 CsI(Tl) crystals, arranged in eight octants. Each octant contains 5 rows of regular shape crystals and 2 rows of crystals specially shaped to provide tight matching with neighbouring octants. The light readout is performed by photomultipliers.

The energy resolution of the CsI calorimeter is of the order of 8% when the energy of the incident photon changes from 100 to 700 MeV. Both azimuthal and polar angle resolutions are of the order of 0.02 radians.

2.4 Endcap BGO calorimeter

The endcap calorimeter [31] consists of 680 25×25×150 mm^3 BGO crystals. The thickness of the calorimeter for normally incident particles is equal to 13.4 X_0.

All the crystals are arranged in rows by 6, 8 or 10. The calorimeter covers polar angles from 0.28 up to 0.86 and from 2.28 up to 2.86 radians for the first and second endcaps respectively, so that its solid angle coverage is equal to $0.3 \times 4\pi$ steradians. BGO crystals are placed in a region of high magnetic field and the light readout is performed with a help of vacuum phototriodes.

The energy and angular resolution of the endcap calorimeter are equal to $\sigma_E/E = 4.6\%/\sqrt{E(GeV)}$ and $\sigma_{\phi,\theta} = 2{\cdot}10^{-2}/\sqrt{E(GeV)}$ radians respectively.

2.5 Muon range system

The muon range system [32] consists of two double layers of streamer tubes operating in a self-quenching streamer mode and is aimed at separation of pions and muons.

The inner part consisting of 8 modules with 48 streamer tubes each and outer part of the system cover 55% and 48% of the solid angle respectively. Five upper modules have 32 tubes each while three lower have 24 tubes each. For a pion with a 500 MeV energy the probability to hit the inner system and imitate a muon is 0.35 for a single track while for the outer system this value is 0.1.

The spatial resolution determined with the help of cosmic rays is 50-70 mm along a wire and the detection efficiency of the double layer is of the order of 99%.

Table 1: CMD-2 data taking information. Arrows show the direction of the beam energy variation during scanning

Legend	Date	C.m. energy, GeV	Run numbers	Wiggler	$\int Ldt$ pb^{-1}
PHI-93	16/02/93÷16/07/93	0.994↔1.040	2100 - 2750	Yes	1.43
PHI-94/1	24/01/94÷01/02/94	1.019→0.980	3001 - 3040	No	0.05
RHOM-94	01/02/94÷26/02/94	0.970→0.810	3041 - 3165	No	0.15
PHI-94/2	13/11/94÷26/11/94	1.018↔1.024	4038 - 4106	No	0.16
RHOM-95	30/11/94÷06/06/95	0.810→0.600	4107 - 4541	No	0.16
PHI-96	12/04/96÷14/07/96	0.984↔1.034	4545 - 5150	No	2.18
LOW-96	20/09/96÷26/10/96	0.512→0.370	5749 - 5961	No	0.10
HIGH-97	29/01/97÷16/06/97	1.040↔1.370	6115 - 7030	No	5.93
PHI-98	10/10/97÷23/03/98	0.984↔1.060	7097 - 8427	Yes	11.93
RHOM-98	24/03/98÷30/06/98	0.970→0.360	8428 - 9345	Yes	3.50
HIGH-99	09/01/99÷	1.080→	9402 -	Yes	

3 Data taking and primary analysis

CMD-2 has been installed at the interaction region in 1992. Data of the 1992 run when 290 nb^{-1} have been collected at the ϕ-meson were used for calibration of the detector subsystems and software development. As a result of the analysis of the 1992 run, basic parameters and major decay modes of the ϕ-meson have been measured with an accuracy close to the world average [8]. From 1993 physical runs started. In Table 1 all runs performed till 1999 are listed.

In total, in experiments with CMD-2 the integrated luminosity of 25 pb^{-1} has been collected so far, a part of it with a superconductive wiggler turned on to increase the luminosity of the VEPP-2M collider. The bulk of data includes $2.1 \cdot 10^7$ events with ϕ-meson production, $3 \cdot 10^5$ multihadron events and $2.1 \cdot 10^6$ $\pi^+\pi^-$ events.

4 Event preselection on secondary tapes

All the events recorded were arranged in the following classes:

- *Neutrals* — events without tracks
- *One Track Events* — only one track was reconstructed
- *Two Tracks coming from One Vertex* — one primary vertex with two tracks

- *Bhabha* $e^+e^- \to e^+e^-$ *events recorded in the BGO calorimeter*
- *All the Others*

Events of well reconstructed background were rejected in the former three classes only. Each class contains its own background so the selections were class dependent.

The major background for *Neutrals* comes from cosmic events escaping detection in DC. The basic signatures of this background are: only one cluster is recorded; all the clusters are on one side from the interaction point either along the Z-direction or in the $R-\varphi$ - plane. The selection criteria for *Neutrals* are:

- $N_{cl} = 2$
  - $\Delta\varphi < 0.55$ **AND**
  - $\Delta\theta < 0.5$

  where $\Delta\varphi$ and $\Delta\theta$ are the acollinearity angles between clusters in the $R-\varphi$ - plane and $R-Z$ - plane respectively.
- $N_{cl} > 2$
  - $\max(\Delta\varphi) < \pi - 0.55$ **AND**
  - $\max(\theta_i) > \frac{\pi}{2} - 0.32$ **OR**
  - $\min(\theta_i) < \frac{\pi}{2} + 0.32$

  where $\Delta\varphi$ is the minimal angle in the $R-\varphi$ - plane containing all the clusters.

The major background for *One Track Events* is produced by showers coming from compensating solenoids or beam interactions with the residual gas in the beam pipe. Events of e^+e^--annihilation can contribute to this class because of two reasons: one of the two tracks is not recorded or the Offline procedure failed to reconstruct it. Events of this class are interesting only for evaluation of reconstruction and trigger efficiencies.

For *Two Tracks One Vertex* events main sources of background are showers from compensating solenoids, conversion at the beam pipe and cosmics crossing DC. Cosmic events were rejected by one of the following cuts:

- $\min(R_{min}) > 1$ **AND** $(\max(p_{tot}) > 2 \cdot E_{beam}$ **OR** $p_1 + p_2 > 3 \cdot E_{beam})$
- $\min(R_{min}) > 2$ **AND** $\Delta\varphi < 0.1$

The events *Bhabha in BGO* were selected in the separate class due to the low reconstruction efficiency for tracks coming at low angles relative to the beam axis. They were selected by the following cut:

- $E_{BGO1} > 0.5 \cdot E_{beam}$ **AND** $E_{BGO2} > 0.5 \cdot E_{beam}$

As a result of the cuts listed above, the number of events on secondary tapes was reduced by a factor of 3 to 5 depending on the beam energy and background conditions at VEPP-2M.

5 Luminosity measurement

Events of the reaction $e^+e^- \to e^+e^-$ were used for the luminosity measurement. The integrated luminosity was calculated as

$$\int Ldt = \frac{N_{ee}}{\sigma_B \cdot (1+\delta) \cdot \varepsilon_{rec}}, \qquad (1)$$

where N_{ee} is the number of collected e^+e^- events, σ_B is the Born cross-section of the $e^+e^- \to e^+e^-$, δ is the radiative correction and ε_{rec} is the reconstruction efficiency.

The collinear events were selected by the following criteria:

- Only one vertex in DC with two opposite charge tracks was found.
- The distance from the vertex to the beam axis $r_{vert} \leq 0.3$ cm.
- Z-coordinate of the vertex $|z_{vert}| \leq 8$ cm.
- Average momentum of two tracks $200 \leq p_{av} \leq 1000$ MeV/c.
- Acollinearity angle of two tracks in the plane transverse to the beam axis $|\Delta\varphi| = |\pi - |\varphi_1 - \varphi_2|| \leq 0.15$ radians.
- Acollinearity angle of two tracks in the plane that contains the beam axis $|\Delta\theta| = |\theta_1 - (\pi - \theta_2)| \leq 0.25$ radians.
- Average polar angle of two tracks $\theta_{min} \leq [\theta_1 + (\pi - \theta_2)]/2 \leq (\pi - \theta_{min})$. All analysis was done separately for $\theta_{min} = 1.0$ and $\theta_{min} = 1.1$.

The selected set consists of $e^+e^- \to e^+e^-$, $e^+e^- \to \pi^+\pi^-$, $e^+e^- \to \mu^+\mu^-$ and the cosmic background events. Energy depositions of both particles of the event are used for event separation. Electrons and positrons unlike

mesons have the large energy deposition in the calorimeter. Therefore for $e^+e^- \to e^+e^-$ both particles usually have the large energy deposition while for events of other types one or both particles usually have the small energy deposition. The example of the energy deposition of collinear events is shown in Fig. 9.

The separation of $e^+e^- \to e^+e^-$ events is performed in two steps. At the first step events with the large energy deposition $(150\,\mathrm{MeV} + E_{beam}/2) < E < E_{beam}$ of one particle are selected (E is the energy deposition). These so called "test" events consist of $e^+e^- \to e^+e^-$ with negligible background from $e^+e^- \to \pi^+\pi^-$ where pion(s) have nuclear interactions in the calorimeter. It is assumed that the energy depositions of both particles in the event are independent (uncorrelated). Therefore while we use the energy deposition of one particle to select "test" $e^+e^- \to e^+e^-$, the energy deposition of another particle gives us energy deposition of electrons and positrons.

At the second step events with the large energy deposition $E > E_{beam}/2$ of both particles are selected. These so called "selected" events are the pure subset of $e^+e^- \to e^+e^-$ events. Knowing the energy deposition of electrons and positrons, the selection efficiency (the probability for electron or positron to have the energy deposition $E > E_{beam}/2$) can be calculated. If the number of "selected" events in N_{sel} and the selection efficiency is ε_{sel}, the total number of $e^+e^- \to e^+e^-$ events N_{ee} is

$$N_{ee} = N_{sel}/\varepsilon_{sel}^2.$$

It is crucial that the energy depositions of electron and positron in the same event are uncorrelated. However a small correlation arises from the dependence of the energy deposition on the polar angle θ. Both particles in the event have about the same θ, and the further is θ from $\pi/2$, the thicker is the calorimeter and the larger energy deposition. To minimize this correlation the corrected energy deposition $\overline{E} = E/\left[1 + \alpha \cdot (\pi/2 - \theta)^2\right]$ is used where the coefficient α is calculated in such a way that dependence of $\overline{E}$ on θ is minimal. Two other sources of correlations — the radiation of initial particles and the nonuniformity of the calorimeter calibration — were estimated both from the simulation and from the real data and their effect was found to be negligible.

The reconstruction efficiency ε_{rec} was measured with the help of the same $e^+e^- \to e^+e^-$ events. At first, the clean subset of $e^+e^- \to e^+e^-$ events is selected using the calorimeter data only. Then, the probability to be properly reconstructed in DC was measured for these events. Since the selection criteria for collinear events are based only on DC data, this probability gives the value of the reconstruction efficiency.

The main sources of the systematic errors are the following.

1. The precision of the calculation of the radiative corrections is about 1%.

2. The trigger efficiency was not taken into account. The estimated trigger efficiency for $e^+e^- \to e^+e^-$ events is about 99%, therefore the corresponding systematic error is about 1%.

3. The precision of the fiducial volume calculation (the accuracy of θ_{min} determination) was estimated from the difference of the integrated luminosity measured for different θ_{min}. The corresponding systematic error is less than 0.5%.

4. The systematic error of $e^+e^- \to e^+e^-$ event separation is determined by the background from $e^+e^- \to \pi^+\pi^-$ events and by the correlation between energy depositions of two particles in the same event. The estimated systematic error is about 0.4% for center-of-mass energies around and above the ϕ-meson.

The overall systematic error is estimated to be about 2%.

The separation procedure, described above, is applicable to the data taken at the center-of-mass energy around and above the ϕ-meson. For lower energies the separation procedure is more complicated and based on the fit of energy deposition. The details about the luminosity measurement for energies below the ϕ-meson can be found in [33].

6 Radiative corrections

The cross sections for all processes of e^+e^- annihilation to leptons and hadrons presented in this work are calculated taking into account radiative corrections (RC). The accuracy of the RC calculation depends on energy and changes for the different decay modes of the ω and ϕ-mesons from 0.2% to 0.5%. For all channels with hadrons in the final state RC were calculated according to [34] excluding lepton and hadron vacuum polarization.

Our method of the RC calculation for the channels $\mu^+\mu^-$ and $\pi^+\pi^-$ is based on two works [34, 35]. In the work [34] the contribution of the RC to the cross section is integrated over kinematics of all final particles except for the total energy radiated by initial particles. It provides an accuracy of about 0.2%. Furthermore, the work [34] is valid only for comparatively small energy losses (under 10% of the beam energy). The second one is less accurate

(about $\sim 1\%$) and assumes only single photon emission but it provides the correct angular distributions for the final particles. It is important when any selection criteria are applied to the events.

The RC calculation procedure combines both approaches in the following way: photons with the energy less than some ΔE are simulated according to [34], while photons with the energy greater than ΔE are simulated according to [35]. The quantity ΔE is a free auxiliary parameter. The simulation shows that there is a wide region of ΔE values where the total cross section does not depend on this parameter at the level of about 0.2% - 0.3%.

The possible values of ΔE are limited by the following factors:

- ΔE should not exceed some upper limit above which [34] is not valid
- it is desirable to have ΔE as large as possible to get better accuracy of the calculation of the RC contribution according to [34], but in this case the angular distributions of the final particles are slightly incorrect
- it is desirable to have ΔE as small as possible to properly take into account the kinematics of the final particles according to [35], but in this case the accuracy of the calculation of the RC contribution to the cross section is not sufficient.

Thus the reasonable value of ΔE is limited for both sides and was chosen to be 10% of the beam energy.

The cross section of large angle Bhabha scattering was calculated with RC according to [36] where only one loop corrections, "soft" and "hard" photon emission are taken into account. The theoretical accuracy of RC formulae is not better than 1%. This RC uncertainty gives a systematic error in the integrated luminosity. Therefore the cross sections for other channels are also restricted by this accuracy. Work is in progress now toward the improvement of the accuracy RC calculation up to 0.2%.

7 Beam energy measurement in the ϕ-meson range

The collider energy was roughly set ($\delta E/E \lesssim 10^{-3}$) by the dipole magnet currents. Precise determination of the beam energy can be performed with the resonant depolarization method [37] providing the accuracy $\delta E/E \sim 10^{-5}$. During all ϕ-meson runs in 1994,1996,1998 twenty two calibration measurements were carried out at 11 energy points. Some points were calibrated

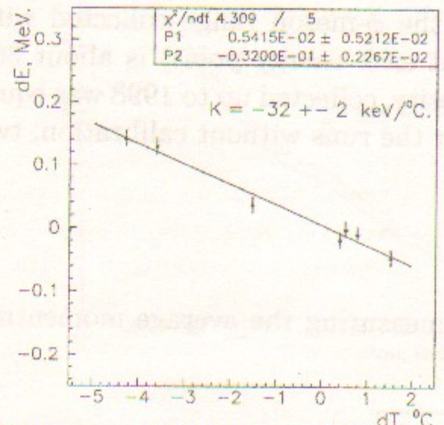

Figure 2: The energy difference between two energy measurements versus the difference between two corresponding temperature measurements. At each energy point the magnetic field in the bending magnets is fixed

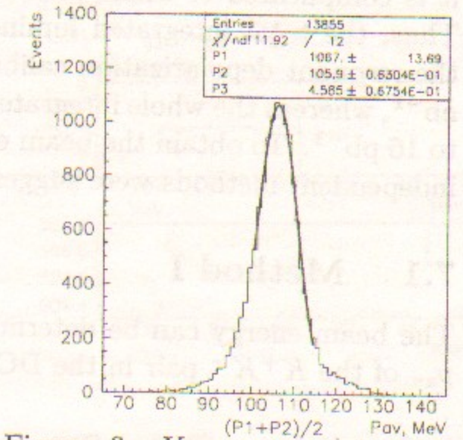

Figure 3: Kaon momentum spectrum. The corresponding beam energy is about 508 MeV

twice: at the beginning and at the end of the run. Analysing these data it was found that at the fixed magnetic field the collider energy slightly depends on the average temperature of all bending magnets (Fig.2). As seen from the fit the energy E_{beam} varies with temperature T as $dE_{beam} = k \cdot dT$, where $k = (-0.032 \pm 0.002)$ MeV/°C. The obtained dependence and temperature monitoring during data taking were used to calculate the average energy for each point.

Since the procedure of the calibration measurement takes a few hours, the majority of data were collected without precise energy calibration. Moreover, it is complicated to make such measurements when the wiggler [38] is on. Thus, the total integrated luminosity in the ϕ-meson range collected with the resonant depolarization calibration (at each energy point) is about 300 nb^{-1}, whereas the whole integrated luminosity, collected up to 1998 was equal to 16 pb^{-1}. To obtain the beam energy for the runs without calibration, two independent methods were suggested.

7.1 Method I

The beam energy can be determined by measuring the average momentum p_{av} of the K^+K^- pair in the DC volume:

$$E_{beam} = \sqrt{p_{av}^2 + m_K^2} + \Delta \qquad (2)$$

where Δ is an additional term, dominated by the contributions of the kaon ionization losses inside the detector and radiative losses of initial electrons. It can also contain the contribution of the DC related systematic effects.

The average momentum resolution σ_p/p for kaons with momenta around 110 MeV/c is about 5% determined mostly by the multiple scattering in DC. The statistical accuracy of the beam energy is determined as:

$$\frac{\sigma_{E_{beam}}}{E_{beam}} = \frac{1}{\sqrt{N}} \beta_K^2 \frac{\sigma_{p_{av}}}{p_{av}} \qquad (3)$$

where N is the number of found K^+K^- pairs. This accuracy is really high $\sim (2-10) \cdot 10^{-5}$ because kaons from the ϕ decay are slow $\beta_K \sim 0.2$ and the number of K^+K^- events at each energy point is about $10^3 - 10^4$. Although the statistical uncertainty of such measurements is small, the accuracy of this method is probably dominated by systematic errors connected with the instability of DC parameters and the drift of the magnetic field inside the chamber volume. It is important to note that since 1994 the permanent

improvement of the system of magnetic field stabilization [39] allowed us to achieve the field stability $\delta H/H \sim 10^{-4}$.

To determine the average value of p_{av} at each energy point the kaon momentum spectrum was fitted by a Gaussian (Fig. 3). The left and right limits of the fit correspond respectively to 0.5 and 0.2 of the Gaussian amplitude. Such procedure was used to decrease the influence of the spectrum distortion due to the radiative photon emission.

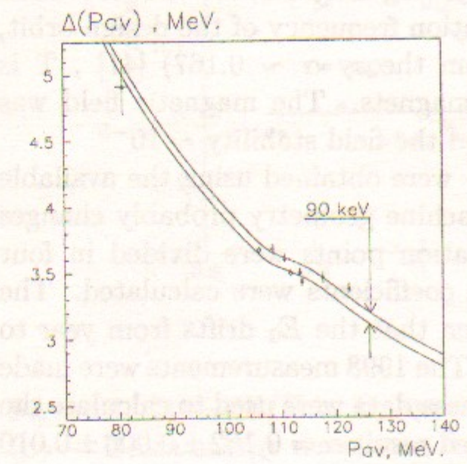

Figure 4: Calibration curves. The lower curve corresponds to 1996,1998 calibrations

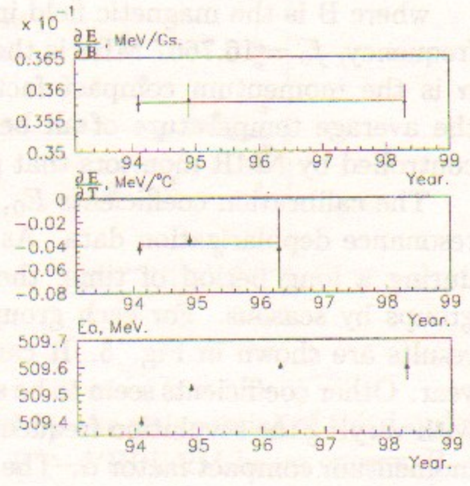

Figure 5: The evolution of calibration coefficients. The coefficient E_0 is transformed to the frequency f=16.7644 MHz

The momentum dependence $\Delta(p_{av})$ was first obtained by GEANT simulation of charged kaons in the detector [40] and approximated by a smooth function. Then the ϕ-meson runs with resonance depolarization were used to correct this function. Finally, the two calibration curves $\Delta(p_{av})$ corresponding to 1994 and 1996,1998 were obtained (Fig. 4). The difference between two calibrations is about 90 keV, whereas each curve is determined with the uncertainty $\sim$ 20 keV.

7.2 Method II

In another way the beam energy defined by the field value in the bending magnets and the revolution frequency of the collider. As mentioned above,

the collider energy also depends on the temperature of the magnetic system. So, to calculate the beam energy in the narrow energy range of the ϕ-meson resonance the following equation can be used:

$$E_{beam}(B,T,f) = [E_0 + \frac{\partial E}{\partial B}(B - B_0) + \frac{\partial E}{\partial T}(T - T_0)] \cdot [1 - \frac{f - f_0}{\alpha f_0}], \quad (4)$$

where B is the magnetic field in the bending magnets, f is the revolution frequency, $f_0 = 16.7667$ MHz is the revolution frequency of the design orbit, α is the momentum compact factor (from theory $\alpha \sim 0.167$) [41] , T is the average temperature of all bending magnets. The magnetic field was controlled by NMR monitors that provided the field stability $\sim 10^{-5}$.

The calibration coefficients $E_0, \frac{\partial E}{\partial B}, \frac{\partial E}{\partial T}$ were obtained using the available resonance depolarization data. As the machine geometry probably changes during a long period of time, the calibration points were divided in four groups by seasons. For each group these coefficients were calculated. The results are shown in Fig. 5. It can be seen that the E_0 drifts from year to year. Other coefficients seem to be stable. The 1998 measurements were made with varying the revolution frequency so these data were used to calculate the momentum compact factor α. The obtained result $\alpha = 0.162 \pm 0.006 \pm 0.010$ is in good agreement with the theory calculation (see above).

It is noteworthy that the collider energy is also affected by the operating wiggler. According to theory, it shifts the beam energy :

$$E_{beam} = E^0_{beam} \cdot [1 - \varrho \cdot (\frac{B_w^2}{E^2_{beam}})],$$

where E^0_{beam} is the beam energy when the wiggler is off, B_w is the magnetic field inside the wiggler, $\varrho = 0.04587$ MeV^2/kGs^2. In the ϕ - meson energy range this shift is about 0.5 MeV.

7.3 Results

Two described methods were applied to determine the energy for three scans of the ϕ-meson in 1996. During this scans there was no calibrations with resonance depolarization. Such consideration allows us to investigate the combined systematic errors of both methods.

These methods gave different results. The average energy difference for the scan 2, 3, 4 is about 50, 100, 120 keV respectively. This difference is really significant for scans 3 and 4. As we don't have any strong argument

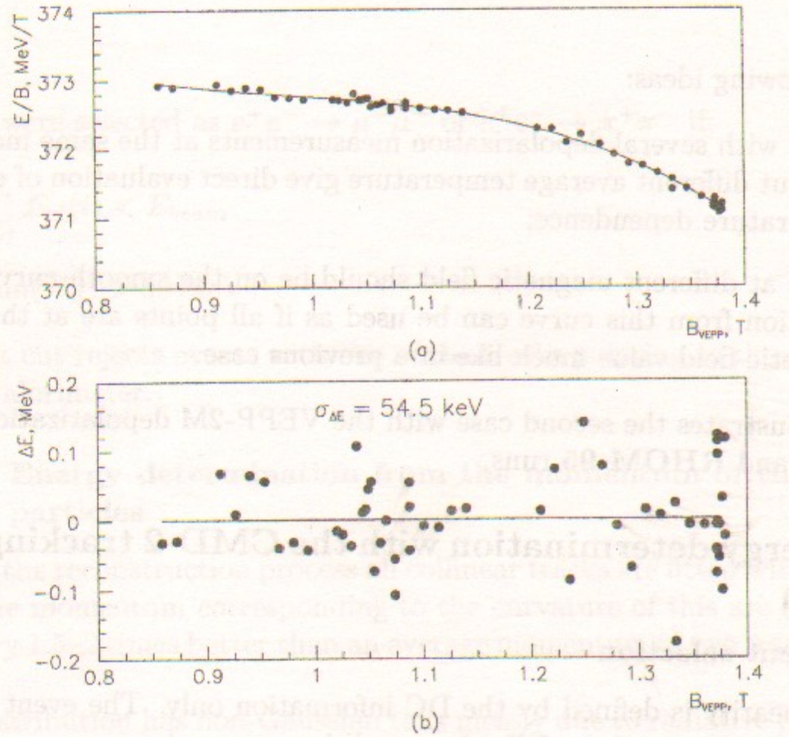

Figure 6: (a) — E/B vs B, approximated by the polynomial of third order, (b) — Beam energy deviations from (a); E — VEPP-2M beam energy, B — VEPP-2M bending magnets field

to prefer one of the methods, the beam energy was calculated as the average energy obtained by these two methods. The systematic error was estimated as a half of the average difference between E_I and E_{II} for each scan, and it is 25, 50, 60 keV for scans 2, 3, 4 respectively.

8 Beam energy determination from the momentum of collinear events

The tracking system of the CMD-2 allows an independent beam energy measurement based on the momenta of the collinear tracks. This technique can be used anywhere in the energy range of VEPP-2M since it uses processes $e^+e^- \to e^+e^-$, $e^+e^- \to \mu^+\mu^-$ and $e^+e^- \to \pi^+\pi^-$.

One can estimate beam energy fluctuations using the depolarization data

and the following ideas:

- points with several depolarization measurements at the same magnetic field but different average temperature give direct evaluation of energy-temperature dependence;
- points at different magnetic field should be on the smooth curve. The deviation from this curve can be used as if all points are at the same magnetic field value much like in a previous case.

Fig. 6 illustrates the second case with the VEPP-2M depolarization data of **PHI-94** and **RHOM-95** runs.

8.1 Energy determination with the CMD-2 tracking system

8.1.1 Event selection

Event collinearity is defined by the DC information only. The event is considered to be collinear if the following conditions are met:

- There are exactly two tracks from the same vertex;
- Tracks belong to the particles with the opposite charges;
- Each track has at least 10 hits in the r-φ plane;
- Track impact parameter relative to the beam axis does not exceed 0.1 cm for each track;
- Absolute Z-coordinate of the vertex is less than 5 cm;
- Polar angle of the first track in the event is inside the $1 \div (\pi - 1)$ interval;
- Acollinearity of two tracks in the r-φ plane is less than 0.02;
- The difference of two track polar angles is inside $\pi \pm .1$.

The energy deposition in the barrel calorimeter was used as the only parameter to distinguish between $e^+e^- \to e^+e^-$ and other collinear events. For $e^+e^- \to e^+e^-$the following conditions should be met:

- $\min(E_{cl}) > 0.65 E_{beam}$
- $\max(E_{cl}) < 1.2 E_{beam}$

Events were selected as $e^+e^- \to \mu^+\mu^-$ or $e^+e^- \to \pi^+\pi^-$ if:

- $\sum_{i=1}^{2} E_{cl}(i) < E_{beam}$
- $\min(E_{cl}) > 50\,\mathrm{MeV}$

The last cut rejects events with one of the tracks pointing to the dead region of the calorimeter.

8.1.2 Energy determination from the momentum of the charged particles

During the reconstruction process all collinear tracks are fitted with the single arc. The momentum corresponding to the curvature of this arc ($\widehat{p}$) has the accuracy 1.5–2 times better than an average momentum of two tracks (Fig. 7).

$\widehat{p}$ distribution has non-Gaussian tails mostly due to radiative photons. To get the reasonable average value of the $\widehat{p}$ two approaches have been used:

1. The distribution is fitted inside the limited range around the maximum, where it is quite close to the standard Gaussian. In that case tails have practically no influence on the average value but interval boundaries are quite arbitrary and may shift the average if changed. We use the following limits:
   $\left|\sqrt{\widehat{p}^2 + m_e^2} - E_{beam}\right| < 10\,\mathrm{MeV}$ for $e^+e^- \to e^+e^-$ and
   $\left|\sqrt{\widehat{p}^2 + m_\pi^2} - E_{beam}\right| < 10\,\mathrm{MeV}$ for $e^+e^- \to \pi^+\pi^-$, $e^+e^- \to \mu^+\mu^-$.
2. The distribution is fitted with the asymmetrical function. For this purpose we use Gram-Charlier approximation series [42], described by:

$$f(z) = \frac{A}{\sqrt{2\pi}} e^{-\frac{z^2}{2}} \left[1 + \frac{\gamma_1}{6}\left(z^3 - 3z\right) + \frac{\gamma_2}{24}\left(z^4 - 6z^2 + 3\right)\right] \quad (5)$$
$$z = \frac{x - x_0}{\sigma};$$

where A, x_0, σ, γ_1, γ_2 are parameters of the fit. Note, that for $\gamma_1 = \gamma_2 = 0$ this distribution becomes standard Gaussian and $\int_{-\infty}^{\infty} f(z)dz = A$ for all γ_1, γ_2. Comparing with the first approach we have more fit parameters, but now the result is independent of the interval boundaries and so they were significantly extended: $\left|\sqrt{\widehat{p}^2 + m_e^2} - E_{beam}\right| <$

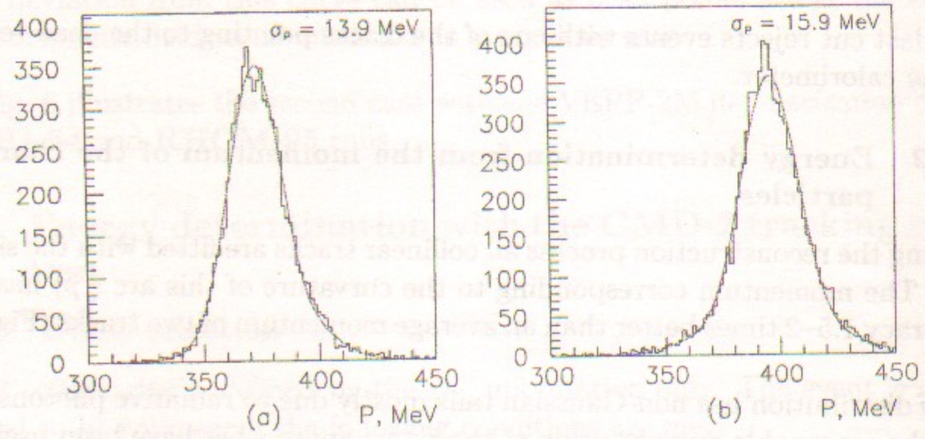

Figure 7: Momentum distribution. (a) – average momentum for $e^+e^- \to \pi^+\pi^-$, $e^+e^- \to \mu^+\mu^-$. (b) – average momentum for $e^+e^- \to e^+e^-$. (c) – one arc momentum for $e^+e^- \to \pi^+\pi^-$, $e^+e^- \to \mu^+\mu^-$. (d) – one arc momentum for $e^+e^- \to e^+e^-$. All distributions are fitted with the function described by (5)

20 MeV for $e^+e^- \to e^+e^-$ and $\left|\sqrt{\widehat{p}^2 + m_\pi^2} - E_{beam}\right| < 20$ MeV for $e^+e^- \to \pi^+\pi^-$, $e^+e^- \to \mu^+\mu^-$.

The accuracy of the average beam energy at each point σ_E depends on the number of collinear events and on the accuracy of the momentum measurement for a single event.

The suggested technique is intended not for the absolute determination of the beam energy but for the check of the beam energy stability. So we have to control not the value of $\Delta E = \sqrt{\widehat{p}^2 + m^2} - E_{beam}$ itself but its dependence on the beam energy. It means that we can combine the results for both classes of event with the average value of ΔE set to an arbitrary constant, e.g. $\Delta E = 0$. In the range of the ω-meson cross sections for $e^+e^- \to e^+e^-$ and processes $e^+e^- \to \pi^+\pi^-$ have the same order of magnitude and their integration can significantly improve the accuracy.

Both approaches give approximately the same result, demonstrated in Fig. 8.

9 Measurement of the pion form factor

Pion form factor measurement is important for a number of physics problems. Detailed experimental data in the timelike region allows to measure the parameters of the $\rho(770)$ meson and its radial excitations. Extrapolation of the energy dependence of the pion form factor to the point $s = 0$ gives the value of the pion electromagnetic radius. Exact data on the pion form factor is necessary for the precise determination of the ratio

$$R = \sigma(e^+e^- \to hadrons)/\sigma(e^+e^- \to \mu^+\mu^-),$$

which in the VEPP-2M energy range is dominated by the $e^+e^- \to \pi^+\pi^-$ cross-section. Knowledge of R with high accuracy is required to evaluate the hadronic contribution to the (g-2) of the muon and to the running electromagnetic constant $\alpha(M_Z{}^2)$. In the case of the (g-2) of the muon, the energy range of VEPP-2M gives the major contribution both to the hadronic contribution itself and to its uncertainty.

The most precise measurement of the pion form factor at VEPP-2M was done in the late 70s – early 80s by OLYA and CMD groups [43]. In the CMD experiment, 24 points from 360 to 820 MeV were studied with a systematic uncertainty of about 2%. In the OLYA experiment, the energy range from 640 to 1400 MeV was scanned with a small energy step and a systematic uncertainty varied from 4% at the ρ-meson peak up to 15% at 1400 MeV.

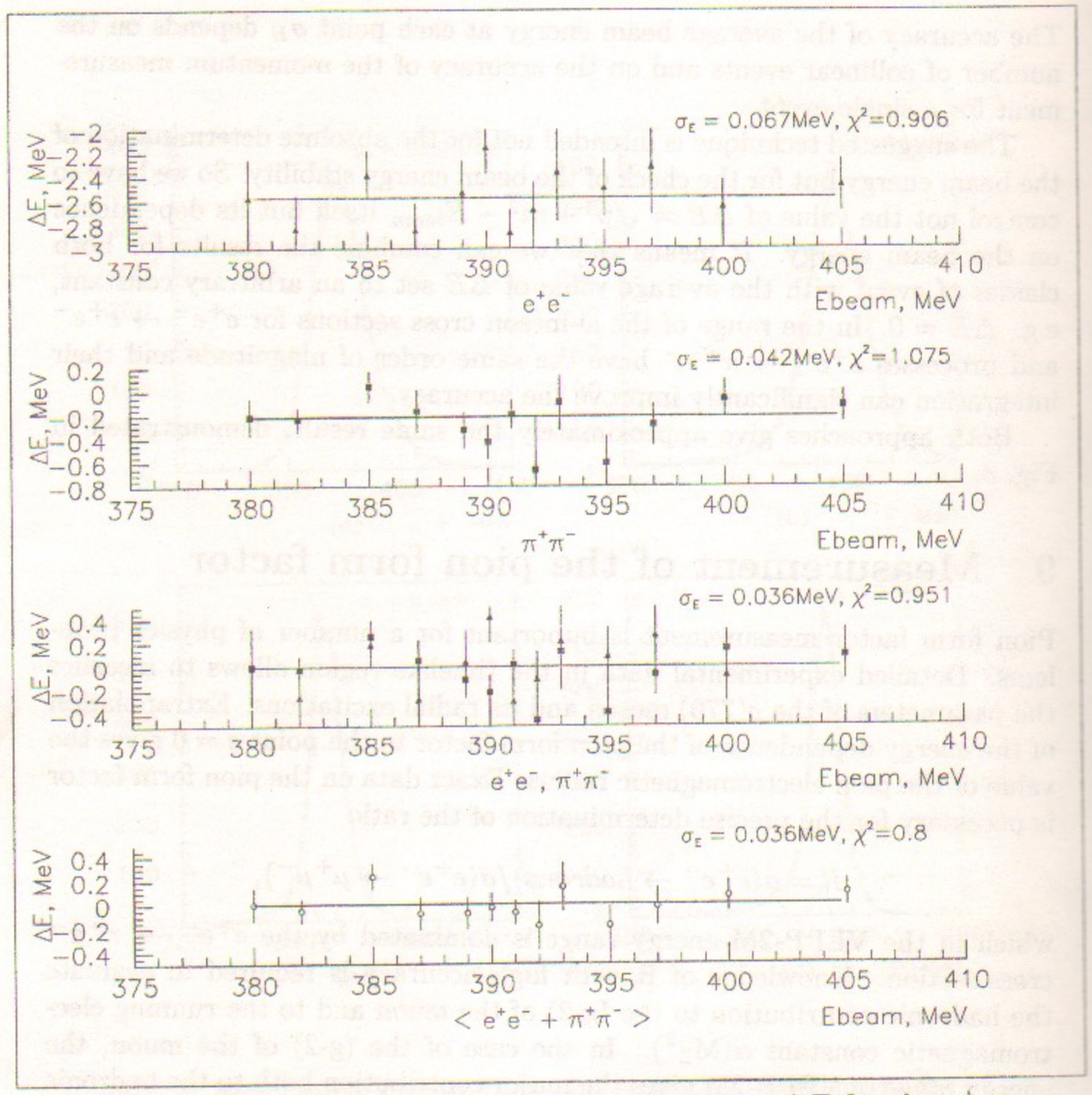

Figure 8: Beam energy stability. From up to down: ΔE for the $e^+e^- \to e^+e^-$ event class, ΔE for the $e^+e^- \to \pi^+\pi^-$ event class, both classes on the same plot with the ΔE set to 0 and the combined result

The large statistics of about 2 million of $e^+e^- \to \pi^+\pi^-$ events was collected by the CMD-2 detector in the whole VEPP-2M energy range. CMD-2 has a lot of advantages which should allow to achieve much smaller systematic error than before. The trigger system has almost 100% efficiency for all collinear events. The tracking system and the electromagnetic calorimeter give good event separation. The Z-chamber allows to measure precisely the fiducial volume.

The analysis scheme is the following. For each energy point, events with two collinear tracks are selected by the following selection criteria:

1. distance from the vertex to the beam axis $r_{vert} < 0.3$ cm,
2. z coordinate of the vertex $|z_{vert}| < 8$ cm,
3. average momentum of two particles p_{av} should be within the range expected for each particular energy point
4. acollinearity of two particles $|\Delta\phi| = |\pi - |\phi_1 - \phi_2|| < 0.15$ rad and $|\Delta\theta| = |\theta_1 - (\pi - \theta_2)| < 0.25$ rad,
5. average polar angle of two particles $\theta_{min} < \theta_{av} < (\pi - \theta_{min})$, where $\theta_{min} = 1.1$ or $\theta_{min} = 1.0$.

The selected sample of events consists of the $e^+e^- \to e^+e^-$, $e^+e^- \to \pi^+\pi^-$, $e^+e^- \to \mu^+\mu^-$ events and the cosmic background events. Then the events are separated and the number of electron N_{ee}, muon $N_{\mu\mu}$ and pion $N_{\pi\pi}$ pairs is calculated. The pion form factor is calculated as:

$$|F_\pi|^2 = \frac{N_{\pi\pi}}{N_{ee}} \cdot \frac{\sigma_{ee}}{\sigma_{\pi\pi}},$$

where σ_{ee} is the "visible" (including all necessary corrections) $e^+e^- \to e^+e^-$ cross-section and $\sigma_{\pi\pi}$ is the "visible" $e^+e^- \to \pi^+\pi^-$ cross-section with $|F_\pi|^2 = 1$.

The collected $e^+e^- \to \pi^+\pi^-$ data is combined into several groups by the energy range and the data taking period.

The **RHOM-95** data sample was collected during 1994-1995 runs at 43 energy points with the center-of-mass energies from 0.61 till 0.96 GeV with a 0.01 GeV energy step. In the narrow energy region near the ω-meson the energy steps were $0.002 \div 0.006$ GeV in order to study the ω-meson parameters and the $\rho - \omega$ interference. The beam energy was measured with the help of the resonance depolarization technique at almost all energy points. The **RHOM-98** data was collected during 1998 run at 37 energy points with the

center-of-mass energies from 0.36 up to 0.97 GeV. As a rule, the larger energy step was used but at the same time much higher statistics was taken than in **RHOM-95**. The **LOW-96** data was collected in 1996 at 10 energy points with the center-of-mass energies from 0.36 up to 0.52 GeV. The **HIGH-97** data was collected in 1997 run at 37 energy points with the center-of-mass energies from 0.98 up to 1.38 GeV.

The data analysis is the same for **RHOM-95** and **RHOM-98** data with $2E > 0.6$ GeV. The energy deposition of both particles in the same event is used for the event separation. The number of $e^+e^- \to \mu^+\mu^-$ events is calculated from the number of $e^+e^- \to e^+e^-$ events according to the QED. Since the number of muon pairs is much smaller than the number of electron and pion pairs, the systematic error of the calculation does not give a significant contribution to the systematic error of the pion form factor value. The energy deposition for collinear events together with the fit is demonstrated in Fig. 9. The measurement of the beam energy with the help of the resonance depolarization technique for **RHOM-95** data allowed to significantly decrease the systematic error coming from the energy uncertainty. But for **RHOM-98** data the corresponding systematic error in the pion form factor value is larger since the precise measurement of the beam energy was not performed. Therefore we prefer to present two independent results for these two data groups.

The event separation in the energy range $2E_{beam} \leq 0.6$ GeV is based on the momenta of both particles in the same event. The momentum distribution for the collinear events is demonstrated in Fig. 10. There are clear signals of electron, muon and pion pairs (from right to left). For some energy points it is possible to apply both methods of event separation performing the cross-check of the procedures.

The event separation in the energy range above the ϕ-meson is based on the energy deposition of both particles in the same event. But since for this energy range the number of pion pairs is less than the number of muon pairs, the systematic error of the calculation of the number of muon pairs from the number of electron pairs gives the significant contribution to the systematic error of the pion form factor value. As a result, the direct pion/muon separation is required.

The analysis of the **RHOM-95** data is completed while other data is still under analysis. The pion form factor, obtained in **RHOM-95** data analysis, is presented in Fig. 11. The systematic error for these data is about 1.4%, coming mainly from the uncertainty of the theoretical calculations for the radiative corrections. The new calculation of the radiative corrections is in process with the goal to reach the uncertainty below 0.3%. A fit of the pion

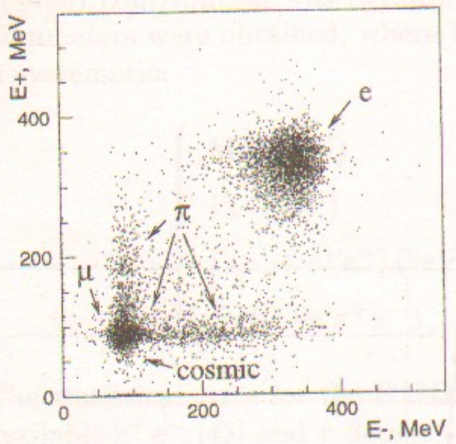

(a) Energy deposition of both particles for the same event

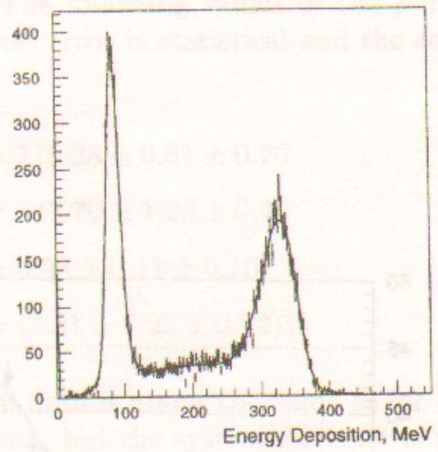

(b) Energy deposition of the particle with positive charge together with the fit

Figure 9: Energy deposition for the collinear events at $2E_{beam} = 0.8$ GeV

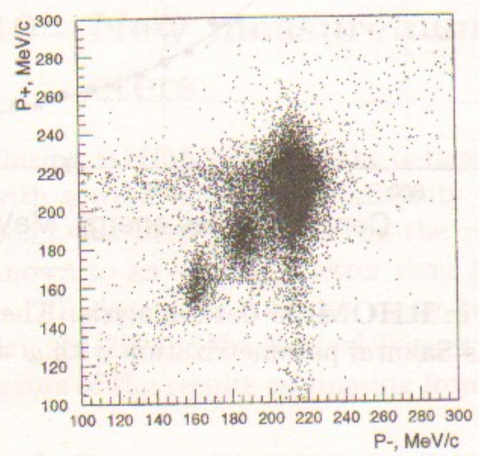

(a) Momentum of both particles for the same event

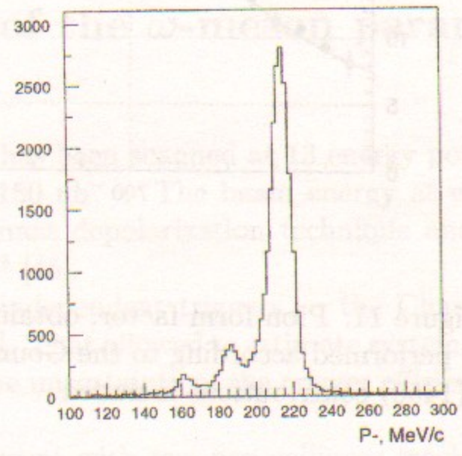

(b) Momentum of the particle with negative charge

Figure 10: Momentum for collinear events at $2E_{beam} = 0.43$ GeV

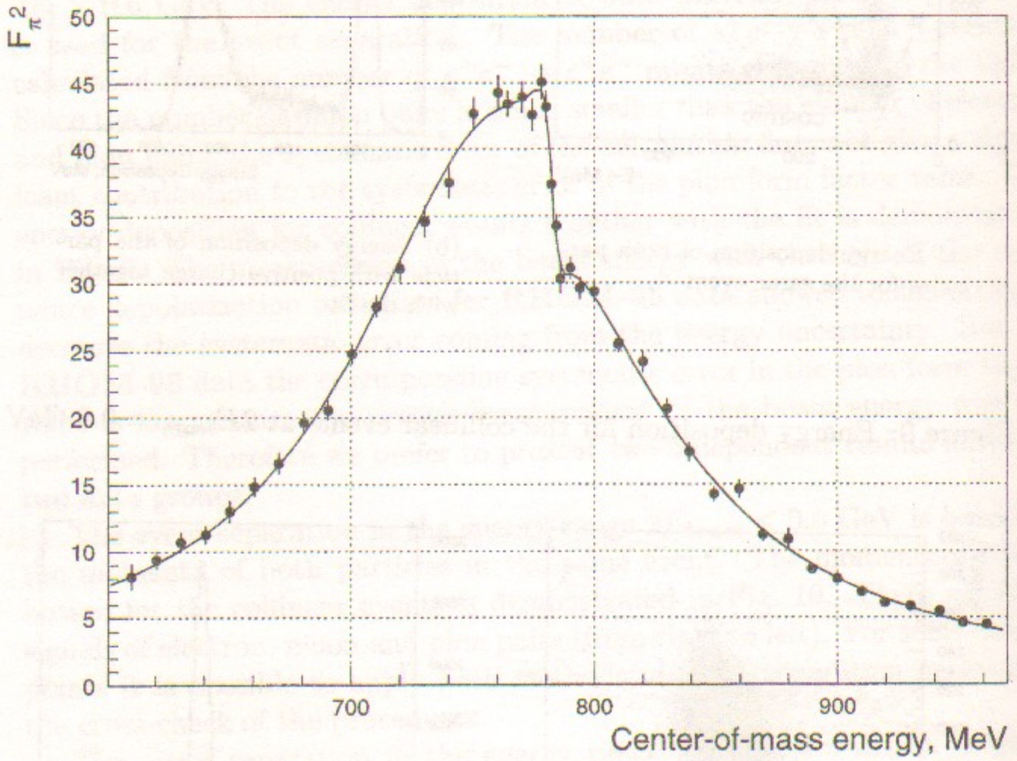

Figure 11: Pion form factor, obtained in **RHOM-95** data analysis. The fit is performed according to the Gounaris-Sakurai parametrization with ω and $\rho(1450)$ contributions included

form factor based on the Gounaris-Sakurai parametrization with the ω and $\rho(1450)$ contribution was performed. The following values of the ρ-meson parameters were obtained, where the first error is statistical and the second is systematic:

$$\begin{cases} M_\rho\,(\text{MeV}) & = 775.28 \pm 0.61 \pm 0.20 \\ \Gamma_\rho\,(\text{MeV}) & = 147.70 \pm 1.29 \pm 0.40 \\ \Gamma(\rho \to e^+e^-)\,(\text{keV}) & = 6.93 \pm 0.11 \pm 0.10 \\ Br(\omega \to \pi^+\pi^-) & = (1.31 \pm 0.23 \pm 0.02)\% \end{cases}$$

The statistical error for the **RHOM-95** data is about the same as for other available e^+e^- [43] and τ decays [44] data, but the systematic error is much smaller. This will allow to significantly reduce the error of the hadronic contribution to the (g-2) of the muon coming from the corresponding energy range, which is completely determined by the systematic errors of the previous experiments. Details about the **RHOM-95** data analysis can be found in [33].

The analysis of the 10 times larger statistics of the remaining data will help to reduce both statistical and systematic experimental errors.

10 New measurement of the ω-meson parameters

During **RHOM-95** runs the ω-meson has been scanned at 13 energy points with a total integrated luminosity of 150 nb^{-1}. The beam energy at each point has been measured by the resonant depolarization technique and is known to an accuracy better than 10^{-4} [45].

All data were collected using two independent triggers — the Charged Trigger [29] and the Neutral Trigger [46]. That allowed to estimate systematic errors of the results originating from the uncertainty of the trigger efficiency.

In the ω-meson energy range any event with two non-collinear tracks is a candidate for an $\omega \to \pi^+\pi^-\pi^0$ decay. Therefore all events with two tracks originating from the same vertex, each having a polar angle $0.85 < \theta < \pi - 0.85$, being within the fiducial volume of the detector, were selected for further analysis.

Since only the DC information has been used for the selection of 3π events, most of the background comes from the processes with a hard photon emission:

$$e^+e^- \to e^+e^-\gamma, \pi^+\pi^-\gamma, \mu^+\mu^-\gamma$$

These processes have the same signature as $\pi^+\pi^-\pi^0$, except that they have a very different acollinearity angle ($\Delta\phi = \pi - |\varphi_1 - \varphi_2|$) distribution peaked near $\Delta\phi = 0$. Thus, the rejection of events with a small $\Delta\phi$ drastically reduces the background, but also decreases the number of 3π events. A value of $\Delta\phi = 0.25$ was used as a reasonable trade out (see Fig. 12).

Additional background suppression can be achieved using the "missing mass" parameter, assuming all charged particles to be pions and taking into account momentum and energy conservation. For real $\pi^+\pi^-\pi^0$ events the distribution over the missing mass squared has a peak in the region of $M^2_{\pi^0}$ contrary to the background processes which have a peak around zero for $e^+e^- \to \pi^+\pi^-\gamma, \mu^+\mu^-\gamma$ or peak in the negative region for $e^+e^- \to e^+e^-\gamma$. Figure 13 shows the squared missing mass of two charged particles versus maximum energy deposition in the calorimeter produced by these two particles. The lines show the cut applied for the separation of $\pi^+\pi^-\pi^0$ events from the background. The effect of this cut is illustrated in Fig. 14.

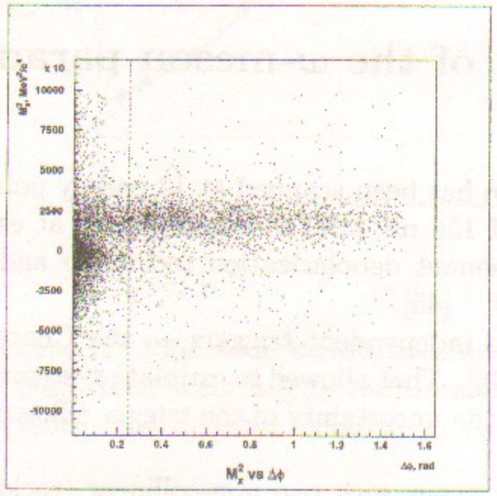

Figure 12: The squared missing mass vs acollinearity angle

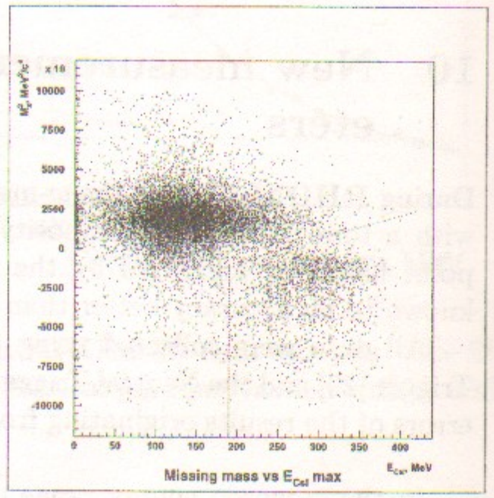

Figure 13: The squared missing mass vs CsI energy

The resulting number of $\pi^+\pi^-\pi^0$ events was obtained by fitting the his-

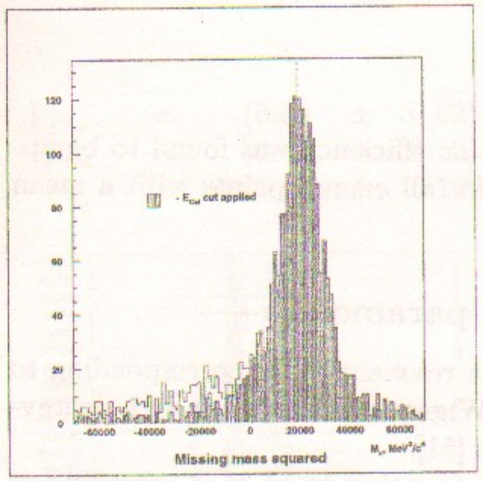

Figure 14: The squared missing mass of two charged particles(taken as pions). The shaded histogram corresponds to the cut shown in Fig. 13. The vertical dashed line points to the $M^2_{\pi^0}$ value

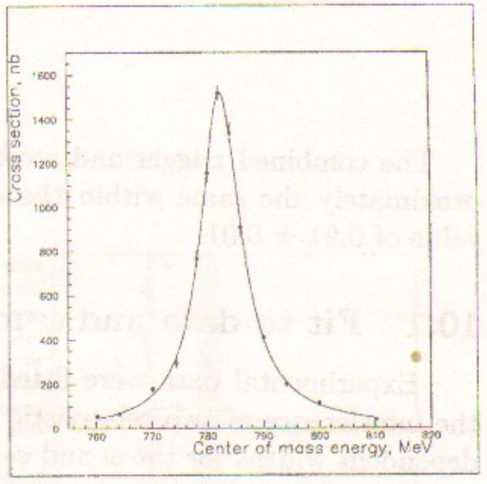

Figure 15: ω-meson excitation curve

tograms similar to the one shown in Fig. 14 with the sum of Gaussian functions describing 3π and background events.

The cross section at each energy point was calculated as follows:

$$\sigma = \frac{N}{L \cdot \varepsilon \cdot (1 + \delta_{rad})},$$

where N is the number of 3π events, L is the luminosity, ε is the total detection efficiency for $e^+e^- \to \pi^+\pi^-\pi^0$ events and δ_{rad} is the radiative correction.

The integrated luminosity was determined from the number of the Bhabha events, selected by the presence of two collinear tracks in the DC [47] and high energy deposition in the CsI barrel calorimeter [48] with the statistical error at each energy point at the level of 1–2%.

Radiative corrections were calculated according to [34] with an accuracy better than 1%.

The geometric efficiency was taken from MC simulation while trigger and reconstruction efficiencies were determined with the help of special "test" events, known to be $\pi^+\pi^-\pi^0$ events with a sufficient level of reliability. Such events were obtained as a result of the constraint fits based on the information from the ZC [47] and CsI calorimeter only.

The combined trigger and reconstruction efficiency was found to be approximately the same within the errors for all energy points with a mean value of 0.91 ± 0.01.

10.1 Fit to data and ω-meson parameters

Experimental data were fitted with a resonant curve corresponding to the interference of two relativistic Breit-Wigner cross sections with energy-dependent widths for the ω and ϕ-mesons [51].

The relative phase of $\omega - \phi$ mixing α was taken to be 155° according to [49].

The leptonic width can be calculated with the help of the formula:

$$\Gamma_{\omega\to e^+e^-} = \Gamma_\omega \cdot \frac{\sigma_0(\omega \to \pi^+\pi^-\pi^0)}{Br(\omega \to \pi^+\pi^-\pi^0)} \cdot \frac{M_\omega^2}{12\pi}.$$

Here $Br(\omega \to \pi^+\pi^-\pi^0) = 0.888 \pm 0.007$ was taken from [7] and all other parameters were defined from the fit.

Currently the main systematic error in the ω leptonic width comes from the uncertainty in the luminosity determination and is about 3%.

Another possible source of a significant systematic error is the efficiency determination which depends on the "purity" of the test event sample. This error should not exceed 2 – 3%, presumably being much lower and is subject of further investigations.

Several other error sources are the accuracy of the radiative corrections, detector fiducial volume determination, pion decays in flight and nuclear interaction processes inside the tracking system. All of them are of the order of 0.5% or less and at present do not contribute significantly to the total systematic error of the ω leptonic width.

The systematic error of the total ω width originates mainly from the background uncertainty and is estimated to be at the level of the statistical error, i.e. $\sim$ 2.5%. It could be reduced by better background suppression with the help of the barrel calorimeter.

Experimental points together with the fitted excitation curve are shown in Fig. 15. The following ω-meson parameters were obtained from the fit:

$$\begin{array}{lcrcrcl} \Gamma_{e^+e^-} & = & (0.63 & \pm & 0.01 & \pm & 0.02) \quad \text{keV} \\ \Gamma_{tot} & = & (8.82 & \pm & 0.18 & \pm & 0.20) \quad \text{MeV} \\ m_\omega & = & (782.65 & \pm & 0.09 & \pm & 0.10) \quad \text{MeV} \end{array}$$

This should be compared to the current PDG values [7]:

$$\begin{array}{lcrcrcl} \Gamma_{e^+e^-} & = & (0.60 & \pm & 0.02) & & \text{keV} \\ \Gamma_{tot} & = & (8.43 & \pm & 0.10) & & \text{MeV} \\ m_\omega & = & (781.94 & \pm & 0.12) & & \text{MeV} \end{array}$$

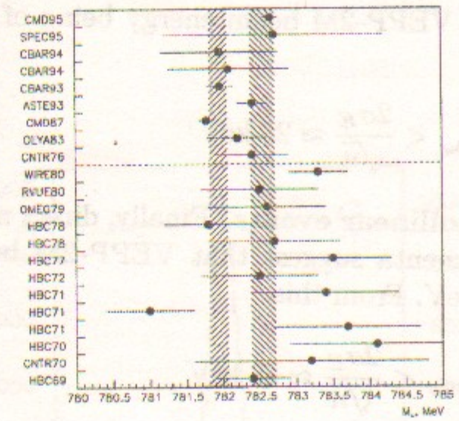

Figure 16: ω-meson mass compared with previous experiments. Left bar shows the current PDG value, right bar - the world average before CMD-87. Experiments below the dashed line are excluded by PDG group from the average value calculation

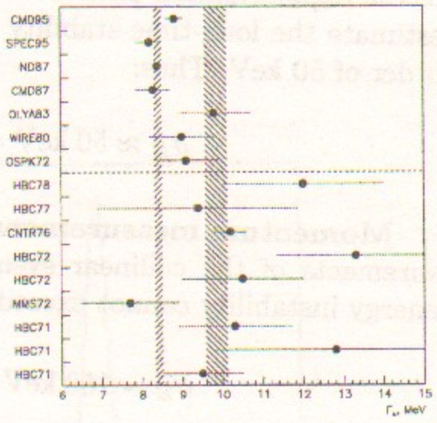

Figure 17: ω-meson width compared with previous experiments. Left bar shows the current PDG value, right bar - the world average before CMD-87. Experiments below the dashed line are excluded by PDG group from the average value calculation

The PDG value of the ω mass is lower by approximately 6 standard deviations but is based practically on the single experiment [50], which is in significant contradiction with the average value of all other experiments [7], the latter being very close to our value.

10.2 Estimation of the possible error of the ω-meson mass

Temperature drift.

Depolarization data in the ω-meson range do not show any clear dependence of the beam energy on the VEPP-2M average temperature, but as a reasonable upper limit one can use the dependence in the ϕ-meson range. Given the temperature fluctuation about 1°C (r.m.s.) the following estimation can be made:

$$\sigma_T \sim 1°\text{C} \Longrightarrow \sigma_E < 30\ \text{keV} \Longrightarrow \sigma_{m_\omega} < \frac{2\sigma_E}{\sqrt{n}} \approx 15\ \text{keV},$$

where n = 13 is the number of energy points.

Long-time stability of the beam energy. Based on the deviation of the depolarization data from the E_{beam}/B dependence curve (Fig. 6) we estimate the long-time stability of the VEPP-2M beam energy being of the order of 50 keV. Thus:

$$\sigma_E \approx 50 \text{ keV} \Longrightarrow \sigma_{m_\omega} < \frac{2\sigma_E}{\sqrt{n}} \approx 25 \text{ keV}$$

Momentum measurement for collinear events. Finally, direct measurements of the collinear events momenta suggest that VEPP-2M beam energy instability cannot exceed 150 keV. From this:

$$\sigma_E \sim 150 \text{ keV} \Longrightarrow \sigma_{m_\omega} < \frac{2\sigma_E}{\sqrt{n}} \approx 75 \text{ keV}$$

Figures 16 and 17 demonstrate results of all experiments quoted by [7] on the ω-meson mass and width respectively.

11 Measurements of ϕ-meson parameters in $K_L^0 K_S^0$ channel

The process $e^+e^- \to \phi \to K_L^0 K_S^0$ with subsequent decay $K_S^0 \to \pi^+\pi^-$ was used to measure the ϕ-meson parameters. The data sample has been analysed corresponding to the integrated luminosity of 2.37 pb^{-1} collected during the **PHI-94/1**, **PHI-94/2** and **PHI-96** runs in the c.m. energy range 984 – 1040 MeV (3.4×10^6 ϕ-mesons).

Events were selected according to the following conditions:

- Two opposite charge tracks, coming from the vertex closest to the beam.
- Both tracks had polar angles $0.95 < \theta < \pi - 0.95$, the distance between the beam and the vertex in the $R-\varphi$ plane: $r_{vert} < 1.5$ cm.
- The invariant mass for two tracks in the vertex was $450 < M_{inv} < 550$ MeV, (see Fig. 18a) and the missing momentum value satisfied the conditions $60 < P_{mis} < \sqrt{E_{beam}^2 - m_{K^0}^2} + 40$ MeV/c, where $m_{K^0} = 497.672$ MeV is the neutral kaon mass.
- Track momenta were $140 < p_{1,2} < 300$ MeV/c, and the average momentum value was $180 < (p_1 + p_2)/2 < 250$ MeV/c as shown in Fig. 18b.

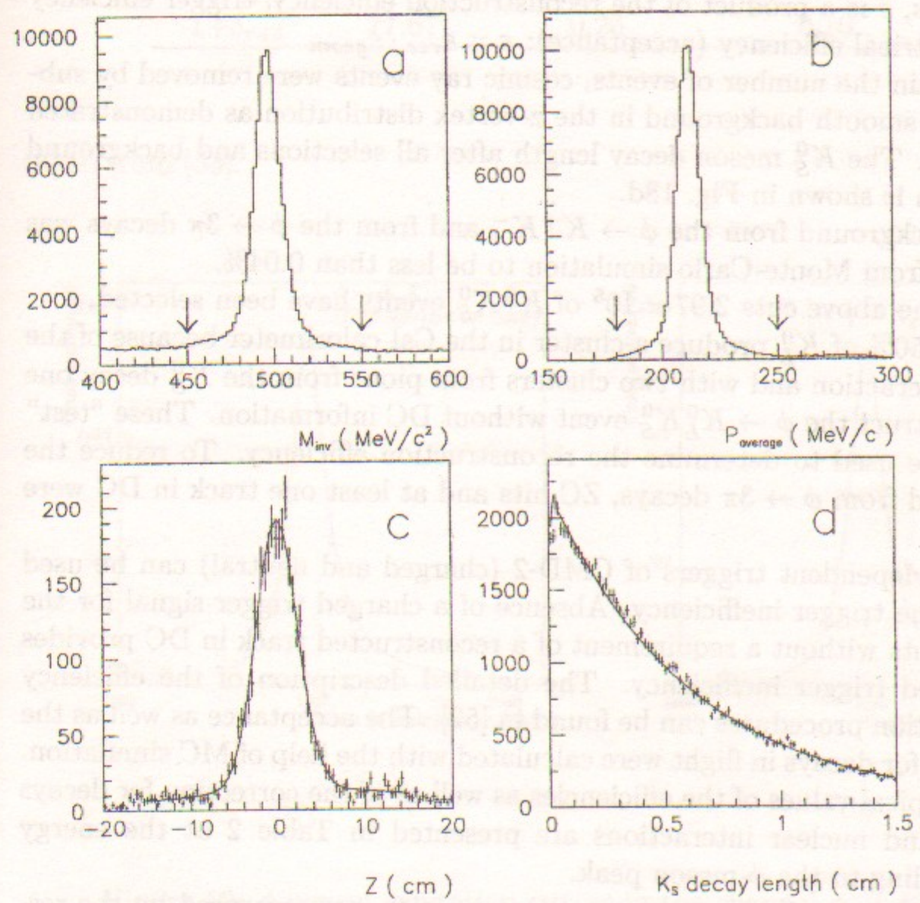

Figure 18: Distributions used in the selection of $e^+e^- \to \phi \to K_L^0 K_S^0$ events

At each energy the cross section of the decay was calculated according to the formula:

$$\sigma = \frac{N}{\varepsilon \cdot L \cdot (1+\delta_{rad}) \cdot (1+\delta_{loss})},$$

where N is the number of events, L is the integrated luminosity, δ_{rad} is the radiative correction [34], δ_{loss} is a correction for decays in flight and nuclear interactions, ε is a product of the reconstruction efficiency, trigger efficiency and geometrical efficiency (acceptance): $\varepsilon = \varepsilon_{rec} \cdot \varepsilon_{geom}$

To obtain the number of events, cosmic ray events were removed by subtraction of smooth background in the z-vertex distribution as demonstrated in Fig. 18c. The K^0_S meson decay length after all selections and background subtraction is shown in Fig. 18d.

The background from the $\phi \to K^+K^-$ and from the $\phi \to 3\pi$ decays was estimated from Monte-Carlo simulation to be less than 0.04%.

With the above cuts 2.97×10^5 of $K^0_L K^0_S$ events have been selected.

About 50% of K^0_L produce a cluster in the CsI calorimeter because of the nuclear interaction and with two clusters from pions from the K^0_S decay one can reconstruct the $\phi \to K^0_L K^0_S$ event without DC information. These "test" events were used to determine the reconstruction efficiency. To reduce the background from $\phi \to 3\pi$ decays, ZC hits and at least one track in DC were required.

Two independent triggers of CMD-2 (charged and neutral) can be used to study the trigger inefficiency. Absence of a charged trigger signal for the "test" events without a requirement of a reconstructed track in DC provides the charged trigger inefficiency. The detailed description of the efficiency determination procedures can be found in [52]. The acceptance as well as the correction for decays in flight were calculated with the help of MC simulation.

The typical values of the efficiencies as well as of the correction for decays in flight and nuclear interactions are presented in Table 2 at the energy corresponding to the ϕ-meson peak.

For 1994 data the beam energy at each point was measured by the resonance depolarization method. For data collected in 1996 the beam energy was determined with the help of charged kaon momenta and by the collider magnetic field analysis.

The obtained cross sections for the process $e^+e^- \to K^0_L K^0_S$ are presented in Figs. 19a,b. The experimental points are fitted by function [8] which includes the contributions of ϕ, ω and ρ as well as higher resonances ($\rho(1450)$, $\phi(1680)$) with the parameters from [7] and the nonresonant background. Relative phases between ρ and $\rho(1450)$ as well as between ϕ and $\phi(1680)$ were

Table 2: Average values of the efficiencies and corrections for $\phi \to K^0_L K^0_S$

Efficiency	Value, %	Stat. error, %	Syst. error, %
ε_{rec}	90.30	1.51	0.80
ε_{trig}	98.32	0.93	0.80
ε_{geom}	32.16	0.53	0.90
$1+\delta_{loss}$	95.53	0.17	0.10
$1+\delta_{rad}$	77.67	0.26	0.10

taken from [53].

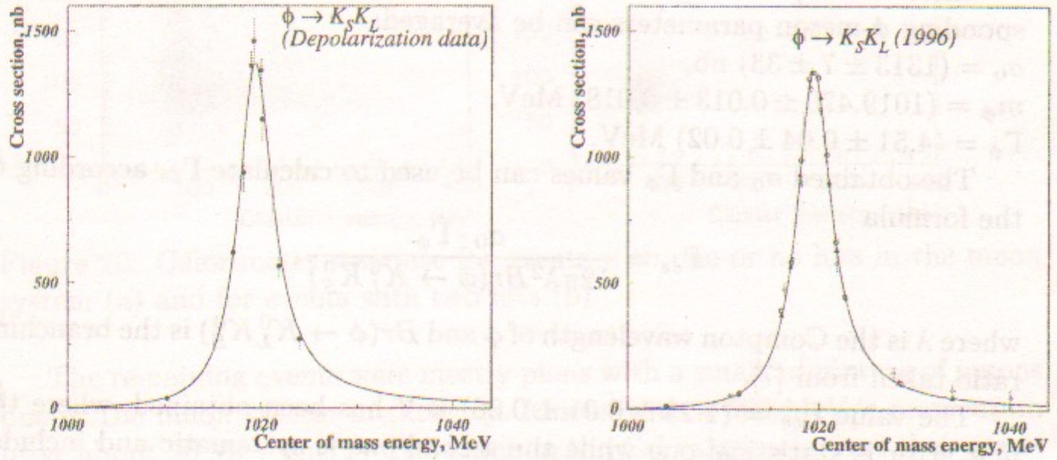

(a) (b)

Figure 19: ϕ-meson excitation curves in the channel $\phi \to K^0_L K^0_S$

The following ϕ-meson parameters have been obtained from the fit:

	PHI-94/1, PHI-94/2	PHI-96
σ_0, nb	$1306 \pm 27 \pm 33$	$1312 \pm 7 \pm 33$
m_ϕ, MeV	$1019.47 \pm 0.06 \pm 0.02$	$1019.471 \pm 0.013 \pm 0.038$
Γ_ϕ, MeV	fixed at the value from [7]	$4.51 \pm 0.04 \pm 0.02$
σ_{back}, nb	fixed at zero	0.02 ± 0.05
$\chi^2_{fit}/d.o.f$	9.09/7	50.36/32

Systematic errors in the mass and width of the ϕ-meson for **PHI-96** data come from the beam energy determination. For the data where the beam energy was determined by the resonant depolarization method the systematic error in the mass value corresponds to the precision of this technique. The main contribution to the systematic error in σ_0 comes from the luminosity uncertainty ($\sim 2\%$) . Other factors contribute about 1.5% :

background subtraction	– 0.3%
reconstruction efficiency	– 0.8%
trigger efficiency	– 0.8%
radiative corrections	– 0.1%
correction for decays in flight and nuclear interaction	– 0.1%
solid angle uncertainty	– 0.9%

Thus, the total systematic error in the σ_0 value was estimated to be 2.5% .

Since the experiments in 1994 and in 1996 are independent, the corresponding ϕ-meson parameters can be averaged:
$\sigma_0 = (1313 \pm 7 \pm 33)$ nb,
$m_\phi = (1019.470 \pm 0.013 \pm 0.018)$ MeV,
$\Gamma_\phi = (4.51 \pm 0.04 \pm 0.02)$ MeV.

The obtained σ_0 and Γ_ϕ values can be used to calculate Γ_{ee} according to the formula

$$\Gamma_{ee} = \frac{\sigma_0 \cdot \Gamma_\phi}{12\pi\lambda^2 Br(\phi \to K_L^0 K_S^0)},$$

where λ is the Compton wavelength of ϕ and $Br(\phi \to K_L^0 K_S^0)$ is the branching ratio taken from [7].

The value $\Gamma_{ee} = (1.23 \pm 0.01 \pm 0.06)$ keV has been obtained, where the first error is statistical one while the second one is systematic and includes the branching ratio uncertainty.

Using Γ_{ee} from [7] with the above formula, the following value has been obtained $Br(\phi \to K_L^0 K_S^0) = 0.317 \pm 0.002 \pm 0.020$.

Values of Γ_{ee} and $Br(\phi \to K_L^0 K_S^0)$ as well as mass and width of ϕ obtained in our experiment are in good agreement with the world average from [7].

12 Study of $\phi \to \pi^+\pi^-$ and $\phi \to \mu^+\mu^-$ decays

The ϕ signal can be seen as an interference pattern in the $e^+e^- \to \pi^+\pi^-$ and $e^+e^- \to \mu^+\mu^-$ cross sections. The event candidates were selected by the requirement of two collinear charged tracks in the DC with the sum of the energy depositions in two CsI clusters associated with them to be less than

450 MeV to remove Bhabha events. The data with the integrated luminosity 1.8 pb^{-1} collected in 1996 were analysed.

Both tracks were required to have a polar angle between 1.05 and 2.1 radians to fit into the muon range system acceptance. The correlation between the energy deposition in the CsI calorimeter and the probability to reach the muon system were used to determine the muon system efficiency which was measured to be $(96.2 \pm 0.3)\%$. The requirement that both particles hit the inner muon system selected muons with about 10% pion admixture.

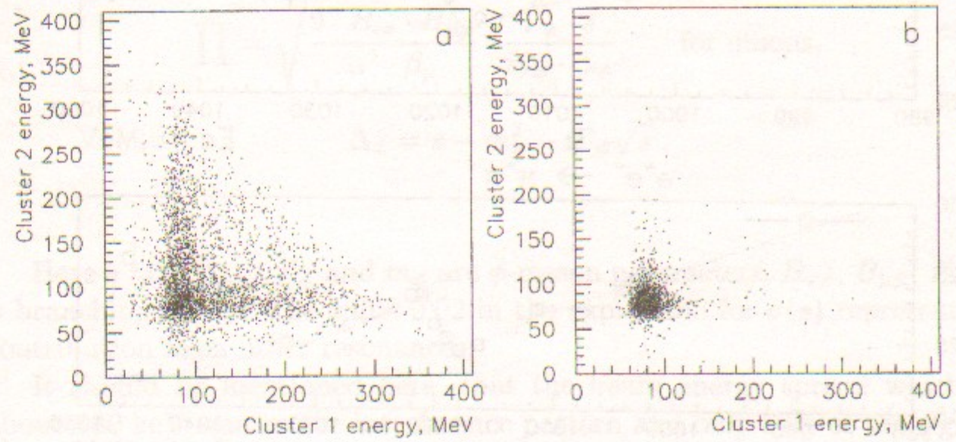

Figure 20: Calorimeter response for events with one or no hits in the muon system (a) and for events with two hits (b)

The remaining events were mostly pions with a small admixture of muons due to the muon system inefficiency. Muons with a 500 MeV/c momentum leave about 90 MeV energy deposition in the CsI calorimeter and their probability to reach the inner muon system is close to 100% while for pions the probability to interact and stop in CsI is about 35%. The calorimeter response for collinear events with and without hits in the muon system is presented in Fig. 20a,b.

The probability for pions to stop in CsI vs polar angle was studied for positive and negative particles and the obtained numbers were used to subtract pions from the muon sample and muons from the pion sample.

The visible cross sections vs energy for pions and muons are presented in Fig. 21. The signal from the ϕ is clearly seen as well as different energy dependence of the pion and muon pair production caused by the pion formfactor.

To get the $\phi \to \pi^+\pi^-$ and $\phi \to \mu^+\mu^-$ branching ratios, the obtained cross sections were fitted by the functions $\sigma_0(s) = const/s$ for muons and

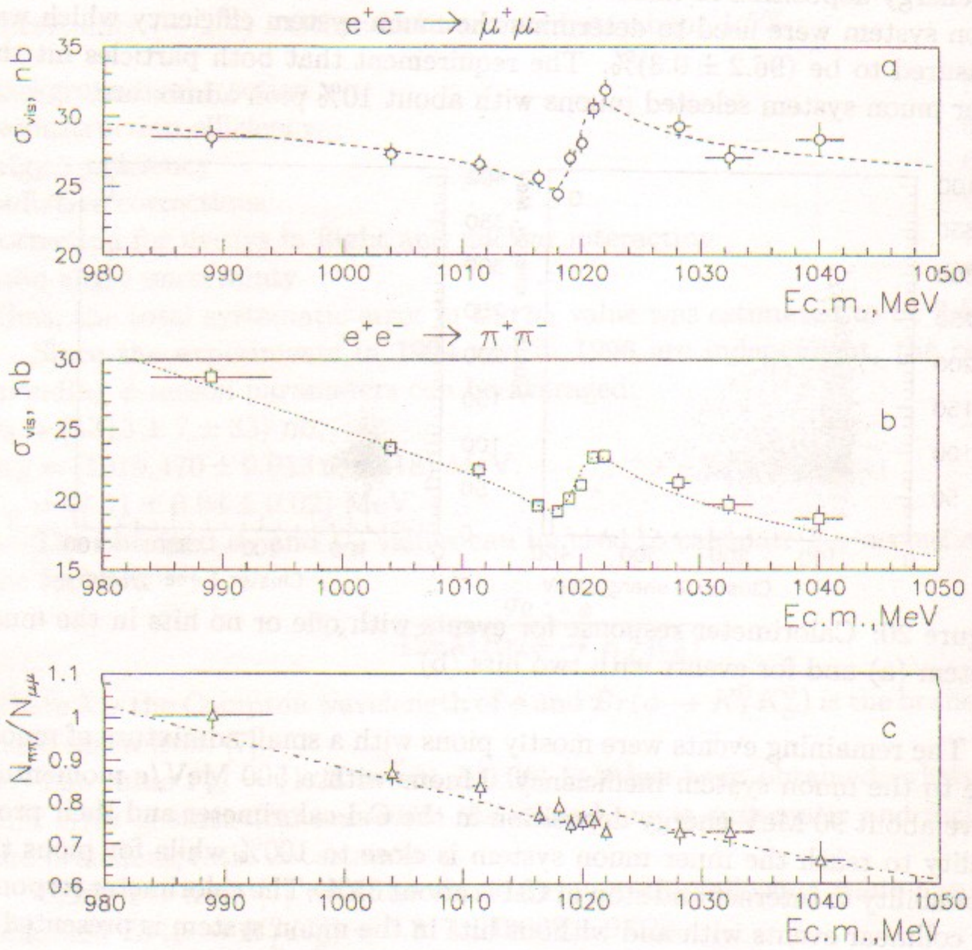

Figure 21: a. Visible cross section for $e^+e^- \to \mu^+\mu^-$ The curve represents the fit with the ϕ signal. b. Visible cross section for $e^+e^- \to \pi^+\pi^-$. The curve represents the fit with the ϕ signal. c. Ratio of number of pions to number of muons vs energy

$\sigma_0(s) = const \cdot |F_\pi(s)|^2/s$ for pions multiplied by the additional term describing vacuum polarization by the ϕ resonance [34]:

$$\sigma(s) = \sigma_0(s)/|1 - \prod -0.02|^2, \qquad \text{where}$$

$$\prod = \sqrt{\frac{36 \cdot B_{ee} \cdot B_{\pi\pi}}{\alpha^2 \cdot \beta_\pi^3 |F_\pi|^2}} \cdot \frac{\Gamma_\phi \cdot s}{m_\phi \cdot \Delta_\phi} \qquad \text{for pions,}$$

$$\prod = \sqrt{\frac{9 \cdot B_{ee} \cdot B_{\mu\mu}}{\alpha^2 \cdot \beta_\mu}} \cdot \frac{\Gamma_\phi \cdot s}{m_\phi \cdot \Delta_\phi} \qquad \text{for muons,}$$

$$\Delta_\phi = s - m_\phi^2 - i\Gamma_\phi\sqrt{s}\,.$$

Here $s = 4E^2_{beam}$, Γ_ϕ and m_ϕ are ϕ-meson parameters, $B_{\pi\pi}$, $B_{\mu\mu}$, B_{ee} are ϕ branching ratios. The value 0.02 in the expression for $\sigma(s)$ represents the contribution from other resonances.

It should be mentioned here, that the beam energy spread which was about 180 keV smears the interference pattern and only 87% of the signal is seen. The obtained visible cross section $\sigma_0(m_\phi)$ for muons is in agreement with the expectation within 4%.

The following results corrected for the beam energy spread have been obtained:

$\sqrt{Br(\phi \to \mu^+\mu^-) \cdot Br(\phi \to e^+e^-)} = (2.89 \pm 0.15 \pm 0.24) \times 10^{-4}$,
$\sqrt{Br(\phi \to \pi^+\pi^-) \cdot Br(\phi \to e^+e^-)} = (2.33 \pm 0.16 \pm 0.10) \times 10^{-4}$,
$Br(\phi \to \mu^+\mu^-) = (2.80 \pm 0.30 \pm 0.46) \times 10^{-4}$,
$Br(\phi \to \pi^+\pi^-) = (1.81 \pm 0.25 \pm 0.19) \times 10^{-4}$.

For the last two branchings above the value of $Br(\phi \to e^+e^-) = (2.99 \pm 0.08) \times 10^{-4}$ was taken from the PDG tables[7]. Systematic errors (given by second error) as we expect, come from the uncertainties in the determination of the beam energy, from the luminosity measurement and from the muon-pion separation at each point. About 2% uncertainty was added to the cross section value representing these factors.

To extract the amplitude of the direct ϕ decay into two pions, the ratio of the number of pions to that of muons was calculated. In this ratio the influence of the ϕ upon the photon propagator cancels and the interference signal of the direct amplitude can be seen. The systematic uncertainties in

this ratio partly cancel, but to be conservative, the same 2% uncertainty was added to the ratio at each energy point.

This ratio is shown in Fig. 21c. No signal is seen and an upper limit has been placed:
$Br(\phi \to \pi^+\pi^-)_{direct} < 0.15 \times 10^{-4}$ at 90% C.L.

13 $\phi \to \pi^+\pi^-\gamma$ channel

The event candidates were selected by a requirement of two charged tracks in DC and one or two photons with the energy greater than 20 MeV in the CsI calorimeter. The data with the integrated luminosity 2.1 pb^{-1} collected in 1993 and 1996 were used for this analysis. Charged particles were required to have the polar angle between 1.05 and 2.1 radians and from 0.85 to 2.25 for photons to suppress bremsstrahlung processes which gave the main contribution to the observed events.

The main background for the studied process came from the $\phi \to \pi^+\pi^-\pi^0$ decay mode when one of the photons from the π^0 decay escaped detection. To reduce this background a constrained fit with the requirement of energy and momentum conservation was used. As a result, after χ^2 cut the 3π background became negligible for the gamma energy range 20 MeV$< E_\gamma <$160 MeV, where the maximum signal from f_0 was expected. For higher photon energies the background spectra at higher χ^2 were used for subtraction. The muon range system was used to separate $\mu^+\mu^-\gamma$ contamination as described in the previous section.

Under these conditions 7309 events of $\pi^+\pi^-\gamma$ and 7590 of $\mu^+\mu^-\gamma$ events were selected. The detection efficiency was found by simulation to be 17%. The experimental cross sections vs center-of-mass energies for events with photons in the 20-120 MeV energy range are presented in Figs. 22a,b.

The observed events are dominated by bremsstrahlung processes and the signal from $\phi \to \pi^+\pi^-\gamma$ decay was searched for as an interference pattern in the energy dependence cross section for the process $e^+e^- \to \pi^+\pi^-\gamma$ (Fig. 22) as well as in the photon spectra of the selected events (Fig. 23) at the ϕ peak.

As it was calculated in [55], in about 2/3 of observed events with above selections the detected photon was emitted by initial electrons (1/2 for muons) and do not contribute to the interference pattern.

A simple "model independent" function with a sum of the power function $\sigma_{br}(s) = const/s^5$ representing $e^+e^- \to \pi^+\pi^-\gamma$ process and Breit-Wigner amplitude from ϕ:

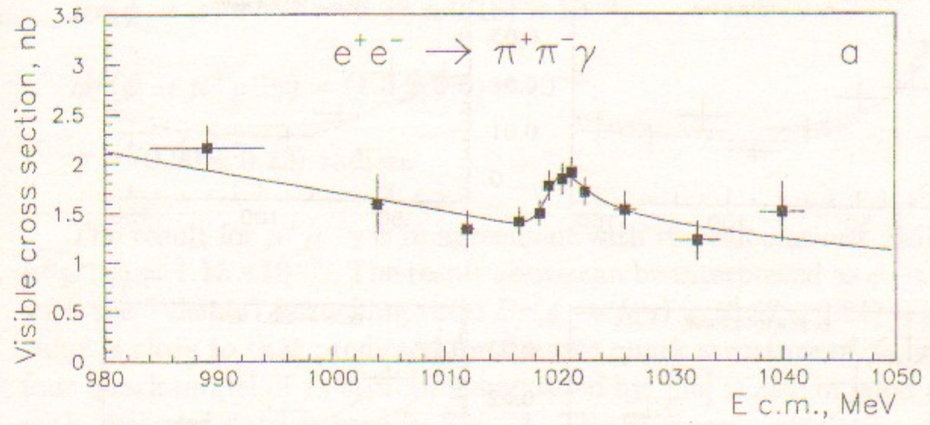

Figure 22: a. Visible cross section for $e^+e^- \to \pi^+\pi^-\gamma$ with $20 < E_\gamma < 120$ MeV. The curve is a fit with $Br(\phi \to \pi^+\pi^-\gamma) = 0.38 \times 10^{-4}$ and a relative phase of 0.6 radian. b. Visible cross section for $e^+e^- \to \mu^+\mu^-\gamma$

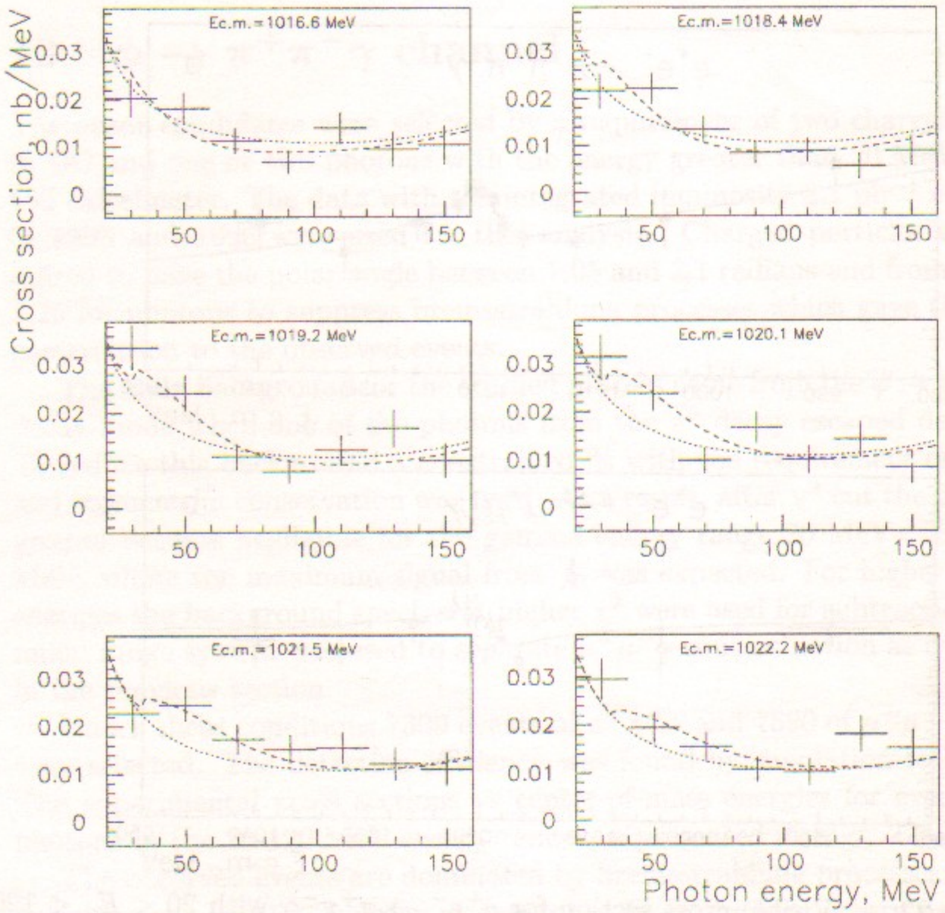

Figure 23: The photon spectra for $\pi^+\pi^-\gamma$ events in the "ϕ" region (a) and out of the "ϕ" region (b) normalized to the integrated luminosity. Lines are the theoretical prediction for the four quark model with 3.0×10^{-4} branching ratio(dashed) and pure bremsstrahlung spectra(dotted)

$\sigma(s) = \frac{2}{3} \cdot \sigma_{br}(s) + \frac{1}{3} \cdot \sigma_{br}(s) \cdot |1 + e^{i\psi} \cdot \sqrt{\frac{3\sigma(\phi \to \pi\pi\gamma)}{\sigma_{br}(s)}} \cdot \frac{m_\phi \Gamma_{tot}}{\Delta_\phi}|^2$
was used for cross section fitting. The observed cross section both for pions and muons is in good agreement with the calculations [55]: $\sigma^{exp}(s)/\sigma^{th}(s) = 1.04 \pm 0.03 \pm 0.05$. The branching ratio was calculated as $Br(\phi \to \pi\pi\gamma) = \sigma(\phi \to \pi\pi\gamma)/\sigma_\phi^{max}$ and gave:

$$Br(\phi \to \pi^+\pi^-\gamma) = (0.38 \pm 0.16) \times 10^{-4},$$

$$Br(\phi \to \mu^+\mu^-\gamma) = (1.3 \pm 0.6) \times 10^{-5},$$

$$\psi = (0.50 \pm 0.23) \text{ radian.}$$

The result for $\mu^+\mu^-\gamma$ is in agreement with the calculations [55]: $Br(\phi \to \mu^+\mu^-\gamma) = 1.15 \times 10^{-5}$. The result above can be interpreted as $\phi \to f_0\gamma$ decay with the "visible" branching ratio $Br(\phi \to f_0\gamma) = (0.57 \pm 0.24) \times 10^{-5}$. This value is close to that predicted for the two quark structure of f_0 in [55]. The four quark model of f_0 structure suggested by [55] is also in good agreement with observed data as seen in Fig. 23. The fit gives:
$Br(\phi \to f_0\gamma) = (2.0 \pm 0.9) \times 10^{-4}$
with the relative phase to bremsstrahlung background (0.7 ± 0.3) radian. The simple explanation of huge "visible" difference in the branching ratio for two models comes from the fact that the relative phase corresponds to strong destructive interference and reduces a visible signal from the ϕ decay in case of the four quark model as was demonstrated in [11]. The above is valid not only for the four quark model but in case if f_0 has a long tail in the mass (recoil photon) spectrum.

The $\pi^+\pi^-\gamma$ events with photons in the 100-300 MeV range after 3π background subtraction were used to search for the C violating process $\phi \to \rho\gamma$. The cross section is shown in Fig. 24.

A new upper limit was obtained: $Br(\phi \to \rho\gamma) < 3 \times 10^{-4}$ at 90% CL.

The $\pi^+\pi^-\gamma$ events with photons in the narrow range $\pm$ 5 MeV around 362 MeV according to the photon resolution after the constrained fit were used to search for CP, P violating decay of η into two charged pions and the new limit is:
$Br(\eta \to \pi^+\pi^-) < 3 \times 10^{-4}$ at 90% CL.

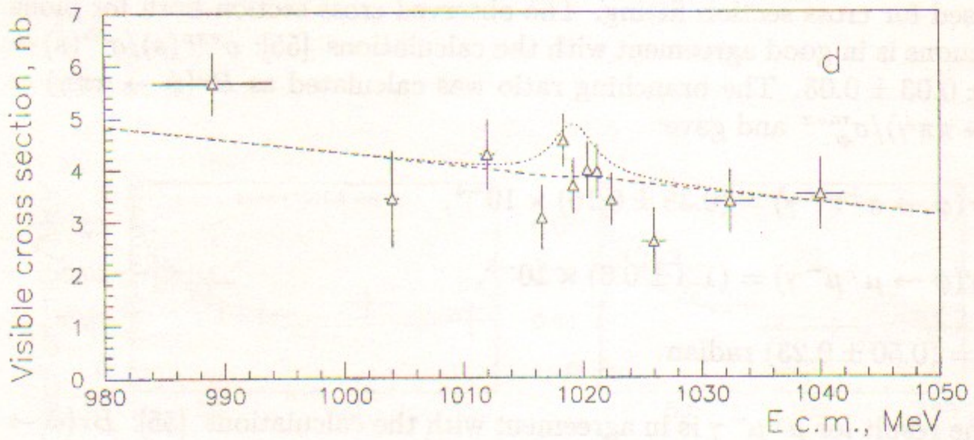

Figure 24: Visible cross section for events with photons in the 100–300 MeV energy range. The signal from the ϕ at the level $3 \cdot 10^{-4}$ is shown

14 Study of $\phi \to \eta\gamma \to \pi^0\pi^0\pi^0\gamma$

This pure neutral channel with 7 photons in final state has relatively small background. The analysis was performed for **PHI-96** and **PHI-98** data. At the first stage all neutral events (no tracks in DC) were selected with the number of photons from 3 to 10, total energy deposition $E_{tot} > 1.5 \cdot E_{beam}$ and at least 3 photons detected in the CsI calorimeter. The obtained events were used for the background study. The noisy spots in the calorimeter were masked and were not used for the next analysis. In addition the minimum polar angle for photon detection was increased from 0.3 to 0.57 radians and detection threshold increased from 20 to 25 MeV. Two last conditions have decreased beam background by a factor of two. Masking and solid angle reduction still left 90% of the geometric efficiency.

The constrained fit with the requirement of energy and momentum conservation was applied to events with the number of photons from 3 to 10 left after "masking". The χ^2 cut gives additional background reduction mostly influencing $K^0_S K^0_L$ events decaying into neutrals.

At the next stage events with seven photons only were selected for the constrained energy-momentum conservation fit with the following additional conditions: all possible pair combinations were formed in search for two π^0's with five softest photons. The combinations with the best χ^2 was chosen.

As a result, three photons not combined into π^0's are left. The invariant

mass of 2 softest of these 3 photons gives π^0 mass except for some fraction of combinatorial errors and if the photon with the smallest energy is a background photon. The events with these background photons were effectively removed by increasing the minimum photon energy in the BGO calorimeter for the third π^0 from 25 to 40 MeV.

The reconstructed energy for the most energetic photon normalized to the beam energy is shown in Fig. 25a. The peak at 0.71 corresponds to 362 MeV photon from the $\phi \to \eta\gamma$ decay. The 10% background under the peak comes mostly from remaining $K^0_S K^0_L$ events. As demonstrated at the scatter plot E_{tot} vs $E_{\gamma max}/E_{beam}$ shown in Fig. 25b the difference in the total energy deposition helps to subtract these events.

About 30% of found signal events initially had more than 7 photons. And it is possible, that after "masking" procedure some events still have more than 7 photons. In this case not to lose signal events, 7 most energetic photons from 8,9,10 photon events with $E_{tot} > 1.5 \cdot E_{beam}$ were selected for the above constrained fit procedure. The distribution of $E_{\gamma max}/E_{beam}$ for this type of events is shown in Fig. 25c. The peak at 0.71 with additional 10% of signal events is seen while simulation gives only 2.7% caused by split photons. The difference was added to the signal event sample.

Comparison of the χ^2 distributions for data and simulated events is shown in Fig. 25d.

The detection efficiency was obtained by simulation and was found to be $(10.8 \pm 0.1)\%$. After background subtraction and correction for "lost" events 8826±101 signal events were selected. The excitation curve for $\phi \to \eta\gamma \to 3\pi^0\gamma$ is shown in Fig. 26a. The following branching ratio has been obtained:

$$Br(\phi \to \eta\gamma) = (1.24 \pm 0.02 \pm 0.06)\%.$$

The second error represents a systematic uncertainty which includes: 0.04 from the electron width taken from PDG [7]; 0.025 from the luminosity determination; 0.03 from the uncertainty in the background subtraction; 0.02 was added as simulated efficiency uncertainty and 0.01 from the uncertainty in the branching ratio of $\eta \to 3\pi^0$ [7].

15 $\phi \to \pi^0\pi^0\gamma$ channel

The decay $\phi \to f_0\gamma$ with $f_0 \to \pi^0\pi^0$ has no bremsstrahlung background and can help to determine the f_0 structure. The observation of this decay was earlier reported by SND [22].

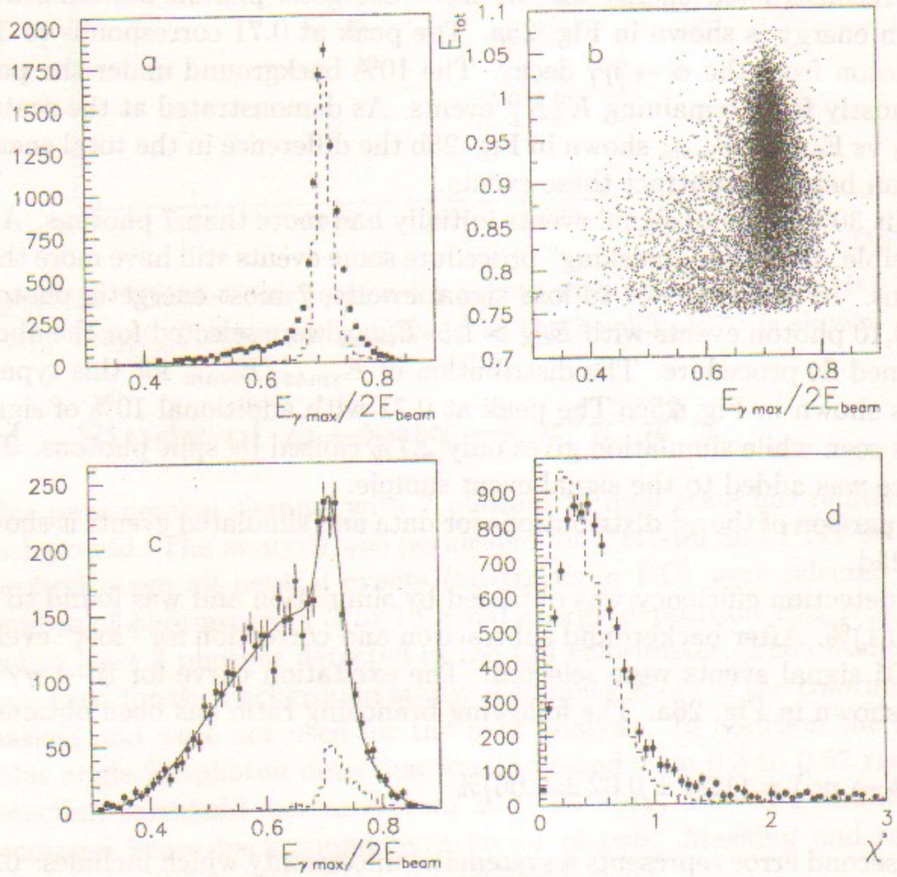

Figure 25: The $e^+e^- \to \pi^0\pi^0\pi^0\gamma$ study. a. Normalized energy of the most energetic photons for data and simulation; b. E_{tot} vs $E_{\gamma max}/E_{beam}$ distribution; c. $E_{\gamma max}/E_{beam}$ for events with $N_\gamma > 7$; d. χ^2 distribution for data (points) and simulation

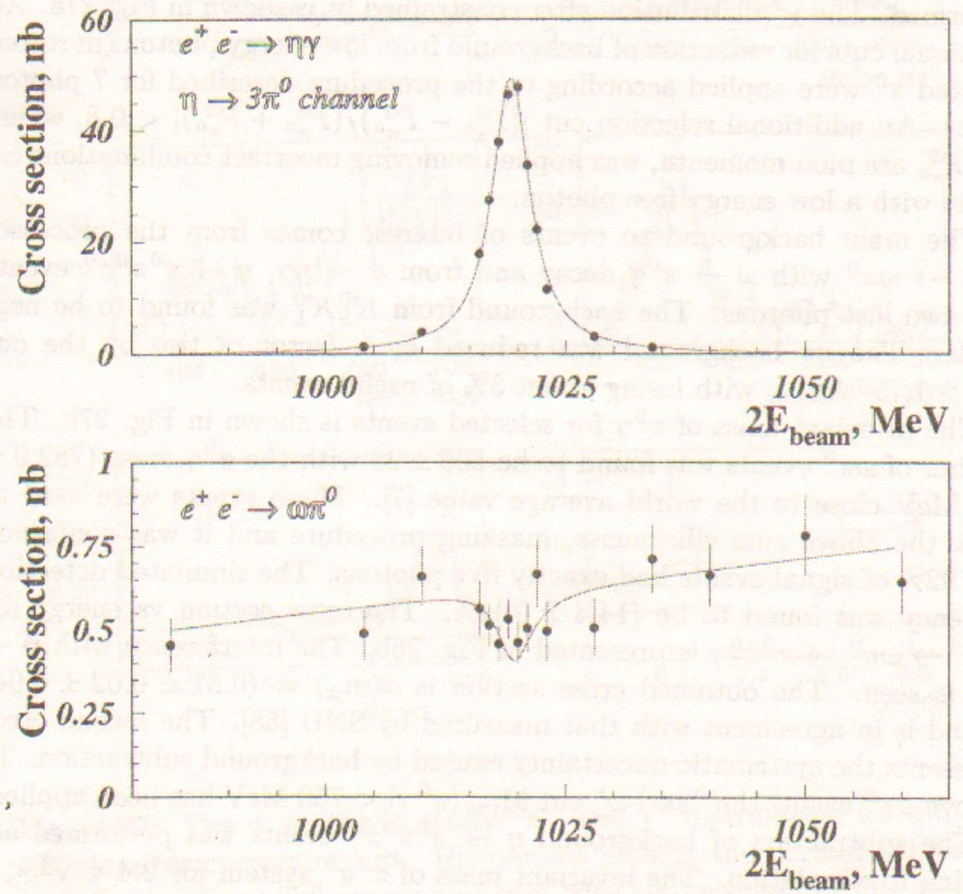

Figure 26: a. Excitation curve for $\phi \to \eta\gamma$ in $\eta \to 3\pi^0$ channel; b. Cross section for $e^+e^- \to \omega\pi^0 \to \pi^0\pi^0\gamma$

Events with 5 photons detected both in the CsI and BGO calorimeter with no charged particles were selected. The masking procedure was performed as described above for 7 photon events.

The constrained fit with the requirement of momentum and energy conservation removes the main background from $K_S^0 \to \pi^0\pi^0$ decays when K_L^0 produces the fifth cluster in the calorimeter. To select $\pi^0\pi^0\gamma$ events the constrained fit finding two best combinations of photon pairs with π^0 masses was performed. The χ^2 distribution after constrained fit is shown in Fig. 27a. All additional cuts for reduction of background from low energy photons in reconstructed π^0 were applied according to the procedure described for 7 photon events. An additional selection cut $|(P^1_{\pi^0} - P^2_{\pi^0})/(P^1_{\pi^0} + P^2_{\pi^0})| < 0.8$, where $P^1_{\pi^0}, P^2_{\pi^0}$ are pion momenta, was applied removing incorrect combinations for events with a low energy free photon.

The main background to events of interest comes from the processes $e^+e^- \to \omega\pi^0$ with $\omega \to \pi^0\gamma$ decay and from $\phi \to \eta\gamma$, $\eta \to \pi^0\pi^0\pi^0$ events with two lost photons. The background from $K_S^0K_L^0$ was found to be negligible. The $\eta\gamma$ background was reduced by a factor of two by the cut $E_{tot} > 1.75 \cdot E_{beam}$ with losing about 3% of useful events.

The invariant mass of $\pi^0\gamma$ for selected events is shown in Fig. 27b. The number of $\omega\pi^0$ events was found to be 506 ± 28 with the $\pi^0\gamma$ mass (782.0 ± 0.9) MeV close to the world average value [7]. These events were used to check the above cuts efficiencies, masking procedure and it was confirmed that 92% of signal events had exactly five photons. The simulated detection efficiency was found to be $(14.4 \pm 0.1)\%$. The cross section vs energy for $e^+e^- \to \omega\pi^0 \to \pi^0\pi^0\gamma$ is presented in Fig. 26b. The interference with $\phi \to \omega\pi^0$ is seen. The obtained cross section is $\sigma(m_\phi) = (0.61 \pm 0.02 \pm 0.04)$ nb and is in agreement with that measured by SND [58]. The second error represents the systematic uncertainty caused by background subtraction. To remove $\omega\pi^0$ events the "anti-ω" cut $M_{inv}(\pi^0\gamma) < 750$ MeV has been applied.

The subtraction of background $\eta \to \pi^0\pi^0\pi^0$ events was performed according to simulation. The invariant mass of $\pi^0\pi^0$ system for $2.4 < \chi^2 < 6$ is shown in Fig. 27d and demonstrates good agreement of observed spectra with simulation. The normalization of observed background events gives $N_\phi = (20.6 \pm 1.0)$ millions in agreement with the (18.8 ± 0.9) millions of ϕ's obtained from the analysis of 7 photon events.

The invariant mass distribution of the $\pi^0\pi^0$ system for $\chi^2 < 2.4$ is shown in Fig. 27c with the expected background from $\omega\pi^0$ after "anti-ω" cut and from $3\pi^0$ events. The distribution demonstrates the increasing of the number of events with high invariant masses (lower photon energy) and after background subtraction $(268 \pm 27)\pi^0\pi^0\gamma$ events have been found. Taking into

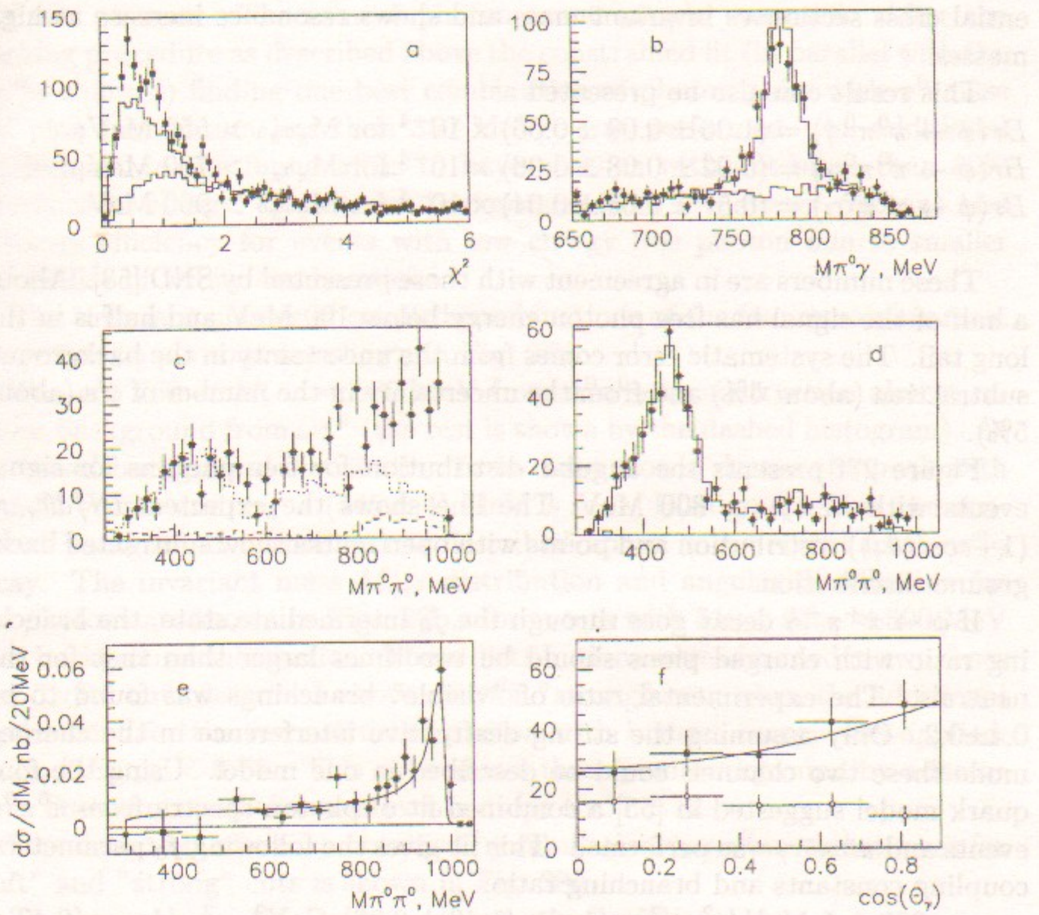

Figure 27: The $\phi \to \pi^0\pi^0\gamma$ study: a. The χ^2 distribution for a 5 photon sample after constrained fit. Histograms present the normalized simulated contribution from $3\pi^0$ events and sum with $\omega\pi^0$ events; b. The $\pi^0\gamma$ invariant mass for events with $\chi^2 < 2.4$; c. The $\pi^0\pi^0$ invariant mass for events with $\chi^2 < 2.4$; d. The $\pi^0\pi^0$ invariant mass for events with $2.4 < \chi^2 < 6$; e. Differential cross section vs invariant mass. The line is the theoretical prediction for f_0 production in case of four quark model for the 3.0×10^{-4} branching ratio; f. Angular distribution for signal events and background. Line is $dN/d\theta_\gamma \approx (1 + cos^2(\theta_\gamma))$

account a 16% detection efficiency the branching ratio
$Br(\phi \to \pi^0\pi^0\gamma) = (1.08 \pm 0.17 \pm 0.09) \times 10^{-4}$
has been obtained for the total mass range. Figure 27e presents the differential cross section vs invariant mass and shows resonance increase at high masses.

This result can also be presented as:
$Br(\phi \to \pi^0\pi^0\gamma) = (1.06 \pm 0.09 \pm 0.06) \times 10^{-4}$ for $M_{\pi^0\pi^0} > 550$ MeV;
$Br(\phi \to \pi^0\pi^0\gamma) = (0.92 \pm 0.08 \pm 0.06) \times 10^{-4}$ for $M_{\pi^0\pi^0} > 700$ MeV;
$Br(\phi \to \pi^0\pi^0\gamma) = (0.57 \pm 0.06 \pm 0.04) \times 10^{-4}$ for $M_{\pi^0\pi^0} > 900$ MeV.

These numbers are in agreement with those presented by SND [58]. About a half of the signal has free photon energy below 100 MeV and half is in the long tail. The systematic error comes from the uncertainty in the background subtraction (about 5%) and from the uncertainty in the number of ϕ's (about 5%).

Figure 27f presents the angular distribution for free photons for signal events with $M_{\pi^0\pi^0} > 800$ MeV. The line shows the expected $dN/d\theta_\gamma \approx (1+cos^2(\theta_\gamma))$ distribution and points with open marks show subtracted background distribution.

If $\phi \to \pi^+\pi^-\gamma$ decay goes through the f_0 intermediate state, the branching ratio with charged pions should be two times larger than that for the neutrals. The experimental ratio of "visible" branchings was found to be 0.4±0.2. Only assuming the strong destructive interference in the charged mode these two channels could be described in one model. Using the four quark model suggested in [55] a combined fit of photon spectra from $\pi^0\pi^0\gamma$ events and $\pi^+\pi^-\gamma$ was performed. This fit gives the following f_0 parameters, coupling constants and branching ratio:
$m_{f_0} = 969 \pm 5$ MeV/c^2, $g^2_{KK}/4\pi = (1.49 \pm 0.36)$ GeV^2, $g^2_{\pi\pi}/4\pi = (0.40 \pm 0.06)$ GeV^2,
$Br(\phi \to f_0\gamma) = (3.24 \pm 0.54) \cdot 10^{-4}$ and relative phase (1.10 ± 0.26) radians.

The obtained results and interpretations are in good agreement with those previously published by SND [22, 58].

The selected events can be used to search for the CP, P violating decay $\eta \to \pi^0\pi^0$. This decay should be seen as a peak at 548 MeV with about ±40 MeV resolution in the distribution presented in Fig. 27e. In this energy range the possible signal does not exceed 0.02 nb and the following upper limit has been obtained:
$Br(\eta \to \pi^0\pi^0) < 5 \times 10^{-4}$ at 90% CL.

16 Search for $\phi \to \eta\pi^0\gamma$

This channel can also be searched for in the 5 photon mode with η decays into two photons. The same 5 photon event sample was used. After the masking procedure as described above the constrained fit (in parallel with the $\pi^0\pi^0\gamma$ channel) finding one best combination of photon pairs with π^0 mass and pion momentum less than 350 MeV/c was performed. An additional requirement to the found π^0 is to have photons with not more than 80% difference in energy. It removes background from low energy photons and increases efficiency for events with low energy free photon due to smaller probability of wrong combinations.

The invariant masses of coupled combinations of the two remaining most energetic two photons are shown in Fig. 28a.

The cut $760 < M_{\pi^0\gamma} < 805$ MeV from $\pi^0\pi^0\gamma$ reconstruction almost removes background from $\omega\pi^0$ (the rest is shown by the dashed histogram). At the broad background distribution from three pion η decays the peak with 80 ± 22 events and $m_\eta = (545 \pm 4)$ MeV is seen. Histograms show the simulated background normalized as described above and a signal from $\eta\pi^0\gamma$ decay. The invariant mass $M_{\eta\pi^0}$ distribution and angular distribution for free photons are shown in Figs. 28b,c for events with $510 < M_{\gamma\gamma} < 590$ MeV after background subtraction. These distributions were obtained in two cases - for "soft" cuts described above and for "strong" cuts when the additional requirement for the reconstructed photon with highest energy was applied: $E_{\gamma max}/2E_{beam} < 0.75$. This cut reduces three pion background by a factor of 4. The number of observed events drops to 37 ± 12.

The detection efficiency obtained by simulation vs $\eta\pi^0$ invariant mass for "soft" and "strong" cuts is shown in Fig. 28d.

The branching ratio corresponding to the "soft" cut
$Br(\phi \to \eta\pi^0\gamma) = (0.90 \pm 0.24 \pm 0.10) \times 10^{-4}$
has been obtained. For the "strong" cut this value was 7% higher or within statistical errors.

The systematic error corresponds to uncertainty in the background subtraction and in the number of ϕ's taken for normalization. The invariant mass distribution shows the increase of the number of events to higher masses supporting the hypothesis about the $a_0(980)$ intermediate state.

The result for the $\eta\pi^0\gamma$ mode is in good agreement with that published recently by SND [23, 58].

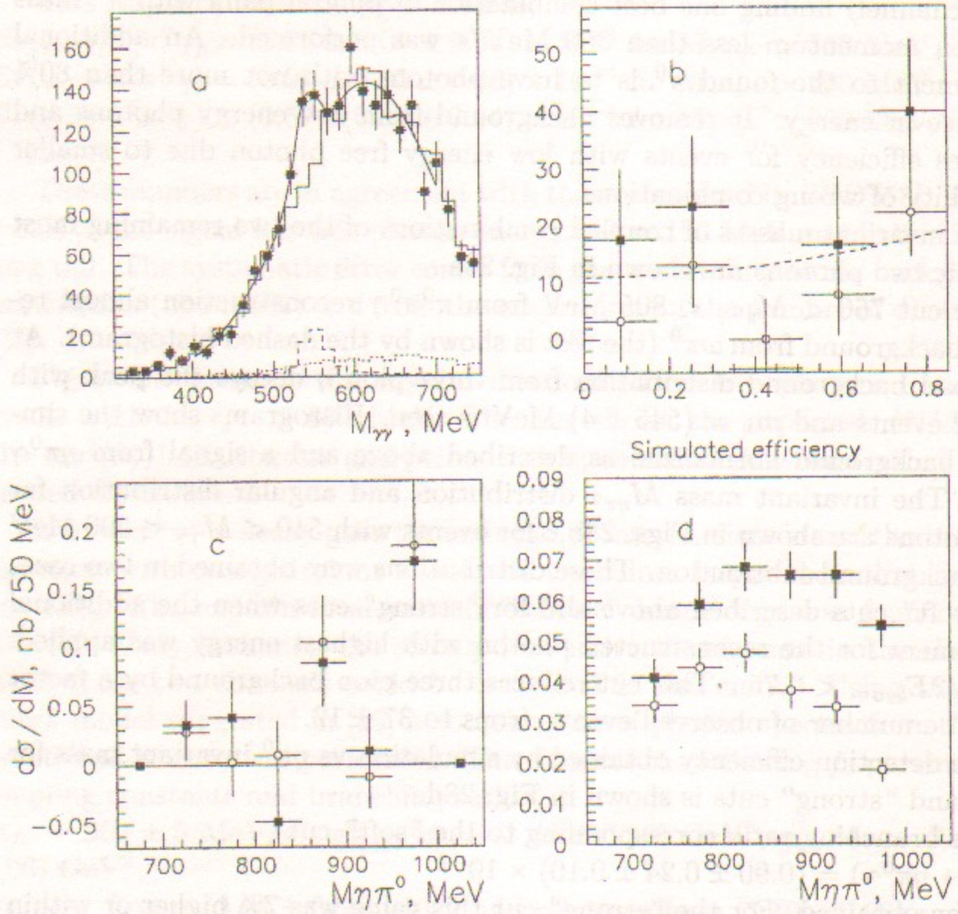

Figure 28: The $\phi \to \eta\pi^0\gamma$ study: a. Invariant masses of two photons with highest energy for data (points) and simulation (histograms); b. Angular distribution for events around η mass after background subtraction for "soft" (dark points) and "strong" cuts; c. The cross section vs $\eta\pi^0$ mass distribution for "soft" and "strong" cuts; d. The simulated detection efficiency vs invariant mass for "soft" and "strong" cuts.

17 Study of $\phi \to \eta\gamma \to \pi^+\pi^-\pi^0\gamma$

The radiative magnetic dipole transition of ϕ into η has been previously studied in many experiments [7, 15] using the neutral final states coming from η decays into $\gamma\gamma$ or $3\pi^0$. In this work we report on the measurement of the $\phi \to \eta\gamma$ decay rate into the mixed charged-neutral final state: $e^+e^- \to \phi \to \eta\gamma \to \pi^+\pi^-\pi^0\gamma$ based on a data sample with the integrated luminosity of about 1.9 pb^{-1} (**PHI-96**).

In this analysis detection of all final particles is not necessary. Instead, one requires the detection of both charged pions and at least one, the recoil photon. As the recoil photon, one selects the photon whose direction is closest to that opposite to the direction of the charged particles $\vec{p}_{\pi^+\pi^-}$. Using the measured momenta of the pions as well as the measured angles φ and θ of the recoil photon and assuming that the energy of the recoil photon is given by $\omega_r = \frac{(2E_{beam})^2 - m_\eta^2}{4E_{beam}}$, one can reconstruct the invariant mass of all other photons in the system, M_{inv}:

$$M_{inv}^2 = (2E_{beam})^2 + \varepsilon_{\pi^+\pi^-}^2 - p_{\pi^+\pi^-}^2 - 4E_{beam}(\varepsilon_{\pi^+\pi^-} + \omega_r) + 2\varepsilon_{\pi^+\pi^-} \cdot \omega_r - 2\vec{p}_{\pi^+\pi^-} \cdot \vec{\omega}_r,$$

where $\varepsilon_{\pi^+\pi^-}$ is the total energy of π^+ and π^-, $\vec{p}_{\pi^+\pi^-}$ is the total momentum of charged pions, $\vec{\omega}_r$ is the momentum of the recoil photon. For the process $e^+e^- \to \phi \to \eta\gamma \to \pi^+\pi^-\gamma$ this parameter $M_{inv} = m_{\pi^0} = 135$ MeV.

Events with 2 tracks and more than one photon were selected using the following criteria:

- One vertex is found in the event
- Two tracks with the opposite charges are reconstructed from this vertex and there are no other tracks
- The angles of both tracks with respect to the beam are limited by $40° < \theta < 140°$ to match the optimal DC coverage
- The number of photons detected in the CsI and BGO calorimeters is more than one and less than six. The cluster in the calorimeter was accepted as a photon when it did not match any charged track and its energy was more than 30 MeV in the CsI calorimeter and more than 40 MeV in the BGO calorimeter
- The distance from each track to the beam $r_{min} < 0.2$ cm

- The distance from the vertex to the interaction point along the beam direction $|z_{vert}| < 10$ cm
- The space angle between the tracks $\Delta\psi < 143°$
- The angle between the track in the r-φ plane $\Delta\varphi < 172°$
- The total energy of the charged particles (assuming that both particles are charged pions) $\varepsilon_{\pi^+\pi^-} < 520$ MeV
- The energy deposition of the photon accepted as a recoil one is more than 250 MeV

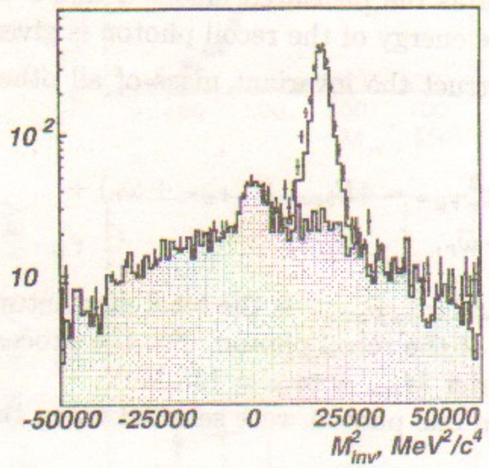

Figure 29: M^2_{inv} distribution. Points with errors present the data. The hatched histogram is the sum of such distributions for simulation of background processes, solid line histogram is the simulation of $\eta\gamma \to \pi^+\pi^-\pi^0\gamma$ together with background simulation

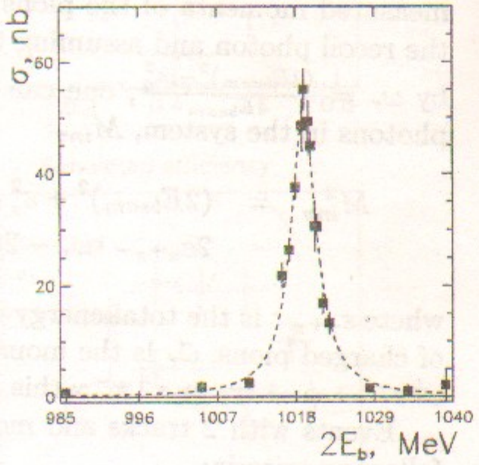

Figure 30: The cross-section $\sigma(e^+e^- \to \phi \to \eta\gamma)$ with fit function

The distribution over the parameter M^2_{inv} for the selected events is presented in Fig. 29. The events from the decay of $\phi \to \eta\gamma$ form the peak near the π^0 mass squared. The background fraction is very small after selection.

The figure is presented in logarithmic scale for better background demonstration. The source of the peak near zero is the events of $\phi \to \eta\gamma$ when η decays to $\pi^+\pi^-\gamma$. The distribution for the simulation of $e^+e^- \to \phi \to \eta\gamma \to \pi^+\pi^-\pi^0\gamma$ is also presented in the figure together with the simulation of the background processes: $\phi \to \pi^+\pi^-\pi^0$, $e^+e^- \to \omega\pi^0$, $\phi \to K^0_S K^0_L$ and $\phi \to \eta\gamma$, $\eta \to \pi^+\pi^-\gamma$. The fraction of each background process in the total number of simulated events was taken in correspondence with its cross section.

Dividing the data in the groups corresponding to different beam energies and fitting the distributions over M^2_{inv} by the sum of the functions describing the effect and background, one can obtain the number of $\phi \to \eta\gamma \to \pi^+\pi^-\pi^0\gamma$ events. After taking into account the radiative corrections the cross-section value for each energy point was obtained. The results for different energy points are presented in Fig. 30.

The efficiency was determined from simulation and the value $\varepsilon = 0.247 \pm 0.004 \pm 0.007$ was obtained. The systematic uncertainty in the efficiency was estimated comparing results of simulation of nuclear interactions by different methods (FLUKA and GHEISHA) [59].

Fitting the energy dependence of the cross-section of $\phi \to \eta\gamma$ (Fig. 30) with the fixed value of the ϕ meson width $\Gamma = 4.43$ MeV and phase of $\omega - \phi$ mixing $\delta_\phi = 180°$ the following results were obtained:

$$\begin{array}{lcrcll} \sigma_{peak} & = & (49.8 & \pm & 1.2) & \text{nb} \\ m_\phi & = & (1019.38 & \pm & 0.07) & \text{MeV} \\ \chi^2/d.f. & = & 18.4 & / & 16 & \end{array}$$

If the value $\Gamma_{ee}/\Gamma_{total} = (2.99 \pm 0.08) \cdot 10^{-4}$ is taken from [7], the branching ratio corresponding the obtained peak cross section is

$$Br(\phi \to \eta\gamma) = (1.18 \pm 0.03 \pm 0.06)\%,$$

where the first error is statistical and the second one is systematic. The systematic error was estimated by taking into account the following contributions:

- luminosity determination (2%)
- the value $\Gamma_{ee}/\Gamma_{total}$ (3%)
- $Br(\eta \to \pi^+\pi^-\pi^0)$ (2.2%)
- detection efficiency (1%)

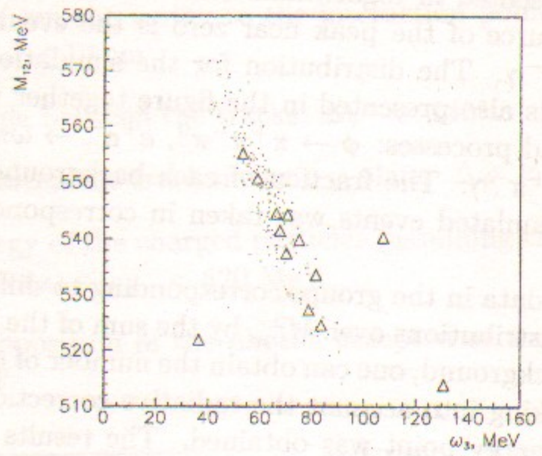

Figure 31: Invariant mass M_{12} vs ω_3. Points present $\phi \to \eta'\gamma$, $\eta' \to \pi^+\pi^-\eta$, $\eta \to \gamma\gamma$ simulation, triangles are events from data

- uncertainty in the signal shape (4%).

The result obtained in the present work is consistent with the world average value $(1.26 \pm 0.06)\%$ [7]. It is the first measurement of this decay rate using the charged mode of η decay.

18 Observation of $\phi \to \eta'\gamma$ decay

The first observation of this rare radiative decay has been reported by the CMD-2 detector in 1997 [10] on the base of data collected during the period of 1992 – 1996. The search has been performed using the mode in which η' decays into $\pi^+\pi^-\eta$ and $\eta \to \gamma\gamma$. Here we present the improved measurement based on the same data sample but with better efficiency due to additional information from the endcap BGO calorimeter.

There are two charged pions and three photons in the final state. The photons are ordered by decreasing energy, from the hardest (ω_1) to the softest (ω_3). The last one is a monochromatic recoil photon, so that its energy $\omega_3 = 60$ MeV. The invariant mass of two hard photons $M_{12} = m_\eta$.

The other process with the similar kinematics is the decay of ϕ to $\eta\gamma$, in which η decays into $\pi^+\pi^-\pi^0$. Here the hardest photon is monochromatic

with $\omega_1 = 362$ MeV and the invariant mass of two others is $M_{23} = m_{\pi^0}$.

The decay $\phi \to \eta\gamma$ is two orders of magnitude more probable and is one of the main sources of background for a $\phi \to \eta'\gamma$ search. At the same time, the decay $\phi \to \eta\gamma$ was used as a monitoring process and the branching ratio of $Br(\phi \to \eta'\gamma)$ was calculated relative to $Br(\phi \to \eta\gamma)$.

The events selected by the same criteria as in the $\phi \to \eta\gamma$ study described in previous section, were kinematically reconstructed, using the maximum likelihood method to improve the values of measured variables from energy and momentum conservation constraints. The additional selection criteria for the $\phi \to \eta'\gamma$ study were the following:

- Three photons are detected in the calorimeter
- $\chi^2/d.f. < 5$
- The ratio of the photon energy measured in the calorimeter ω_{cal} to that from the constrained fit ω is $\omega_{cal}/\omega < 1.5$
- $\frac{(\omega_1 + 0.45\cdot(M_{23}-m_{\pi^0}) - \omega_{\eta\gamma})^2}{\Delta_\omega^2} + \frac{(M_{23}-m_{\pi^0})^2}{\Delta_M^2} > 1$.

The last cut is to exclude $\phi \to \eta\gamma$ events which are inside this ellipse region (for more detail see [10]). The number of reconstructed $\phi \to \eta\gamma$ events $N_{\eta\gamma} = 1518$. The efficiency from the simulation is $\varepsilon_{\eta\gamma} = (16.6 \pm 0.3)\%$.

After all the cuts the scatter plot of the invariant masses for two hardest photons M_{12} versus the weakest photon energy ω_3 was studied. Figure 31 presents the data together with simulation of $\phi \to \eta'\gamma$.

The one-dimensional distribution over $\omega_3 + M_{12} - m_\eta$ (projection of Fig. 31 plot to the axis perpendicular to the correlation line) is shown in Fig. 32c. The same projection for the events from the $\eta\gamma$ ellipse is shown in Fig. 32a. This distribution was fit to fix the background behaviour. Reconstructed simulation events (from a sample of 20000 events generated $\phi \to \eta'\gamma$, $\eta' \to \pi^+\pi^-\eta$, $\eta \to \gamma\gamma$) are shown together with fit in Fig. 32b, and the determined efficiency $\varepsilon_{\eta'\gamma} = (12.2 \pm 0.4)\%$. The data were fit using the background shape fixed from Fig. 32a together with that of the signal from simulation in Fig. 32b.

The result of the fit is $N_{\eta'\gamma} = 9.2^{+3.5}_{-2.9}$ events.

The relative branching ratio is:

$$\frac{Br(\phi \to \eta'\gamma)}{Br(\phi \to \eta\gamma)} = \frac{N_{\eta'\gamma}}{N_{\eta\gamma}} \cdot \frac{Br(\eta \to \pi^+\pi^-\pi^0)}{Br(\eta' \to \pi^+\pi^-\eta)} \cdot \frac{Br(\pi^0 \to \gamma\gamma)}{Br(\eta \to \gamma\gamma)} \cdot \frac{\varepsilon_{\eta\gamma}}{\varepsilon_{\eta'\gamma}}.$$

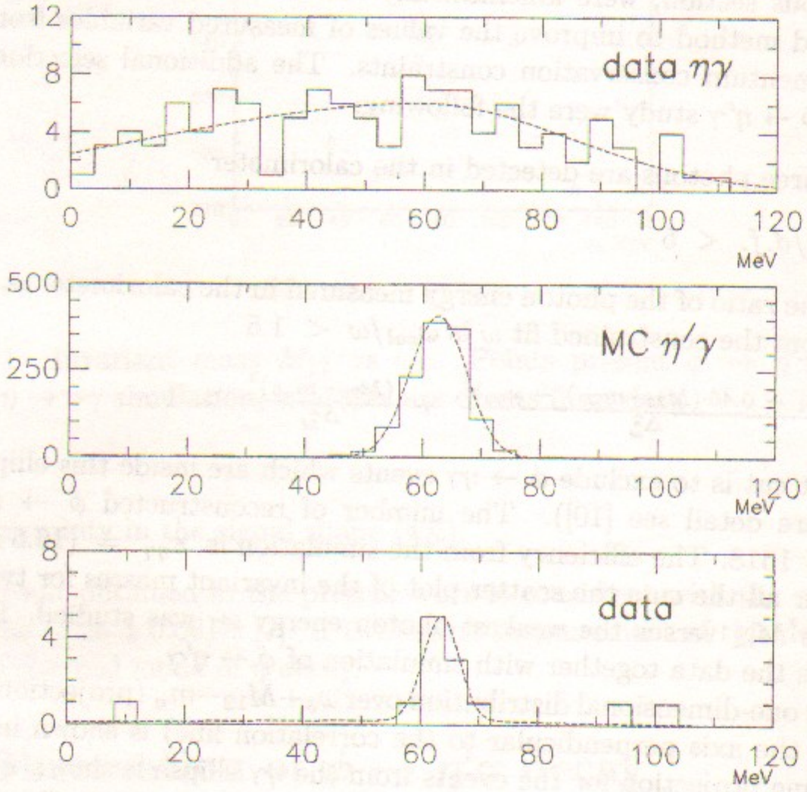

Figure 32: The distribution over $\omega_3 + M_{12} - m_\eta$ together with the fit function (dashed line). From upper to lower: background from $\phi \to \eta\gamma, \eta \to \pi^+\pi^-\pi^0$ events; the simulation of $\phi \to \eta'\gamma,\ \eta' \to \pi^+\pi^-\eta,\ \eta \to \gamma\gamma$; data

Using the values of all branching ratios from [7]

$$Br(\phi \to \eta'\gamma) \ = \ (13.5^{+5.5}_{-4.5} \pm 2.0) \cdot 10^{-5}.$$

The last error is systematic one. As the branching ratio of $Br(\phi \to \eta'\gamma)$ is calculated relative to $Br(\phi \to \eta\gamma)$, the systematic errors due to luminosity, detector inefficiency etc. cancel. The systematic uncertainty was estimated using different parameters of the constrained fit procedure and simulation, changes in selection criteria and different shape of background.

19 Study of $K^0_S K^0_L$ coupled decays

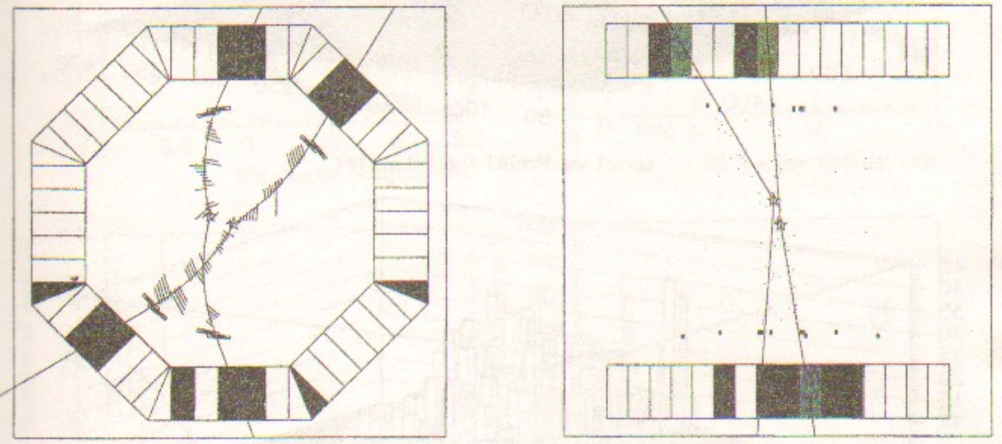

Figure 33: Display of the $\phi \to K^0_S K^0_L$ event with a coupled decay

Candidates were selected from a sample in which two vertices were found within 15 cm from the beam axis each with two opposite charged tracks. Tracks in both vertices should have an acollinearity angle of more than 0.1 radians. An example of such event is shown in Fig. 33..

Figure 34a shows the lego plot of invariant mass M_{inv} vs missing momentum P_{mis} for tracks in the closest to the beam vertex assuming them to be pions. The peak at the kaon mass and kaon momentum shows that the decay $K^0_S \to \pi^+\pi^-$ dominates in the first vertex.

The cuts $470 < M_{inv} < 525$ MeV and $80 < P_{mis} < 140$ MeV/c with an additional requirement to have another reconstructed vertex in the missing momentum direction select $K^0_S \to \pi^+\pi^-$ events in one of the vertices. In this case K^0_L is expected to be in the other one. With these conditions about 14000 events with double vertices have been selected.

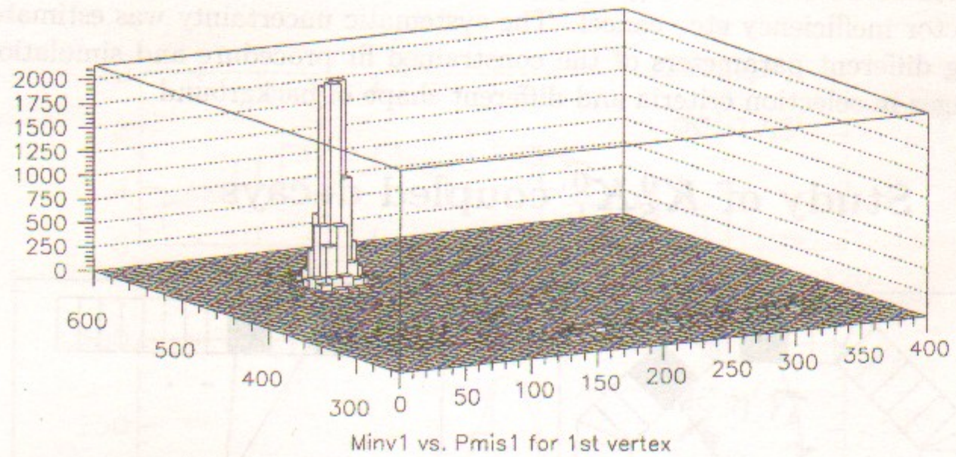

Figure 34: a. The M_{inv} vs P_{mis} distribution for tracks in the first vertex; b. The M_{inv} vs P_{mis} distribution for tracks in second vertex when K^0_S is selected in the first vertex

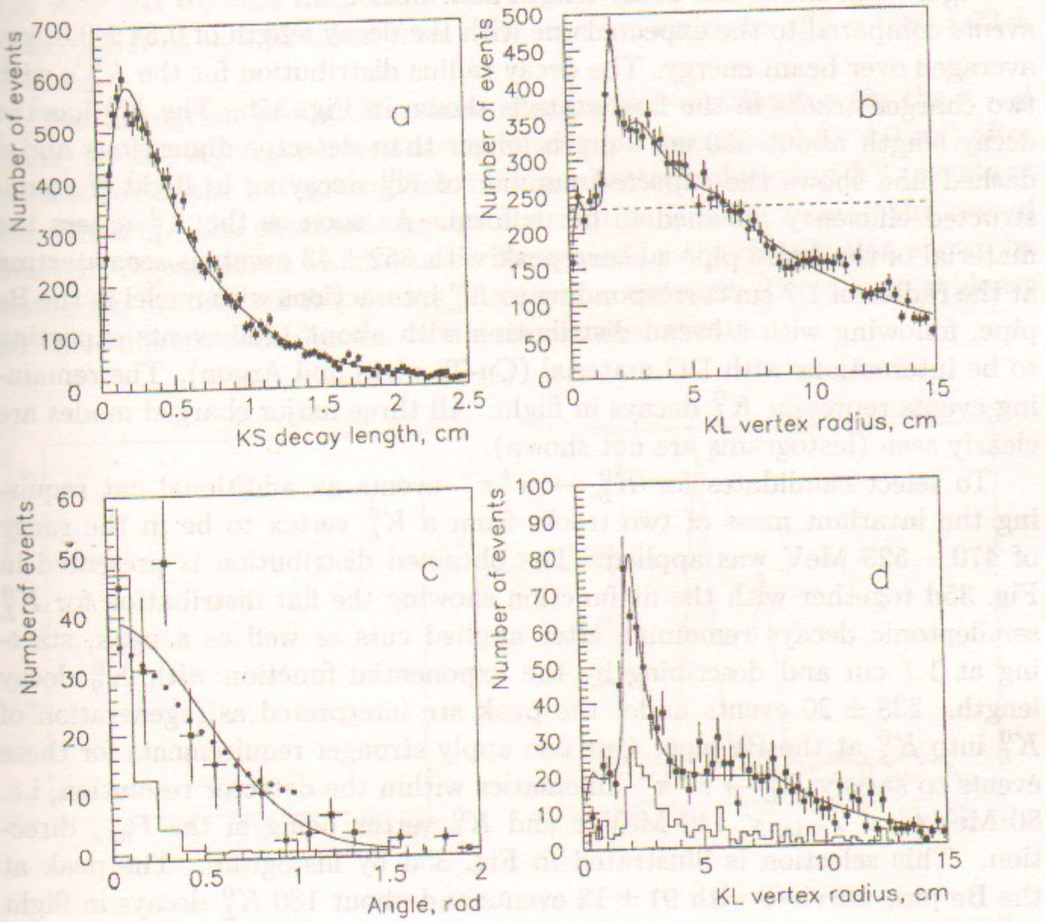

Figure 35: a. Decay length for K^0_S; b. Decay radius for K^0_L; c. Projected angular distribution for "tube" events after background subtraction (points with errors), for K^0_S two pions decays (histogram) and theoretical prediction (dots); d. Decay radius for K^0_L after M_{inv} cut and after K^0_S selecting cut (histogram)

Figure 34b shows lego plot M_{inv} vs P_{mis} for tracks in the second vertex when $K_S^0 \to \pi^+\pi^-$ decay is selected in the first one. The three body decay distribution dominates, but the peak at the kaon mass is seen demonstrating the presence of a two pion final state in both vertices.

Figure 35a shows the decay length distribution for selected $K_S^0 \to \pi^+\pi^-$ events compared to the expected one with the decay length of 0.54 ± 0.01 cm averaged over beam energy. The decay radius distribution for the K_L^0's with two charged tracks in the final state is shown in Fig. 35b. The K_L^0 has the decay length about 350 cm - much longer than detector dimensions and a dashed line shows the expected number of K_L^0 decaying in flight if reconstructed efficiency assumed to be uniform. As soon as the K_L^0 enters the material of the beam pipe a sharp peak with 562 ± 43 events is seen starting at the radius of 1.7 cm corresponding to K_L^0 interactions with nuclei in the Be pipe, following with a broad distribution with about 1100 events expecting to be interactions with DC material (Cu-Ti wires and Argon). The remaining events represent K_L^0 decays in flight. All three major charged modes are clearly seen (histograms are not shown).

To select candidates for $K_L^0 \to \pi^+\pi^-$ events an additional cut requiring the invariant mass of two tracks from a K_L^0 vertex to be in the range of 470 – 525 MeV was applied. The obtained distribution is presented in Fig. 35d together with the fit function showing the flat distribution for K_L^0 semileptonic decays remaining after applied cuts as well as a peak, starting at 1.7 cm and describing by the exponential function with K_S^0 decay length. 238 ± 20 events under the peak are interpreted as regeneration of K_L^0 into K_S^0 at the Be pipe. One can apply stronger requirements for these events to satisfy $K_L^0 \to \pi^+\pi^-$ kinematics within the detector resolution, i.e. 80 MeV/c $< P_{mis} <$ 140 MeV/c and K_S^0 vertex being in the P_{mis} direction. This selection is illustrated in Fig. 35d by histogram. The peak at the Be pipe survives with 91 ± 12 events and about 180 K_L^0 decays in flight and interactions in DC material remain. About 40 CP violation decays of $K_L^0 \to \pi^+\pi^-$ are expected but cannot be identified because of background from K_L^0 semileptonic decays and nuclear interactions.

Using the number of events above and simulated efficiencies for estimation of the total number of K_L^0 passed through the Be pipe, the following cross sections for the regeneration and visible inelastic scattering have been obtained:

$\sigma_{reg}^{Be} = (55.1 \pm 5.9 \pm 5.0)$ mb

$\sigma_{vis}^{Be} = (72 \pm 9)$ mb.

The sources of the inelastic scattering events are reactions with Σ and Λ production. About 10% admixture of these reactions to regenerated events and corrections for the presence of other material (0.1 mm mylar DC window) give the main contribution to the systematic error.

To estimate the total cross section, the relative weight of these reactions was taken to be 0.21 from the CERN GEANT code (NUCRIN). With the ratio $\sigma_{inel}/\sigma_{tot} = 0.52$ taken from [61], one can estimate $\sigma_{tot}^{Be} = (580 \pm 72 \pm 174)$ mb.

The histogram in Fig. 35c shows the angular distribution (in the $r - \phi$ plane) for the K_S^0 regenerated at the beam pipe (events at 1.5 - 4.0 cm) after subtraction of the background from the semileptonic decays of K_L^0 (events at 4.0 - 6.5 cm). The obtained angular distribution is wider than in the case of coherent regeneration which can be illustrated by the distribution shown by histogram for original K_S^0 decays at the same distance. There is no evidence for the coherent contribution to the regenerated events.

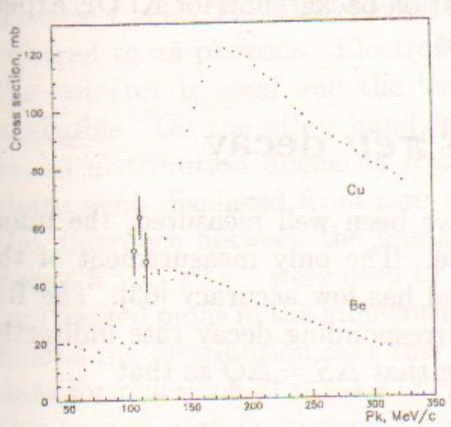

Figure 36: Experimental regeneration cross section and theoretical calculations for Be and Cu

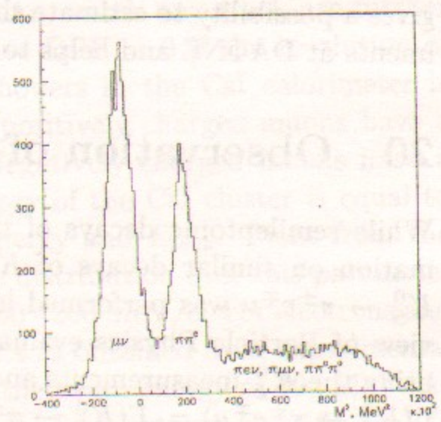

Figure 37: Missing mass distribution for events with kaons decaying in flight

The data were obtained at different energies around the ϕ. The regeneration cross section can be calculated for different kaon momenta. For the average momenta (105 ± 2), (110 ± 2) and (115 ± 2) MeV/c the cross sections (51.9 ± 8.5), (63.5 ± 7.4) and (48.0 ± 10.5) mb have been obtained respectively.

The selection of candidates for $K_L^0 \to \pi^+\pi^-$ events faced two problems. First was a background from the dominant semileptonic K_L^0 decays which

already was discussed in [62] and seemed to be solvable with better DC resolution.

A second problem was relatively high background from nuclear interactions of K_L^0 and regeneration effect which was for the first time experimentally observed for slow kaons with the CMD-2 detector.

In Fig. 36a the measured regeneration cross section is plotted together with the theoretical calculations [61] for Be and Cu. The comparison of the calculated regeneration cross sections for these two different materials shows, that at momenta below 200 MeV/c one cannot scale them by a simple $A^{2/3}$ dependence. Unfortunately, our momentum range is too narrow to prove it experimentally. The experimental angular distribution of the regenerated K_S^0 after background subtraction is presented in Fig. 36b together with a fitted exponential function and theoretical prediction [61] and seems to be more narrow.

The obtained regeneration cross section for Be for low momentum kaons gives a possibility to estimate the regeneration background for KLOE experiments at DAΦNE and helps to subtract it.

20 Observation of $K_S^0 \to \pi e \nu$ decay

While semileptonic decays of the K_L^0 have been well measured, the information on similar decays of K_S^0 is scarce. The only measurement of the $K_S^0 \to \pi^\pm e^\mp \nu$ was performed long ago and has low accuracy [63]. The Review of Particle Physics evaluates the corresponding decay rate indirectly, using the K_L^0 measurements and assuming that $\Delta S = \Delta Q$ so that $\Gamma(K_S^0 \to \pi^\pm e^\mp \nu) = \Gamma(K_L^0 \to \pi^\pm e^\mp \nu)$ [7].
We present results of the direct measurement of the branching ratio for the $K_S^0 \to \pi e \nu$ using the unique opportunity to study events containing a pure $K_L^0 K_S^0$ state produced in the reaction $e^+e^- \to \phi \to K_L^0 K_S^0$. The statistics was collected during 1993–1998 (**PHI-93**, **PHI-96**, **PHI-98**).

Some characteristics of the detector relevant to this analysis are:

- Charged particles in the neutral kaon decays have momenta less than 290 MeV/c and stop within CsI crystals of the barrel calorimeter (the information from the BGO endcap was not used in this analysis)
- The momentum resolution for 200 MeV/c charged particles is 3%
- The barrel calorimeter is placed at 40 cm from the beam axis so that about a half of K_L^0 mesons with $\lambda = 3.3$ m interact within CsI crystals

- The beam pipe with a radius of 1.8 cm is placed inside DC and most of K_S^0 mesons with $\lambda = 0.6$ cm decay inside it.

K_S^0 decays can be tagged using the presence of the second vertex with two charged particles at a long distance from the e^+e^- interaction region or the CsI cluster from K_L^0 interactions in CsI. The most probable decay channel $K_S^0 \to \pi^+\pi^-$ was used for the normalization of the semileptonic $K_S^0 \to \pi e \nu$ decay. Both channels have a vertex with two charged particles near the beam axis.

To identify electrons in the decay under study, we are using the difference between a measured momentum and energy loss in the detector material for stopped particles. The basic parameter used for charged particle identification was

$$DPE = p - E_{loss} - E_{cluster},$$

where p is a particle momentum measured in DC, E_{loss} is an ionization energy loss in the material in front of the CsI calorimeter (this value is about 10 MeV), $E_{cluster}$ is an energy deposition in a CsI cluster matched with a particle track. The CsI clusters which do not match any track are further referred to as photons. Electrons must have DPE = 0 if the resolution of the detector is ideal and the leakage of showers in the CsI calorimeter is negligible. On the other hand, pions and positively charged muons have a broad distribution displaced from zero. Negatively charged muons have a sharp peak displaced from zero as the energy of the CsI cluster is equal to the difference between the muon kinetic energy and E_{loss}. Pions from the decay $K_S^0 \to \pi^+\pi^-$ were used to obtain the distribution over this parameter for charged pions in the momentum range 160 - 200 MeV/c. For electrons and muons the distribution over this parameter was obtained from experimental data for reactions $e^+e^- \to e^+e^-, \mu^+\mu^-$ at the beam energy of 195 MeV. At this energy particle momenta are 195 MeV/c for electrons and 164 MeV/c for muons. The distribution for muons overlaps with the one for pions and this circumstance is correspondingly taken into account.

Some kinematic features for the decay mode $K_S^0 \to \pi e \nu$ are :

- The momenta of charged particles are less than 290 MeV/c
- The total energy of charged particles (assuming that both particles are charged pions) is between 330 and 550 MeV.

The same parameters for the decay mode $K_S^0 \to \pi^+\pi^-$ are :

- The opening angle between two tracks is more than 2.6 radians

- The pion momenta are between 160 and 270 MeV/c.

The selection criteria for both modes of K_S^0 decay were:

- One or two vertices are found in the event
- Two minimum ionizing tracks with the opposite charge signs are reconstructed from the first vertex (nearest to the beam) and there is no other track with the distance to the beam less than 1.4 cm
- The distance from the first vertex to the beam is between 0.2 cm and 1.4 cm
- The distance from the first vertex to the interaction point along the beam direction is less than 7 cm
- Each charged particle at the first vertex has a momentum from 90 to 270 MeV/c since particles with a momentum less than 90 MeV/c can not reach the CsI calorimeter in the magnetic field of DC
- Each track at the first vertex crosses all sensitive layers in DC in the radial direction and therefore has a polar angle θ from 0.87 to 2.27 radians
- Each charged particle at the first vertex fires ZC and does not fire the muon range system
- The azimuthal angle difference between two tracks at the first vertex ($\Delta\varphi$) is between 0.17 and 2.97 radians
- The azimuthal angle difference ($\Delta\varphi$) between the direction from the first vertex (K_S^0) to the interaction point and a photon with the energy greater than 50 MeV (supposedly the K_L^0 cluster) or the second vertex in DC (supposedly K_L^0 decay in DC) is within ± 0.5 radian
- There are no photons with the energy greater than 15 MeV outside the direction from the first vertex to the interaction point ± 1 radian in the $r-\varphi$-plane. This cut rejects background from processes with the neutral pions.

To select the decay mode $K_S^0 \to \pi e \nu$ the following complementary criteria for the first vertex were used:

- The opening angle between two tracks is between 0.35 and 2.50 radians

- The total energy of charged particles (assuming that both particles are charged pions) is between 300 and 470 MeV
- The invariant mass squared of the assumed neutrino is greater than -10000 MeV^2 and less than 6000 MeV^2.

To select the decay mode $K_S^0 \to \pi^+\pi^-$ the following complementary criteria for the first vertex were used:

- The opening angle between two tracks is more than 2.55 radians
- The total energy of charged particles (assuming that both particles are charged pions) is between 480 and 540 MeV
- The pion momenta are between 140 and 270 MeV/c
- The average momentum of two charged pions is between 190 and 230 MeV/c
- The invariant mass squared of the assumed photon is greater than -10000 MeV^2 and less than 6000 MeV^2

The DPE distribution for events selected as candidates for the decay $K_S^0 \to \pi e \nu$ is shown in Fig.38. The data were fit using the DPE distribution for e, μ and π measured in experiment. The result of the fit for the number of the electrons is $N_e = 83.5 \pm 12.7$. The number of mesons is equal to $N_m = 354 \pm 21$. The distribution over the distance between the vertex and beam axis for these events is consistent with that for $K_S^0 \to \pi^+\pi^-$ decays.

The main background for the $K_S^0 \to \pi e \nu$ decay mode after applying the above cuts comes from the decays $K_S^0 \to \pi^+\pi^-\gamma$, $K_S^0 \to \pi\mu\nu$ and $K_L^0 \to \pi e \nu$. The former two processes are taken into account while fitting the histogram over DPE. The same procedure was applied to events with the distance from the first vertex to the beam between 3 and 7 cm to take into account the background from the K_L^0 decays. The resulting number of electrons for these events is 24.2 ± 6.1. Taking into account the dependence of the efficiency of vertex reconstruction on the distance from the beam axis it was found that the contribution of the K_L^0-decays to effect is equal to 8.6 ± 2.2. Thus, the number of electrons and correspondingly the number of events of the $K_S^0 \to \pi e \nu$ decay, is equal to

$$N_e = 75 \pm 13$$

Under the applied cuts the number of $K_S^0 \to \pi^+\pi^-$ detected decays equals 178110 (of about 7 million produced $K_S^0 K_L^0$ pairs). Applying the selection

criteria above to the events from simulation, one obtains that the ratio of the number of events due to the process under study and the normalization process should be 1 : 2550 if their branching ratios are taken from [7]. Then one would expect 69.8 events for the branching ratio of 6.7 $\times 10^{-4}$ evaluated by the Review of Particle Physics. From 75 $\pm$ 13 events observed by us the following result was obtained for the branching ratio:

$$Br(K^0_S \to \pi e \nu) = (7.19 \pm 1.35) \cdot 10^{-4}.$$

The quoted error contains the statistical error of the number of events and the systematic uncertainty (5% from the simulation detection efficiency and 5% from the selection criteria) added in quadrature. This result is consistent with the only previous determination of $Br(K^0_S \to \pi e \nu)$ [63] as well as with the Review of Particle Physics evaluation [7] which was obtained by the calculation from K^0_L semileptonic rates.

21 Study of charged kaon decays

Charged kaons from the ϕ decays have a 120 MeV/c momentum and correspondingly about 50 cm decay length. Within 10 cm radius about 6% of charged kaon decays are completely reconstructed. Most of the major charged kaon decays have one charged particle in the final state with some number of neutrals (neutrino and π^0). Only $K^\pm \to \pi^\pm\pi^+\pi^-$ with a (5.59 $\pm$ 0.05)% probability has three charged particles in the final state. This analysis uses the data collected in the **PHI-96** run.

Candidates were selected by the presence of two charged tracks in the DC — one track coming from the interaction point with the 120 MeV/c momentum and high dE/dx and second track with the low dE/dx signal, acollinearity angle greater than 0.15 radian and impact parameter greater than 0.2 cm. The decay point was reconstructed by prolongating the kaon track to the intersection with a second track which was assumed to come from the decay of another kaon. Under these conditions about 50000 tagged kaon decays were selected with a decay radius less than 9 cm. The momentum and the direction of the decayed kaon are completely determined by a tagging kaon and the missing mass can be calculated assuming the decay particle to be a pion. Figure 37 presents the distribution of squared missing masses calculated for two detected tracks. Peaks correspond to two body decays $K^\pm \to \mu^\pm\nu$ and $K^\pm \to \pi^\pm\pi^0$. Using the number of events under the peaks and with the efficiencies obtained by simulation the following ratio has been obtained:

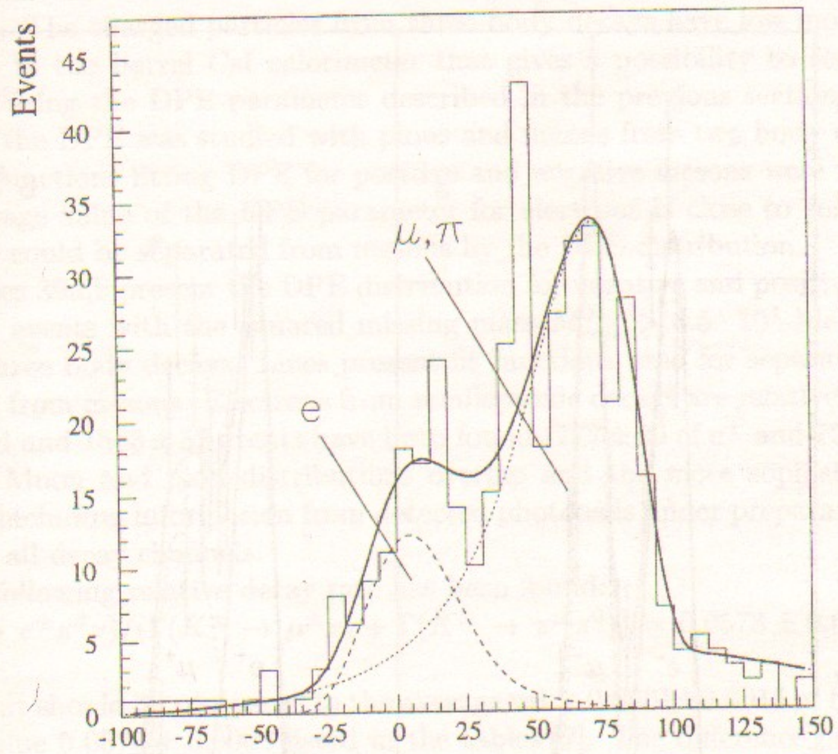

Figure 38: DPE distribution for charged particles in K^0_S decays; dashed line — electrons; dotted line — muons and pions

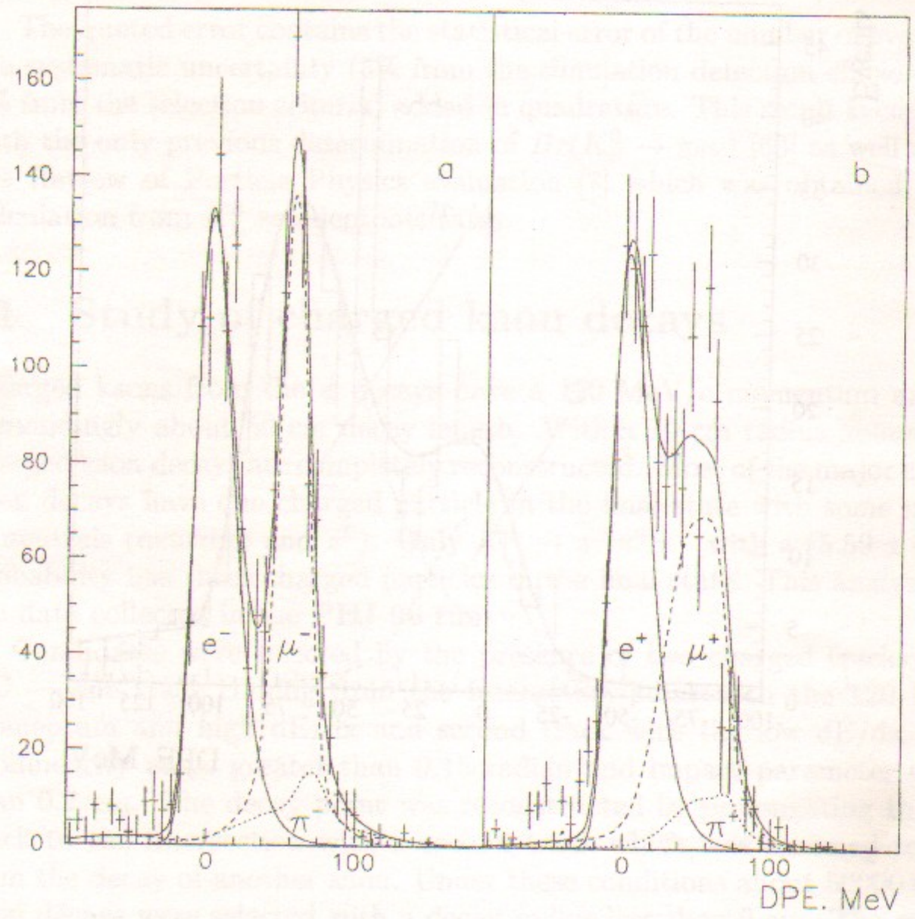

Figure 39: The DPE parameter distributions for negative (a) and positive (b) decay particles

$\Gamma(K^\pm \to \pi^\pm\pi^0)/\Gamma(K^\pm \to \mu^\pm\nu) = 0.340 \pm 0.008 \pm 0.017$.
This result should be compared with that listed in tables [7]:
$\Gamma(K^\pm \to \pi^\pm\pi^0)/\Gamma(K^\pm \to \mu^\pm\nu) = 0.3316 \pm 0.0032$.

The broad distribution in Fig. 37 represents the three body decays of charged kaons to $\pi^0\mu\nu$, $\pi^0 e\nu$ and $\pi\pi^0\pi^0$. The reconstruction of π^0's from detected photons can help to separate the channels mentioned above. In the present analysis the different calorimeter response for electrons and mesons was used. The charged particles from three-body decays have low momenta and stop in the barrel CsI calorimeter that gives a possibility to separate particles using the DPE parameter described in the previous section. The shape of the DPE was studied with pions and muons from two body decays and the functions fitting DPE for positive and negative mesons were found. The average value of the DPE parameter for electrons is close to zero and electrons could be separated from mesons by the DPE distribution.

Figures 39a,b present the DPE distribution for negative and positive particles for events with the squared missing mass $M^2_{mis} > 3.5 \cdot 10^4$ MeV^2 selecting three body decays. Lines present fit functions used for separation of electrons from mesons. Electrons from semileptonic decays are relatively well separated and 1503 ± 52 events have been found (777 ± 29 of e^+ and 726 ± 31 of e^-). Muon and pion distributions overlap and the more sophisticated analysis including information from detected photons is under preparation to separate all decay channels.

The following relative decay rate has been found:
$\Gamma(K^\pm \to e^\pm\pi^0\nu)/(\Gamma(K^\pm \to \mu^\pm\nu) + \Gamma(K^\pm \to \pi^\pm\pi^0)) = 0.0578 \pm 0.0020 \pm 0.0020$.
This result should be compared to the average value 0.0601 ± 0.0015 or fit with S=1.4 value 0.0570 ± 0.0008 listed in the tables [7]. The difference between the average and fit values is probably due to a big spread of the measured branching ratios making interesting new independent experiments.

22 Study of conversion decays

Conversion decays are closely related to corresponding radiative decays. In conversion decays a virtual photon is converted into a lepton pair.

This work is devoted to determination of the branching ratios for conversion decays $\phi \to \eta e^+e^-$, $\phi \to \pi^0 e^+e^-$ as well as Dalitz decay $\eta \to e^+e^-\gamma$. A data sample corresponding to the integrated luminosity of 15.5 pb^{-1} collected in the groups of runs **PHI-93**, **PHI-96** and **PHI-98** has been used.

The decay $\phi \to \eta e^+e^-$ was detected via the mode $\phi \to \eta e^+e^-$, $\eta \to \gamma\gamma$, the decay $\phi \to \pi^0 e^+e^-$ via the $\phi \to \pi^0 e^+e^-$, $\pi^0 \to \gamma\gamma$ and the decay $\eta \to e^+e^-\gamma$ – via the mode $\phi \to \eta\gamma$, $\eta \to e^+e^-\gamma$.

The process $\phi \to \eta\gamma$, $\eta \to \pi^+\pi^-\gamma$ was used to determine the number of ϕ-mesons. All processes have two charged particles and two photons in the final state.

Events were selected with two charged particles in DC and two photons in the CsI calorimeter. Information from the BGO calorimeter was not used in this analysis. The selected events were subject to kinematic reconstruction taking into account energy-momentum conservation.

In Fig. 40a we plot the invariant mass of the $\pi^+\pi^-\gamma_{min}$ system for the data of **PHI-98** where γ_{min} is a photon with the minimal energy.

The number of ϕ-mesons was determined from the formula

$$N_\phi = \frac{N_0}{Br(\phi \to \eta\gamma) \cdot Br(\eta \to \pi^+\pi^-\gamma) \cdot \varepsilon}, \qquad (6)$$

where N_0 is the number of $\pi^+\pi^-\gamma$ events, ε is the detection efficiency which equals $(13.24 \pm 0.26)\%$ as the MC simulation of the experiment shows [59].

To select conversion decays one used the specific feature of their kinematics: the angle between e^+ and e^- is as a rule close to zero.

Significant background to events of conversion decays comes from the γ-quantum conversion in the detector material. The detection efficiency for this process was also determined from the simulation. The number of conversion events was calculated from the formula:

$$N_{conv} = N_\phi \cdot Br(\phi \to P\gamma) \cdot Br(P \to \gamma\gamma) \cdot \varepsilon_{conv}, \qquad (7)$$

where P stands for η (for $\eta \to e^+e^-\gamma$ and $\phi \to \eta e^+e^-$) or π^0 (for $\phi \to \pi^0 e^+e^-$).

The number of events of $\phi \to \eta\gamma$, $\eta \to e^+e^-\gamma$ was determined from the spectrum of the invariant mass of the $e^+e^-\gamma$ state (Fig. 40b). The following criterion was used to select a photon:

$$\gamma_{max} \text{ if } (M_{e^+e^-\gamma_{max}} + M_{e^+e^-\gamma_{min}}) < 2 \cdot M_\eta,$$
$$\gamma_{min} \text{ if } (M_{e^+e^-\gamma_{max}} + M_{e^+e^-\gamma_{min}}) > 2 \cdot M_\eta,$$

where γ_{max} is a photon with the maximum energy, γ_{min} is a photon with the minimum energy. The angle ψ between e^+e^- is less than 0.5. The detection efficiency of the effect was $(10.51 \pm 0.22)\%$ and for conversion events – $(5.08 \pm 0.36) \cdot 10^{-4}$.

The number of events of $\phi \to \eta e^+e^-$, $\eta \to \gamma\gamma$ was determined from the spectrum of the invariant mass of the $\gamma\gamma$ state (Fig. 40c). The angle ψ

Table 3: The relative branching ratios

	N_ϕ $(\times 10^6)$	$Br(\eta \to e^+e^-\gamma)$ $(\times 10^{-4})$	$Br(\phi \to \eta e^+e^-)$ $(\times 10^{-4})$	$Br(\phi \to \pi^0 e^+e^-)$ $(\times 10^{-4})$
PHI-93	1.18 ± 0.16	8.08 ± 3.18	1.44 ± 0.67	1.70 ± 1.19
PHI-96	2.43 ± 0.25	5.13 ± 1.66	1.22 ± 0.40	0.76 ± 0.70
PHI-98	11.83 ± 0.82	8.71 ± 1.18	1.07 ± 0.19	1.38 ± 0.33
PHI-98*		8.41 ± 1.29	1.12 ± 0.23	1.02 ± 0.42
Total	15.44 ± 0.87	7.56 ± 0.92	1.12 ± 0.17	1.29 ± 0.29

between e^+e^- is less than 0.5. The detection efficiency was $(13.73 \pm 0.26)\%$ and for conversion events — $(3.15 \pm 0.31) \cdot 10^{-4}$.

The number of $\phi \to \pi^0 e^+e^-$, $\pi^0 \to \gamma\gamma$ events was also determined from the spectrum of the invariant mass of the $\gamma\gamma$ state (Fig. 40d). The main background for this process comes from the events of $\phi \to \pi^+\pi^-\pi^0$, $\pi^0 \to \gamma\gamma$. But for this process the angle between charged particles does not have a peak around zero, therefore this background can be suppressed by making more strict the criterion for the angle between charged particles. The angle ψ between e^+e^- is less than 0.15. The detection efficiency was $(20.62 \pm 0.32)\%$ and for conversion events was $(5.59 \pm 0.39) \cdot 10^{-4}$.

The relative branching ratios were determined from the formula:

$$Br_i = \frac{N_{0_i} - N_{conv_i}}{N_\phi \cdot \overline{Br_i} \cdot \varepsilon_{0_i}} \qquad (8)$$

where $i = 1, 2, 3$ corresponds to $\eta \to e^+e^-\gamma$, $\phi \to \eta e^+e^-$ and $\phi \to \pi^0 e^+e^-$

Br_i is the relative branching ratio,

N_{0_i} is the number of events of the effect,

N_ϕ is the number of the ϕ-mesons determined from the formula (6),

N_{conv_i} is the number of conversion events from the formula (7),

$\overline{Br_i}$ is the probability of the decays:
$Br(\phi \to \eta\gamma)$ for $\eta \to e^+e^-\gamma$
$Br(\eta \to \gamma\gamma)$ for $\phi \to \eta e^+e^-$
$Br(\pi^0 \to \gamma\gamma)$ for $\phi \to \pi^0 e^+e^-$,

ε_{0_i} is the detection efficiency.

The results are shown in Table 3.

For the **PHI-98** data we performed a fit of the energy dependence of the cross sections with the ϕ-meson excitation curve. In Fig. 41 visible cross

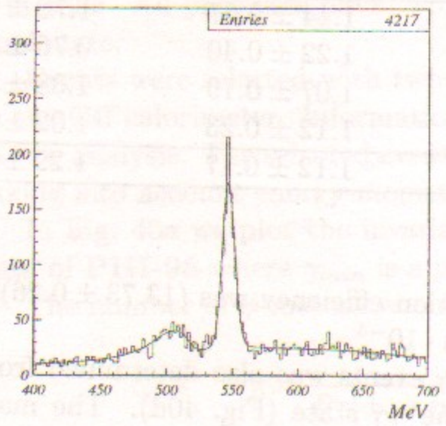

a) – $M_{\pi^+\pi^-\gamma}$, for $\phi \to \eta\gamma$, $\eta \to \pi^+\pi^-\gamma$

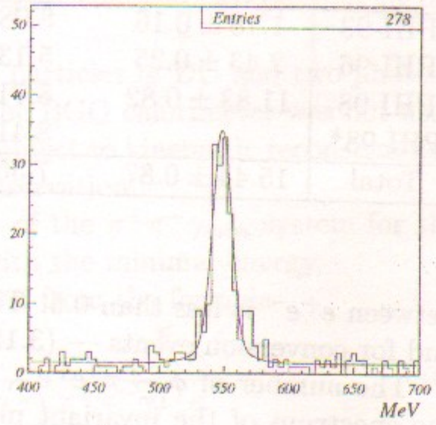

b) – $M_{e^+e^-\gamma}$, for $\phi \to \eta\gamma$, $\eta \to e^+e^-\gamma$

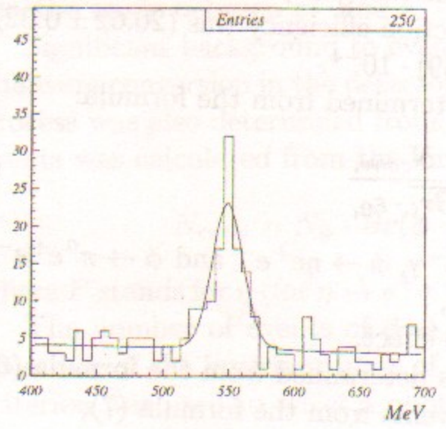

c) – $M_{\gamma\gamma}$, for $\phi \to \eta e^+e^-$, $\eta \to \gamma\gamma$

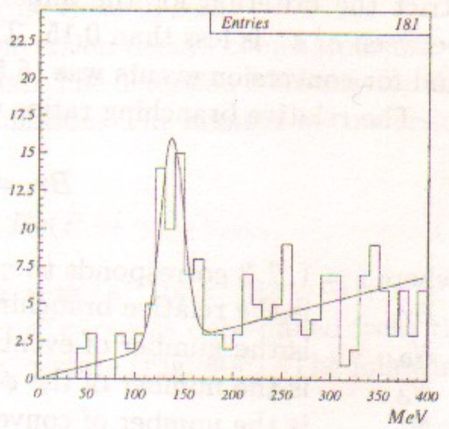

d) – $M_{\gamma\gamma}$, for $\phi \to \pi^0 e^+e^-$, $\pi^0 \to \gamma\gamma$

Figure 40: Invariant masses for conversion decays, **PHI-98** data

Table 4: Comparison with theoretical predictions and other experiments

Decay	$Br(\eta \to e^+e^-\gamma)$	$Br(\phi \to \eta e^+e^-)$	$Br(\phi \to \pi^0 e^+e^-)$
Theory	$(6.60 \pm 0.80) \cdot 10^{-3}$	$(1.10 \pm 0.10) \cdot 10^{-4}$	$(1.44 \pm 0.10) \cdot 10^{-5}$
PDG	$(4.9 \pm 1.1) \cdot 10^{-3}$	$(1.3^{+0.8}_{-0.6}) \cdot 10^{-4}$	$< 1.2 \cdot 10^{-4}$
CMD-2	$(7.56 \pm 0.92 \pm 1.13) \cdot 10^{-3}$	$(1.12 \pm 0.17 \pm 0.17) \cdot 10^{-4}$	$(1.29 \pm 0.29 \pm 0.19) \cdot 10^{-5}$

sections of the processes under the study are shown parametrized with the Breit-Wigner function plus constant. At each point the procedure above was used to calculate the visible cross section by dividing the number of events over the integrated luminosity. The relative branching ratios of conversion decays were determined as a ratio of the corresponding maxima of the cross sections to the maximum of the cross section of the monitoring process $\phi \to \eta\gamma$, $\eta \to \pi^+\pi^-\gamma$ taking into account corresponding detection efficiencies and decay branching ratios.

The obtained results (Table 3, line "PHI-98*") are consistent with those from the previous method (Table 3, line "PHI-98").

The following sources of the systematic uncertainties were considered: efficiency of reconstruction and detection of the tracks with a small angle between them, extra photons from the cluster splitting in the calorimeter, extra photons from the noisy crystals and electronics channels in the calorimeter. The overall systematic uncertainty was estimated to be 15%.

The obtained results do not contradict to theoretical predictions [64] and have better statistical accuracy than the previous measurements quoted by the Review of Particle Physics [7] (Table 4).

Using the data sample from the end-cap BGO calorimeter should result in the efficiency increase by a factor of $\sim 1.5 \div 2$. Investigation of the transition form factors of pseudo-scalar mesons will require a detailed study of the efficiencies of reconstruction and detection of tracks at a small angle.

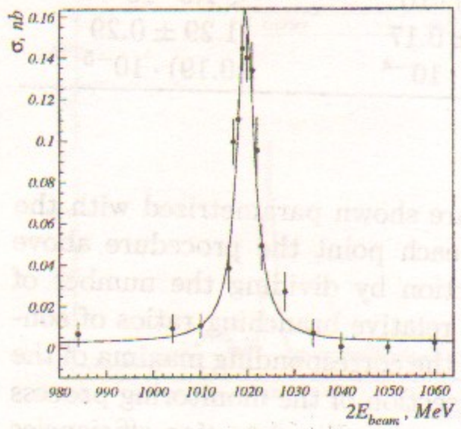

a) – $\phi \to \eta\gamma$, $\eta \to \pi^+\pi^-\gamma$

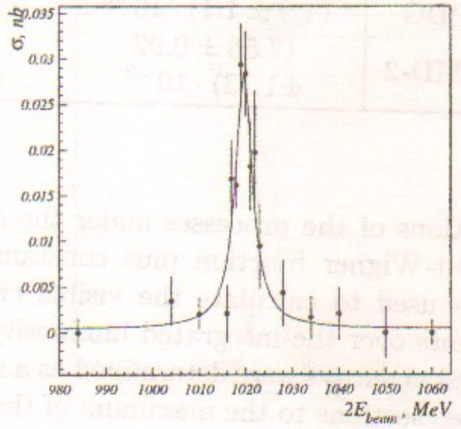

b) – $\phi \to \eta\gamma$, $\eta \to e^+e^-\gamma$

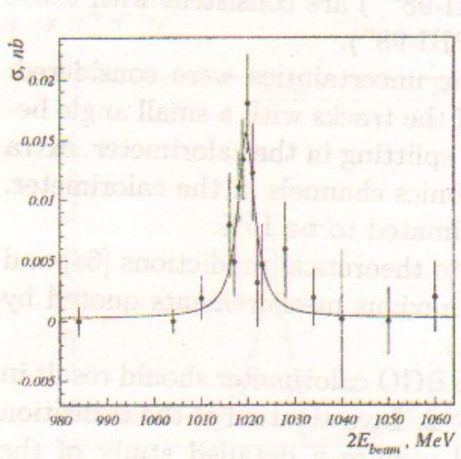

c) – $\phi \to \eta e^+e^-$, $\eta \to \gamma\gamma$

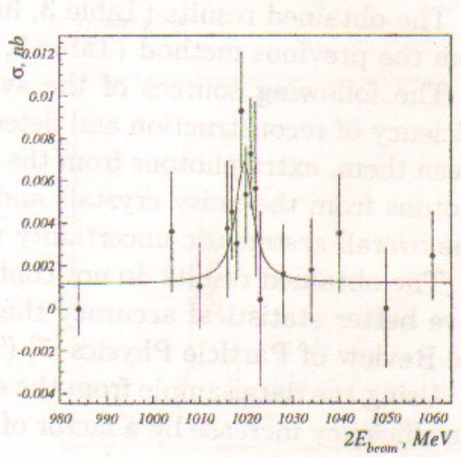

d) – $\phi \to \pi^0 e^+e^-$, $\pi^0 \to \gamma\gamma$

Figure 41: Visible cross sections for conversion decays, **PHI-98** data

23 Observation of decay $\phi \to \eta'\gamma$ in the final state with four charged particles and photons

A search for the decay $\phi \to \eta'\gamma$ was performed using data collected in the **PHI-98** experiment in the decay channels (9) and (10):

$$\phi \to \eta'\gamma, \quad \eta' \to \eta\pi^+\pi^-, \quad \eta \to \pi^+\pi^-\pi^0 \quad \text{or} \tag{9}$$

$$\phi \to \eta'\gamma, \quad \eta' \to \eta\pi^+\pi^-, \quad \eta \to \pi^+\pi^-\gamma \tag{10}$$

The main characteristic feature of the studied processes is the presence in the final state of 4 charged pions coming from the interaction region and two or more photons. That certainly gives clues for event selection and possible sources of background. One of the main problems in the analysis presented here is detection in the calorimeter of "extra" photons induced by the products of nuclear interactions of charged pions in the detector material. Since the probability of the decay $\phi \to \eta'\gamma$ is rather low ($\sim 10^{-4}$), practically all processes from $\phi \to K^+K^-$ and $\phi \to K^0_S K^0_L$ with four particles in the final state could contribute to the background because of their several orders of magnitude higher cross section. The main background, however, comes from the process $\phi \to K^0_S K^0_L$, where $K^0_S \to \pi^+\pi^-$ and $K^0_L \to \pi^+\pi^-\pi^0$.

Analysis included full kinematic reconstruction taking into account energy – momentum conservation. All charged particles in the reconstruction procedure were considered as pions. The following simple method was used for suppression of "extra" photons. Angular coordinates of all detected photons were input parameters for the kinematic reconstruction. As output parameters of reconstruction procedure photon energies were obtained. Photons with the reconstructed energy below threshold (E_{th} = 30 MeV) were considered as "extra" photons and were excluded from the subsequent analysis.

The following criteria were used for event selection:

- $N_{track} = 4$, $P < 700$ MeV , $N_\gamma > 1$
- $dE/dx < 2000$ and min $M_{inv}(3\pi) > 510$ MeV — these suppressed background from the decays of charged kaons
- The following condition suppressed background from the decays of neutral kaons: max $M_{inv}(\pi^+, \pi^-) < 450$ MeV

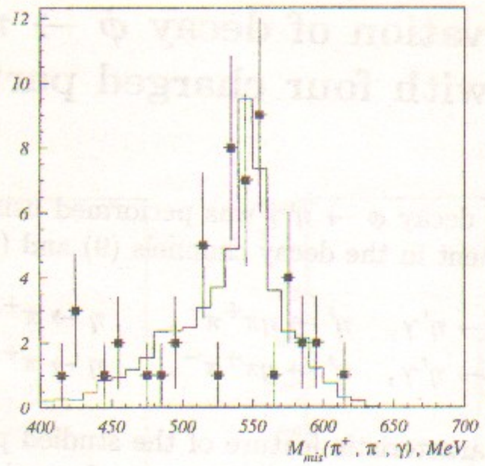

Figure 42: The missing mass distribution of the pair of pions and the photon $E_\gamma = 60$ MeV; histogram — Monte Carlo, black squares with error bars — data

- Background from conversion decays was suppressed by the cut over the space angle between opposite charged tracks: $\min\psi(\pi^+,\pi^-) > 0.3$

- Track impact parameters: $r_{min} < 0.3$ cm.

The number of survived events after application of all these selection conditions was $\tilde{N}_{\eta'\gamma} = 13$. The efficiency of the listed criteria was obtained from the simulation of the processes (9) and (10):

$$\begin{aligned} \varepsilon_{\eta\to 3\pi} &= 0.084 \pm 0.003\,, \\ \varepsilon_{\eta\to\pi^+\pi^-\gamma} &= 0.111 \pm 0.003\,. \end{aligned}$$

The simulated spectra on the following pictures were obtained as a sum of the contributions of the processes (9) and (10) with the numbers of events proportional to the corresponding decay probabilities.

Figure 42 shows the distribution over the missing mass of the pair of charged pions and the photon with the energy closest to the energy of the monochromatic photon from the decay $\phi \to \eta'\gamma$. As one can see, the experimental data does not contradict to the simulation. To estimate number of remaining background events in $\tilde{N}_{\eta'\gamma}$, simulation was done for the processes with charged and neutral kaons. The number of simulated events for each decay mode was approximately equal to the expected number of events for

this mode in the **PHI-98** experiment. It was found that the only contribution to the $\tilde{N}_{\eta'\gamma}$ could come from the process $\phi \to K^0_S K^0_L$, $K^0_S \to \pi^+\pi^-$ and $K^0_L \to \pi^+\pi^-\pi^0$. In practice, it is not possible to determine this contribution from Fig. 42 because of the rather big combinatorial background in the $M_{mis}(\pi^+\pi^-\gamma)$ distribution — each event gives four entries into these spectra.

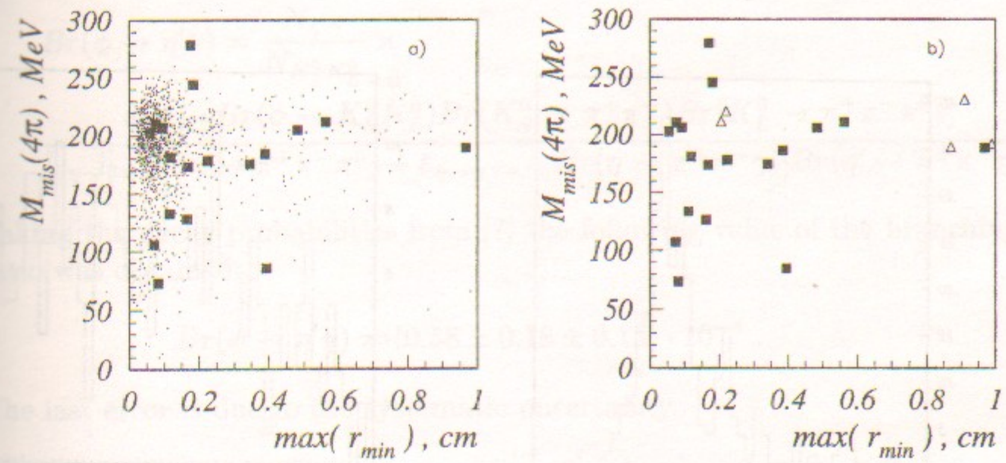

Figure 43: The distribution of the missing mass of 4π versus the maximum of the track impact parameters; a) black squares — experimental data, dots — sum of Monte Carlo of the processes (9) and (10); b) black squares — data, light triangles — simulation of $K^0_S K^0_L$

Figure 43a shows the distribution over the missing mass of all four charged pions versus maximum of the track impact parameters. Good agreement is seen on this picture between the Monte Carlo and the experimental data for $r_{min} < 0.3$ cm. The expected number of events with $r_{min} > 0.3$ cm is $N^{>0.3}_{\eta'\gamma} = 1.4 \pm 1.2$, while the number of detected events in this region is $\tilde{N}^{>0.3}_{\eta'\gamma} = 6$. In Fig. 43b the same distribution of the experimental data is shown in comparison with the simulation of the process $\phi \to K^0_S K^0_L$. It is seen from this picture that $K^0_S K^0_L$ gives the main contribution to $\tilde{N}^{>0.3}_{\eta'\gamma}$. Thus, the parameters $M_{mis}(4\pi)$ and r_{min} could be used together to control the background from the decays of neutral kaons.

The process $\phi \to K^0_S K^0_L$ was also used for the normalization and calcu-

lation of the probability of decay $\phi \to \eta'\gamma$. The following requirements were applied to select events:

- $N_{track} = 4$, $p < 700$ MeV, $\min \psi(\pi^+, \pi^-) > 0.3$, $N_\gamma > 1$
- $dE/dx < 2000$, $\min M(3\pi) > 510$ MeV
- And finally, the selection of $\phi \to K_S^0 K_L^0$ itself: $M_{inv}(\pi^+, \pi^-) > 450$ MeV for at least one of $\pi^+\pi^-$ pairs.

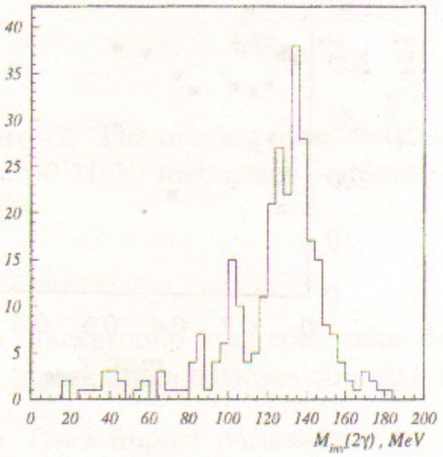

Figure 44: The distribution over the invariant mass of 2γ in the decay $\phi \to K_S^0 K_L^0, K_S^0 \to \pi^+\pi^-, K_L^0 \to \pi^+\pi^-\pi^0$

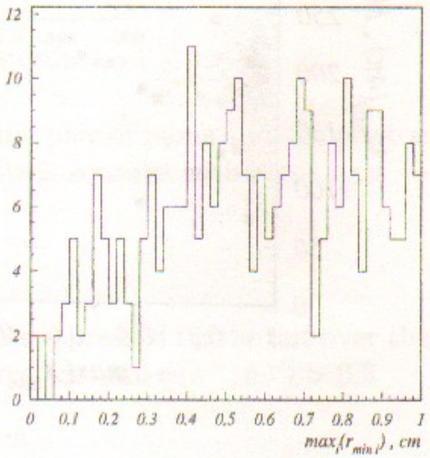

Figure 45: The distribution over the maximum of track impact parameters for $K_S^0 K_L^0$

Figure 44 shows the distribution over the invariant mass of a pair of photons for selected events. The clear peak is observed around $m_{\pi^0} \simeq 135$ MeV. The selection efficiency was determined from MC:

$$\varepsilon_{K_S^0 K_L^0} = (5.1 \pm 0.3) \cdot 10^{-4}.$$

The number of detected events: $N_{K_S^0 K_L^0} = 278$.

Figure 45 shows distribution of the maximum of all four tracks impact parameter. The probability to detect $K_S^0 K_L^0$ events with $r_{min} < 0.3$ cm:

$$W_{K_S^0 K_L^0} = \frac{N_{K_S^0 K_L^0}(r_{min} < 0.3 \text{ cm})}{N_{K_S^0 K_L^0}(r_{min} > 0.3 \text{ cm})} = \frac{45}{233} = 0.19 \pm 0.03\,. \qquad (11)$$

This probability mostly depends on the shape of the r_{min} distribution and is weakly affected by the other requirements used for selection of $K_S^0 K_L^0$ events. According to this consideration, the contribution of $K_S^0 K_L^0$ to $N_{\eta'\gamma}$ was estimated and the number of $\eta'\gamma$ events was obtained as follows:

$$N_{\eta'\gamma} = \tilde{N}_{\eta'\gamma} - W_{K_S^0 K_L^0}(\tilde{N}_{\eta'\gamma}^{>0.3} - N_{\eta'\gamma}^{>0.3}) = 11.6 \pm 3.6\,.$$

The probability of the decay $\phi \to \eta'\gamma$ was calculated using the formula:

$$Br(\phi \to \eta'\gamma) = \frac{N_{\eta'\gamma}}{N_{K_S^0 K_L^0}} \times \frac{\varepsilon_{K_S^0 K_L^0} Br(\phi \to K_S^0 K_L^0) Br(K_S^0 \to \pi^+\pi^-) Br(K_L^0 \to \pi^+\pi^-\pi^0)}{[\varepsilon_{\eta\to 3\pi} Br(\eta \to \pi^+\pi^-\pi^0) + \varepsilon_{\eta\to\pi^+\pi^-\gamma} Br(\eta \to \pi^+\pi^-\gamma)] Br(\eta' \to \pi^+\pi^-\eta)}\,.$$

Taking the decay probabilities from [7] the following value of the branching ratio was obtained:

$$Br(\phi \to \eta'\gamma) = (0.58 \pm 0.18 \pm 0.15) \cdot 10^{-4}\,.$$

The last error is due to the systematic uncertainty.

24 Analysis of $\phi \to \eta e^+e^-$, $\eta \to \pi^+\pi^-\pi^0$ decay

In analysis of events of $\phi \to \eta e^+e^-$ decay the kinematic reconstruction was performed with energy-momentum conservation taken into account. The pair of opposite charge particles with the smallest angle between them was considered as a e^+e^- pair. Two remaining charged particles were considered as pions. The procedure described in Section 23 was applied for suppression of "extra" photons.

Criteria used for the selection of the events of $\phi \to \eta e^+e^-$, $\eta \to \pi^+\pi^-\pi^0$ decay are listed below:

- $N_{track} = 4$, $P < 700\,MeV$, $N_\gamma > 1$, $r_{min}(\pi^\pm) < 0.3$ cm — events with pions coming from the interaction region selected.

Since conversion decays feature a small angle between e^+ and e^- the following requirement was applied:

- $\psi(e^+, e^-) < 0.3$

- $M_{inv}(e^+e^-\gamma) > 200$ MeV — events of $\phi \to \pi^+\pi^-\pi^0, \pi^0 \to e^+e^-\gamma$ decay excluded.

For events satisfying all these conditions the distribution over the invariant mass of two pions and two photons $M_{inv}(\pi^+\pi^-\gamma_1\gamma_2)$ is shown in Fig. 46 where the peak around $m_\eta \simeq 548$ MeV is clearly seen. After the additional requirement:

- $M_{inv}(\pi^+\pi^-\gamma_1\gamma_2) < 590$ MeV

$\tilde{N}_{\eta e^+e^-} = 44$ events survived.

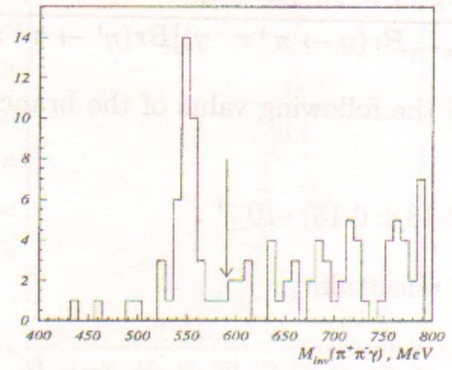

Figure 46: Distribution over the invariant mass $M_{inv}(\pi^+\pi^-\gamma\gamma)$

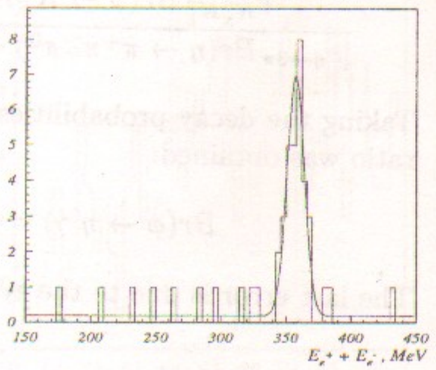

Figure 47: Distribution over the sum energy of e^+e^--pair

Figure 47 shows the distribution over the total energy of the e^+e^- pair. The peak at ~ 360 MeV corresponds to the energy of the virtual photon in the conversion decay $\phi \to \eta\gamma^*, \gamma^* \to e^+e^-$. The fit of the $E_{e^+} + E_{e^-}$ spectrum was performed by the sum of a Gaussian and the flat background distribution. Thus, the number of events from the decay $\phi \to \eta e^+e^-, \eta \to \pi^+\pi^-\pi^0$ was found to be:

$$N_{\eta e^+e^-} = 30 .$$

The efficiency of the selection requirements was determined from the simulation:

$$\varepsilon_{\eta e^+e^-} = 0.130 \pm 0.003 .$$

To calculate the probability of the decay $\phi \to \eta e^+e^-$ and for the normalization the process $\phi \to \pi^+\pi^-\pi^0, \pi^0 \to e^+e^-\gamma$ was used. Selection of events of this process was done according to the following condition:

- $N_{track} = 4$, $P < 700$ MeV, $N_\gamma > 0$, $r_{min}(\pi^\pm) < 0.3$ cm, $\psi(e^+e^-) < 0.3$
- $|M_{inv}(e^+e^-\gamma) - 135| < 40$ MeV.

The selection efficiency is:

$$\varepsilon_{\pi^0\to e^+e^-\gamma} = 0.0675 \pm 0.0025 .$$

The number of selected events was: $N_{\pi^0\to e^+e^-\gamma} = 1248$. The probability of the $\phi \to \eta e^+e^-$ decay was calculated from the formula:

$$Br(\phi \to \eta e^+e^-) = \frac{N_{\eta e^+e^-}}{N_{\pi^0\to e^+e^-\gamma}} \times \frac{Br(\phi \to \pi^+\pi^-\pi^0)Br(\pi^0 \to e^+e^-\gamma)\varepsilon_{\pi^0\to e^+e^-\gamma}}{Br(\eta \to \pi^+\pi^-\pi^0)\varepsilon_{\eta e^+e^-}} .$$

Using the number of events and efficiencies found previously and the decay probabilities from [7], the following branching ratio was obtained:

$$Br(\phi \to \eta e^+e^-) = (1.00 \pm 0.18) \cdot 10^{-4} .$$

25 Search for $\eta \to \pi^+\pi^-e^+e^-$ decay

The decay mode $\phi \to \eta\gamma$ serves as a source of η-mesons tagged by a monochromatic photon with the energy $E_\gamma \simeq 360$ MeV.

A search for the decay $\eta \to \pi^+\pi^-e^+e^-$ was performed using the data sample collected in **PHI-98** experiment. Data analysis included full kinematic fit as described in Section 24. The following criteria were used for event selection:

- $N_{track} = 4$, $P < 700$ MeV, $N_\gamma = 1$, $r_{min}(\pi^\pm) < 0.3$ cm
- The angle between e^+e^- tracks: $\psi(e^+, e^-) < 0.5$
- The requirement $M(e^+, e^-, \gamma_1) > 200$ MeV rejected events of the process $\phi \to \pi^+\pi^-\pi^0, \pi^0 \to e^+e^-\gamma$

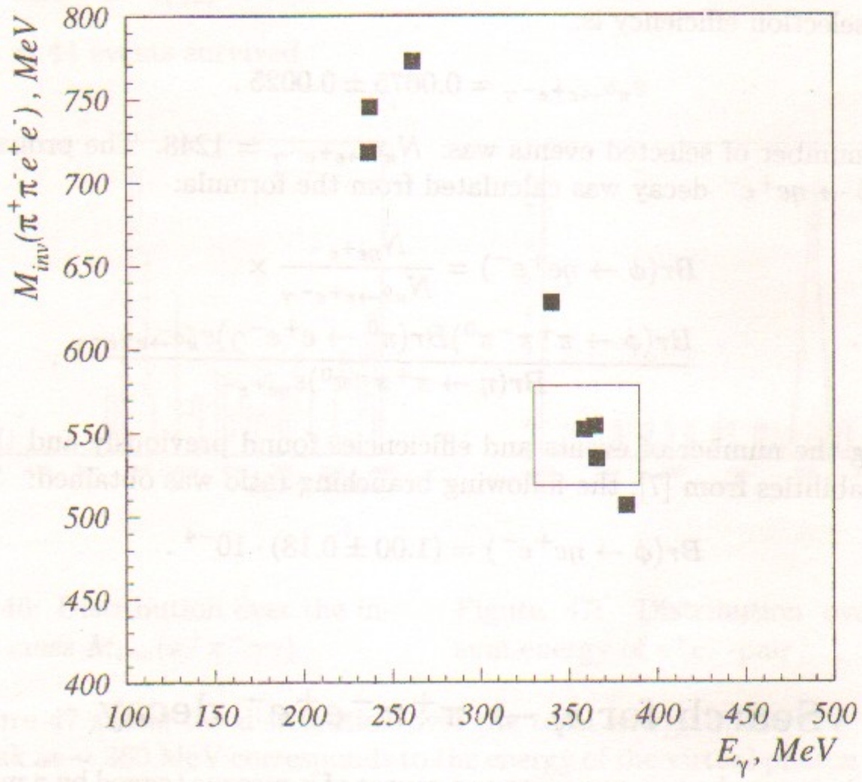

Figure 48: Distribution of the invariant mass of $\pi^+\pi^-e^+e^-$ vs the photon energy

- Events of conversion decay $\phi \to \eta e^+e^-$ were suppressed by the condition: $E_{e^+} + E_{e^-} < 330$ MeV.

Figure 48 shows distribution over the invariant mass of all four charge particles versus the photon energy. For the decay under consideration, the distributions over these parameters should have peaks around $m_\eta \simeq 548$ MeV and $E_\gamma \simeq 360$ MeV. As it is seen in Fig. 48, this region is actually populated with few events. After the requirement:

- $|M(\pi^+\pi^-e^+e^-) - 548| < 30$ MeV, $|E_\gamma - 360| < 30$ MeV

$N_{\eta\to\pi^+\pi^-e^+e^-} = 3$ events were selected.

The main background for the decay $\eta \to \pi^+\pi^-e^+e^-$ comes from the process $\phi \to \eta\gamma\,, \eta \to \pi^+\pi^-\pi^0$ and $\pi^0 \to e^+e^-\gamma$ when the photon from π^0 decay escapes detection in the calorimeter. But the distribution of invariant mass $M_{inv}(\pi^+\pi^-e^+e^-)$ for these events is broad and does not have any peak near $m_\eta \simeq 548$ MeV. Number of expected background events was found from simulation: $N_{bg} = 0.5 \pm 0.2$.

The decay probability was determined from the formula:

$$Br(\eta \to \pi^+\pi^-e^+e^-) = \frac{N_{\eta\to\pi^+\pi^-e^+e^-}}{N_{\pi^0\to e^+e^-\gamma}} \frac{Br(\phi \to \pi^+\pi^-\pi^0)Br(\pi^0 \to e^+e^-\gamma)}{Br(\phi \to \eta\gamma)}\,.$$

The following value was obtained:

$$Br(\eta \to \pi^+\pi^-e^+e^-) = (3.5 \pm 2.0) \cdot 10^{-4}\,.$$

26 $e^+e^- \to \pi^+\pi^-\pi^+\pi^-$ below ϕ-meson

For analysis of the process $e^+e^- \to \pi^+\pi^-\pi^+\pi^-$ in the c.m. energy range 600–1060 MeV the data samples collected in **PHI-98** and **RHOM-98** experiments were used. Analysis of the data included the kinematic fit with the constraint $\sum_i \vec{p}_i = 0$. All charged particles were considered as pions.

The following criteria were used for event selection:

- $N_{track} = 4$, $\max|\cos\theta_i| < 0.8$, $r_{min} < 0.3$ cm
- To suppress conversion decays the requirement was applied: $\min\psi(\pi^+,\pi^-) > 0.3$

- $|\sum_i \sqrt{\vec{p}_i^{\,2} + m_{\pi^\pm}^2}/2E_{beam} - 1| < 0.1$.

The cross section of the process $e^+e^- \to \pi^+\pi^-\pi^+\pi^-$ was calculated using the formula:

$$\sigma = \frac{N_{4\pi}}{L\varepsilon}$$

The detection efficiency for each energy point was determined from the simulation of the process $e^+e^- \to 4\pi$ with the uniform distribution of the final particles in phase space. The obtained cross section is shown in Fig. 49.

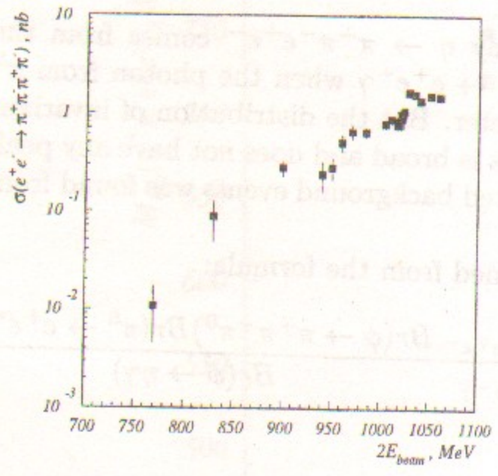

Figure 49: Cross section of the process $e^+e^- \to \pi^+\pi^-\pi^+\pi^-$ below ϕ-meson

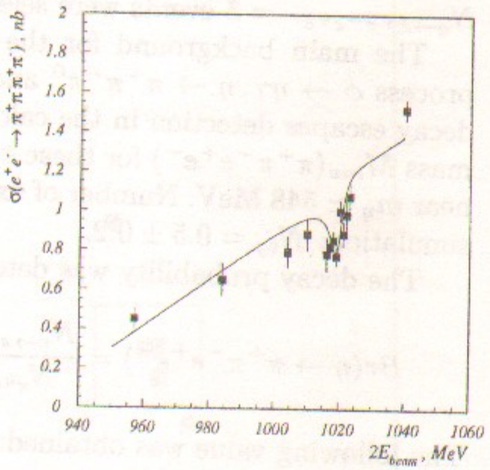

Figure 50: Cross section of the process $e^+e^- \to \pi^+\pi^-\pi^+\pi^-$ near ϕ-meson

In the energy range $E_{beam} = 365$–405 MeV (around the maximum of ρ-meson) $N_{4\pi} = 3$ events were selected. The number of expected background events was estimated to be ~ 1. The main source of the background was the decay $\omega \to \pi^+\pi^-\pi^0$,$\pi^0 \to e^+e^-\gamma$. Assuming that the contribution of the higher ρ recurrences ($\rho(1450)$, $\rho(1700)$) to the observed 4π events is negligible so that all of them come from the ρ-meson decay, the following upper limit was set:

$$\sigma(e^+e^- \to \rho \to \pi^+\pi^-\pi^+\pi^-) < 0.024\,\text{nb} \quad \text{at } 90\%\ \text{CL.}$$

The corresponding upper limit for the partial decay width is

$$\Gamma(\rho \to \pi^+\pi^-\pi^+\pi^-) < 3\,\text{keV} \quad \text{at } 90\%\ \text{CL.}$$

This value is 10 times lower than previous measurement [68]. Several theoretical calculations [65]–[67] exist for $\Gamma(\rho \to \pi^+\pi^-\pi^+\pi^-)$. Table 5 summarizes these predictions. Our result certainly excludes theoretical models considered in [65] and [66] and does not contradict to the calculations in [67].

Table 5: Theoretical predictions for the decay width $\Gamma(\rho \to \pi^+\pi^-\pi^+\pi^-)$

Work	$\Gamma_{\rho\to\pi^+\pi^-\pi^+\pi^-}$, keV
[65]	6
	25
	57
[66]	16
[67]	0.59–1.03

The behaviour of the cross section near the ϕ-meson is shown in more detail in Fig. 50. The cross section was fitted using the following formula:

$$\sigma_{4\pi} = \sigma_0\,(1 + A(E - m_\phi))\left|1 - Z\frac{m_\phi\Gamma_\phi}{m_\phi^2 - E^2 - iE\cdot\Gamma_\phi}\right|^2,$$

where $E = 2E_{beam}$, σ_0 is a non resonant cross section of the process $e^+e^- \to \pi^+\pi^-\pi^+\pi^-$ at $E = m_\phi$, A is a slope parameter, m_ϕ and Γ_ϕ are the ϕ-meson mass and width and $Z = e^{i\psi}$ is a complex interference amplitude. The following values were obtained from the fit:

$$\begin{aligned} \sigma_0 &= 1.08 \pm 0.03\,\text{nb}, \\ A &= 0.011 \pm 0.001\,\text{MeV}^{-1}, \\ Im(Z) &= 0.080 \pm 0.024, \\ Re(Z) &= -0.150 \pm 0.022. \end{aligned}$$

This allows to obtain $|Z|$ and ψ:

$$\begin{aligned} |Z| &= 0.170 \pm 0.024, \\ \phi &= (-62 \pm 8)^\circ. \end{aligned}$$

Then the branching ratio of the decay $\phi \to 4\pi$ can be obtained:

$$Br(\phi \to \pi^+\pi^-\pi^+\pi^-) = \frac{\sigma_0|Z|^2}{\sigma_\phi} = (0.77 \pm 0.21 \pm 0.20)\cdot 10^{-5},$$

where σ_ϕ is the cross section in the maximum of ϕ-meson. The last error in this result is the systematic one. It takes into account the model dependency in the calculation of the detection efficiency and σ_0. Some work is still needed for correct understanding of the systematic errors. Nevertheless, evidence for the decay $\phi \to \pi^+\pi^-\pi^+\pi^-$ could be claimed.

27 Study of the process $e^+e^- \to 4\pi$ above ϕ-meson

The process of 4π production is one of the dominant in the total cross section of e^+e^- annihilation into hadrons in the energy range from 1.05 to 2.5 GeV. For the first time it was observed in Frascati [69] and Novosibirsk [70]. The first experiments with limited data samples allowed a qualitative study of the new phenomenon of multiple production of hadrons and estimated the magnitude of the corresponding cross sections. Subsequent measurements by M2N [71], DM1 [72] and DM2 [73] in Orsay as well as by OLYA [68], CMD [78] and ND [74] in Novosibirsk obtained more detailed information on the energy dependence of the cross sections of the processes $e^+e^- \to 4\pi^\pm$ and $e^+e^- \to \pi^+\pi^-2\pi^0$.

The abundance of the different mechanisms and their complicated interference results in the necessity of simultaneous analysis of two possible final states ($2\pi^+2\pi^-$ and $\pi^+\pi^-2\pi^0$) which requires a general purpose detector capable of measuring energies and angles of both charged and neutral particles.

Our analysis is based on the data sample corresponding to the integrated luminosity of 5.8 pb^{-1} collected in 1997 **HIGH-97** while scanning the c.m.energy range 1.05–1.38 GeV. To describe four pion production we used a simple model assuming quasitwoparticle intermediate states taking into account identical final pions (see [75]) and the interference of all possible amplitudes.

To select events of the process $e^+e^- \to \pi^+\pi^-\pi^0\pi^0$, the following criteria were applied :

- $N_{track} = 2$
- $N_{vert} = 1$
- $Q_1 + Q_2 = 0$
- $\max(r_{min}) < 0.3\ cm$
- $|z_{vert}| < 10\ cm$

- $|\Delta\phi| > 0.1$
- $\theta_{min} > 0.54$
- $N_\gamma(E_\gamma > 20\ MeV) > 3$
- $N_{\pi^0} > 1$.

For all possible combinations of $\pi^0\pi^0$, the kinematic fit was performed with the following constraints :

- $\sum_i E_i = 2E_{beam}$
- $\sum_i \vec{p_i} = 0$
- $M_{\gamma_1\gamma_2} = m_{\pi^0}$
- $M_{\gamma_3\gamma_4} = m_{\pi^0}$.

For further analysis the combination with $\min(\chi^2)$ was selected under the condition $\chi^2 < 16$. After such selection 22128 events remained.

Figure. 51 shows the distribution over $M_{recoil}(\pi^0)$ at the energy $E_{beam} =$ 690 MeV. Each event gives two entries to the histogram corresponding to two π^0. Points with errors are the data, the histogram shows MC simulation. A signal from the process $\omega\pi^0$ is clearly seen.

To select the process $\omega\pi^0$, all the data was divided into two classes:

1. $\min(|M_{recoil}(\pi^0) - m_\omega|) < 70$ MeV
2. $\min(|M_{recoil}(\pi^0) - m_\omega|) > 70$ MeV

The first class contains mainly $\omega\pi^0$ events while the second one has a relatively small admixture of $\omega\pi^0$ ($1 \div 5\%$). Since the matrix element for the channel $\omega\pi^0$ can be written unambiguously, one can use the events from the first class to test the adequacy of the total MC simulation [59].

Figures 52, 53 show the distributions over $M_{inv}(\pi^\pm\pi^0)$, $M_{recoil}(\pi^\pm)$, $M_{inv}(\pi^+\pi^-)$, $M_{inv}(\pi^0\pi^0)$, $\cos(\psi_{\pi^\pm\pi^0})$, $\cos(\psi_{\pi^+\pi^-})$, $\cos(\psi_{\pi^0\pi^0})$ and $M_{recoil}(\pi^0)$. Good consistence of the data and MC makes us confident that MC simulation adequately reproduces both the kinematics of produced particles and the detector response to them.

Similar distributions for the events of the second class are shown in Figs. 54, 55. A clear signal of $\rho^\pm$ is observed while there is no signal of the ρ^0. Thus, one can assume that these events originate from a heavy isospin 1 resonance. The best candidate for this intermediate state is $a_1(1260)$.

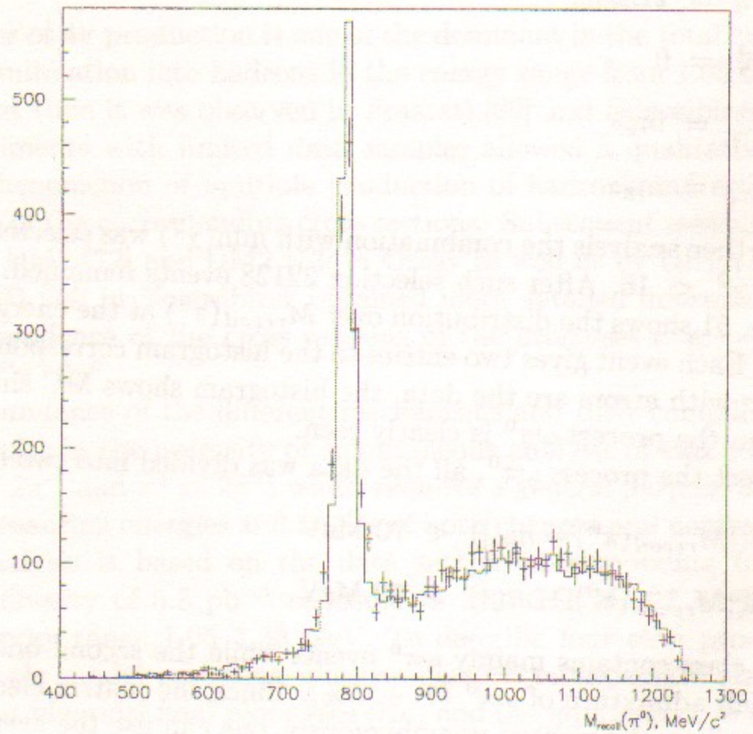

Figure 51: Distribution over π^0 recoil mass for $\pi^+\pi^-2\pi^0$

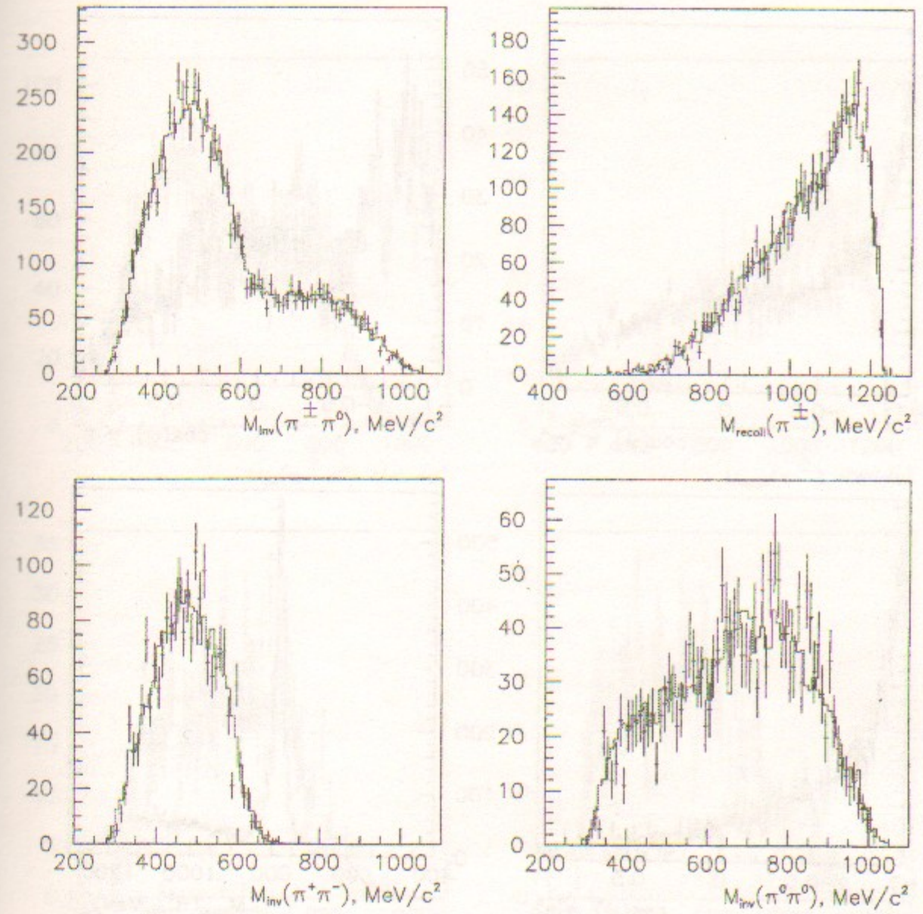

Figure 52: Distributions over $M_{inv}(\pi^{\pm}\pi^0)$, $M_{recoil}(\pi^{\pm})$, $M_{inv}(\pi^+\pi^-)$, $M_{inv}(\pi^0\pi^0)$ for $\pi^+\pi^-2\pi^0$ events from the class (1)

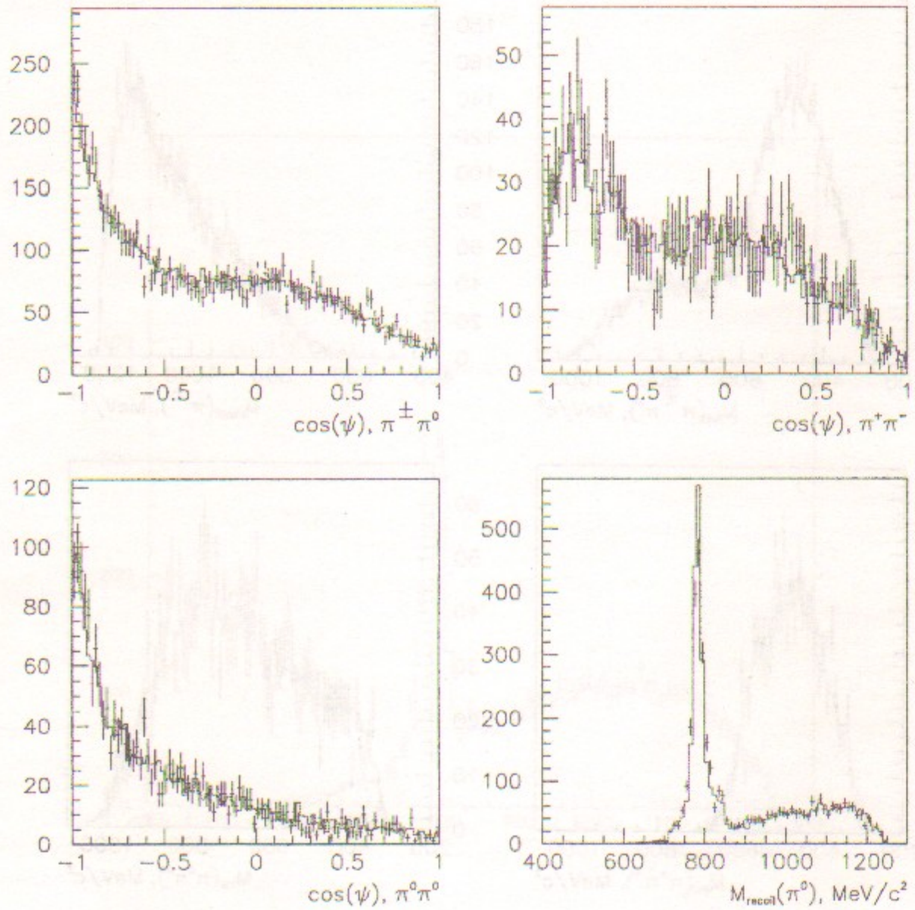

Figure 53: Distributions over $\cos(\psi_{\pi^\pm\pi^0})$, $\cos(\psi_{\pi^+\pi^-})$, $\cos(\psi_{\pi^0\pi^0})$ and $M_{recoil}(\pi^0)$ for $\pi^+\pi^-2\pi^0$ events from the class (1)

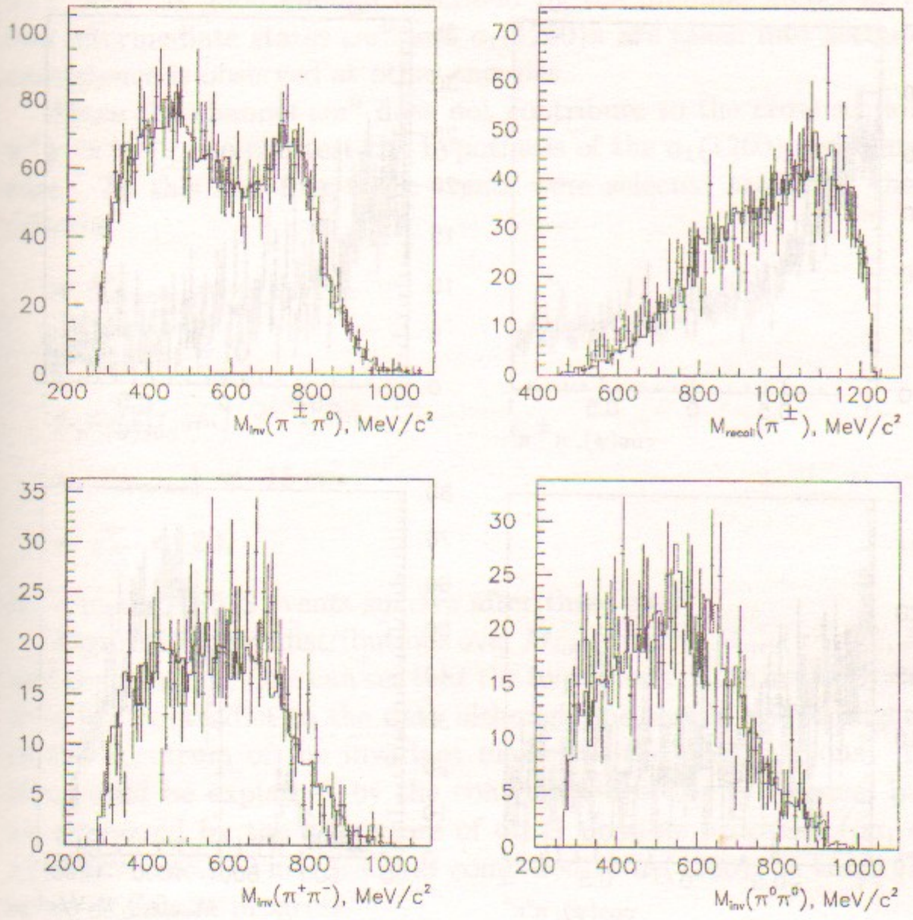

Figure 54: Distributions over $M_{inv}(\pi^\pm\pi^0)$, $M_{recoil}(\pi^\pm)$, $M_{inv}(\pi^+\pi^-)$, $M_{inv}(\pi^0\pi^0)$ for $\pi^+\pi^-2\pi^0$ events from the class (2)

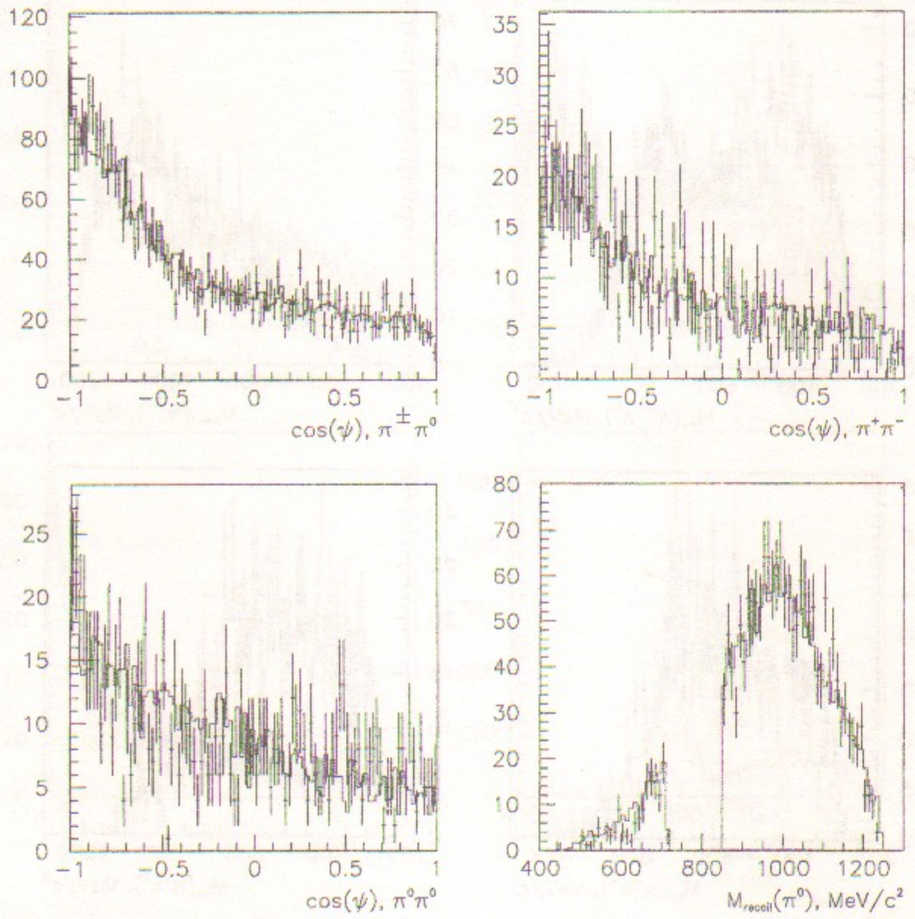

Figure 55: Distributions over $\cos(\psi_{\pi^\pm\pi^0})$, $\cos(\psi_{\pi^+\pi^-})$, $\cos(\psi_{\pi^0\pi^0})$ and $M_{recoil}(\pi^0)$ for $\pi^+\pi^-2\pi^0$ events from the class (2)

Histograms in Figs. 51, 52, 53, 54, 55 correspond to the simulation of the processes $\omega\pi^0$ and $a_1(1260)\pi$ taking into account their interference as well as the interference of the diagrams differing by permutations of identical final pions [76]. In the simulation the mass $m_{a_1} = 1230$ MeV was fixed [7], while the free parameters were Γ_{a_1}, the normalization and phase of the interference amplitude of these two contributions. One can see that the process $\pi^+\pi^-\pi^0\pi^0$ is good enough described by the minimal model in which only two intermediate states $\omega\pi^0$ and $a_1(1260)\pi$ are taken into account. Similar consistence is observed at other energies.

Since the channel $\omega\pi^0$ does not contribute to the cross section $e^+e^- \to \pi^+\pi^-\pi^+\pi^-$, one can test the hypothesis of the $a_1(1260)$ dominance for this case. To this end four-track events were selected satisfying the following criteria:

- $N_{track} = 4$
- $\sum_i Q_i = 0$
- $\max(r_{min}) < 1\ cm$
- $|Z_{tracks}| < 15\ cm$
- $\chi^2_E < 20$.

As a result, 28552 events survive after these cuts.

Figure 56 shows distributions over $M_{inv}(\pi^\pm\pi^\mp)$, $M_{inv}(\pi^\pm\pi^\pm)$, $M_{recoil}(\pi^\pm)$ and $\cos(\psi_{\pi^\pm\pi^\mp})$. One can see that the hypothesis of the $a_1(1260)\pi$ dominance does not contradict to the data although one should note a slight deviation in the spectrum of the invariant masses of the likesign pions. This deviation could be explained by the contribution of the $D-wave$, but can not be explained by the admixture of other possible processes ($\rho\sigma$, $a_2(1320)\pi$, $\pi(1300)\pi$, etc.). Their fraction compared to $a_1(1260)\pi$ is small [76] and its study is now in progress.

It is important to note that due to the strong interference ($5 \div 10\%$) between $\omega\pi^0$ and $\pi^+\pi^-\pi^0\pi^0$, extraction of the cross sections of the separate channels loses its usual meaning. Nevertheless, to simplify the presentation, we neglect the interference effects while showing the cross sections of $\omega\pi^0$ and $\pi^+\pi^-\pi^0\pi^0$ and include the arising uncertainty into the systematic error.

To determine total cross sections selection criteria were modified and the cut $\cos(\psi) < 0.7$ was applied where ψ is the angle between the photon direction in the π^0 rest frame and its momentum. This cut allowed to improve the stability of the detection efficiency.

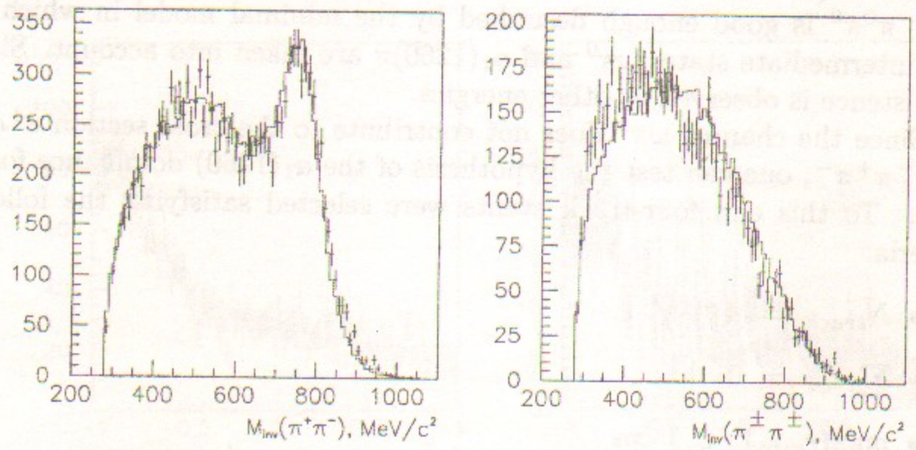

Figure 56: Distributions over $M_{inv}(\pi^\pm\pi^\mp)$, $M_{inv}(\pi^\pm\pi^\pm)$, $M_{recoil}(\pi^\pm)$ and $\cos(\psi_{\pi^\pm\pi^\mp})$ for $4\pi^\pm$ events

Cross sections were calculated from the formulae:

$$\sigma_{\omega\pi^0} = \frac{N_\omega}{Br(\omega \to 3\pi)\cdot(1+\delta)\cdot L\cdot\varepsilon},$$

$$\sigma_{\pi^+\pi^-\pi^0\pi^0} = \frac{N_{a_1}}{(1+\delta)\cdot L\cdot\varepsilon},$$

where L is the luminosity, ε is the detection efficiency from MC, δ is a radiative correction calculated according to [34].

The number of events N_ω N_{a_1} was determined from:

$$N_\omega = \frac{\beta\cdot N_1 - (1-\beta)\cdot N_2}{\alpha+\beta-1},$$

$$N_{a_1} = \frac{\alpha\cdot N_2 - (1-\alpha)\cdot N_1}{\alpha+\beta-1},$$

where N_1 and N_2 are the number of events in class (1) and (2), α is the probability for the $\omega\pi^0$ event to enter class (1) and β is the probability for the $a_1\pi$ event to enter class (2). α and β were taken from MC. The overall systematic uncertainty for $\pi^+\pi^-\pi^0\pi^0$ was estimated to be $\sim$ 15%.

Figure 57 shows the obtained cross sections for $e^+e^- \to \omega\pi^0$ and $e^+e^- \to \pi^+\pi^-\pi^0\pi^0$.

Figure 59 shows the total cross section which is consistent with the previous measurement at OLYA and within systematic errors does not contradict to the recent result from SND. Also shown are results from other Novosibirsk, Orsay and Frascati groups.

To determine the cross section $e^+e^- \to \pi^+\pi^-\pi^+\pi^-$ the selection criteria were also modified:

- $\chi^2_E < 50$
- $\theta_{min} > 0.67$
- $|\sum_i E_i - E_{beam}| < 0.2\cdot E_{beam}$
- $|\sum_i \vec{p_i}| < 0.3\cdot E_{beam}$,

where E_i, $\vec{p_i}$ are pion energies and momenta before the kinematic reconstruction.

The cross section was determined from the formula:

$$\sigma_{\pi^+\pi^-\pi^+\pi^-} = \frac{N_{4\pi}}{(1+\delta)\cdot L\cdot\varepsilon}.$$

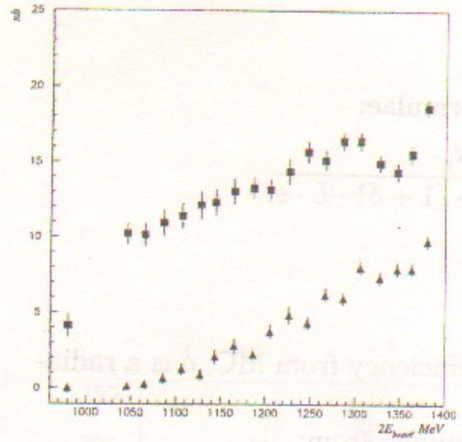

Figure 57: Energy dependence of $\sigma(e^+e^- \to \omega\pi^0)$—upper and $\sigma(e^+e^- \to \pi^+\pi^-2\pi^0)$—lower where the contribution of $\omega\pi^0$ is subtracted

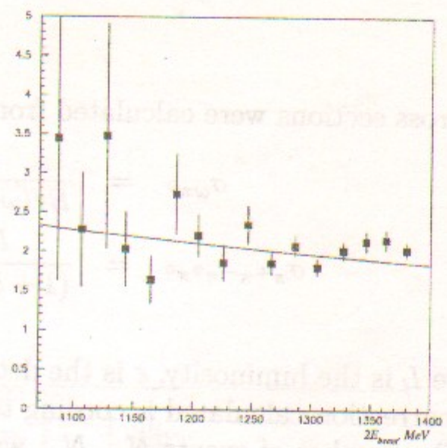

Figure 58: Energy dependence of the ratio $\frac{\sigma(e^+e^- \to \pi^+\pi^-\pi^+\pi^-)}{\sigma(e^+e^- \to \pi^+\pi^-\pi^0\pi^0)}$. The contribution of $\omega\pi^0$ is subtracted. The solid curve shows the theoretical prediction based on the $a_1\pi$ dominance

The systematic uncertainty for $\pi^+\pi^-\pi^+\pi^-$ is also $\sim$ 15%.

The obtained cross section is shown in Fig. 60. It is consistent with the previous measurement at OLYA and within systematic errors does not contradict to the recent result from SND. Also shown are results from other Novosibirsk, Orsay and Frascati groups.

Figure 58 presents the ratio of the cross sections $\sigma(e^+e^- \to \pi^+\pi^-\pi^+\pi^-)$ and $\sigma(e^+e^- \to \pi^+\pi^-\pi^0\pi^0)$ where the contribution of $\omega\pi^0$ is subtracted. The solid curve shows the theoretical prediction based on the $a_1\pi$ dominance.

Thus, in this work it is shown for the first time that in addition to the $\omega\pi^0$ the considerable contribution to the cross section of the process $e^+e^- \to \pi^+\pi^-\pi^0\pi^0$ comes from the $a_1(1260)\pi$ channel. The later simultaneously accounts for the dynamics of $\pi^+\pi^-\pi^+\pi^-$ production in the energy range 1.05 to 1.40 GeV.

28 Evidence for $\omega\pi^0\pi^0$ production

In order to investigate the background to $e^+e^- \to \pi^+\pi^-2\pi^0$ coming from the processes with extra π^0 in the final state, we select the events with $N_{track} = 2$ and $N_\gamma > 5$. The event selection and procedure of kinematical reconstruc-

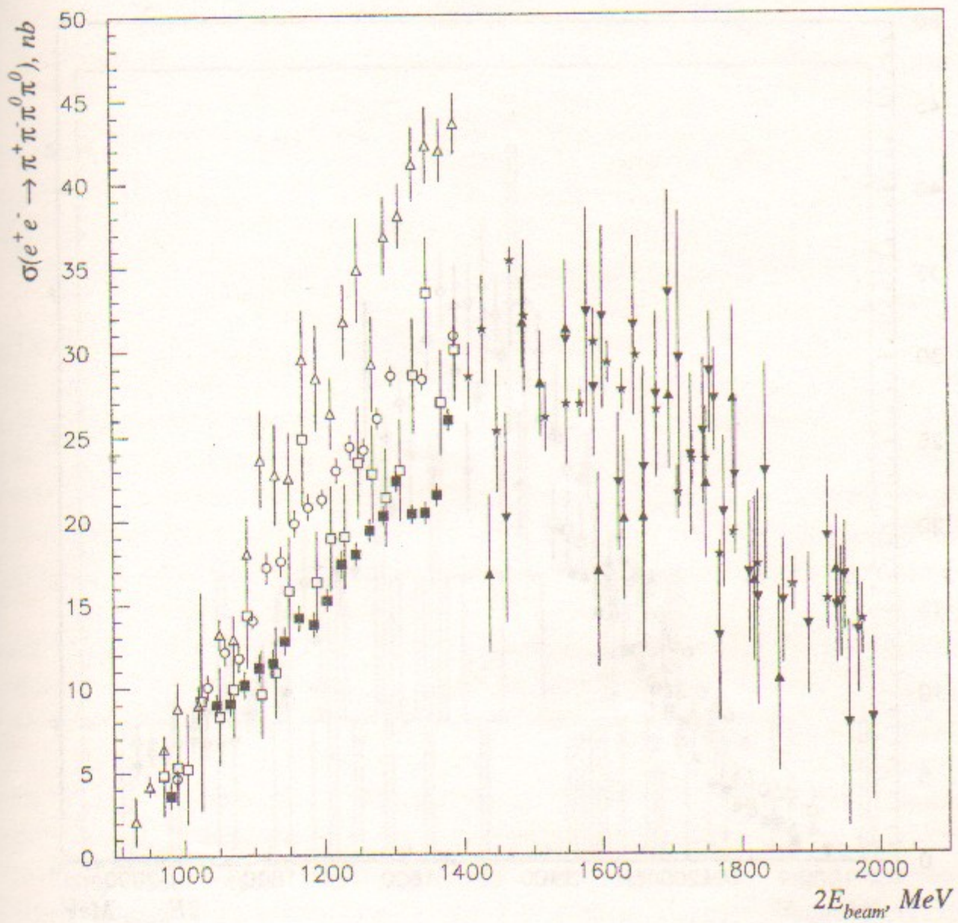

Figure 59: Energy dependence of the $\pi^+\pi^-2\pi^0$ cross section. Below 1.4 GeV solid squares are results of this work

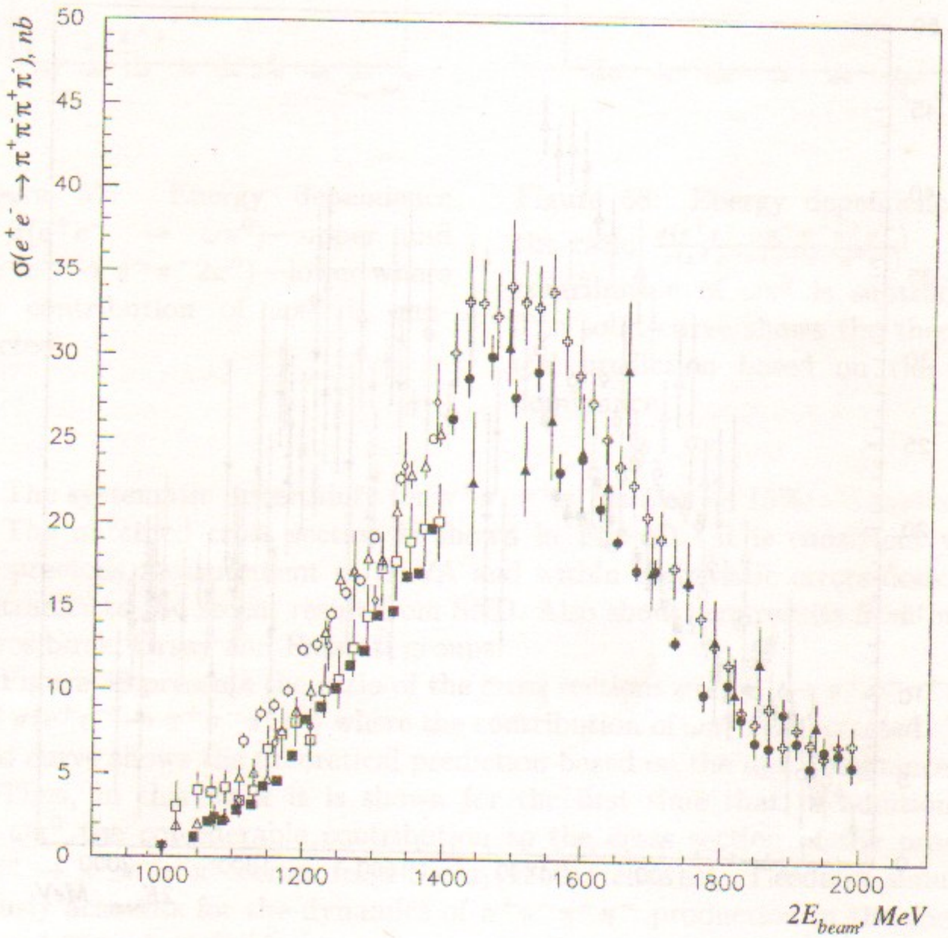

Figure 60: Energy dependence of $\pi^+\pi^-\pi^+\pi^-$ cross section. Below 1.4 GeV solid squares are results of this work

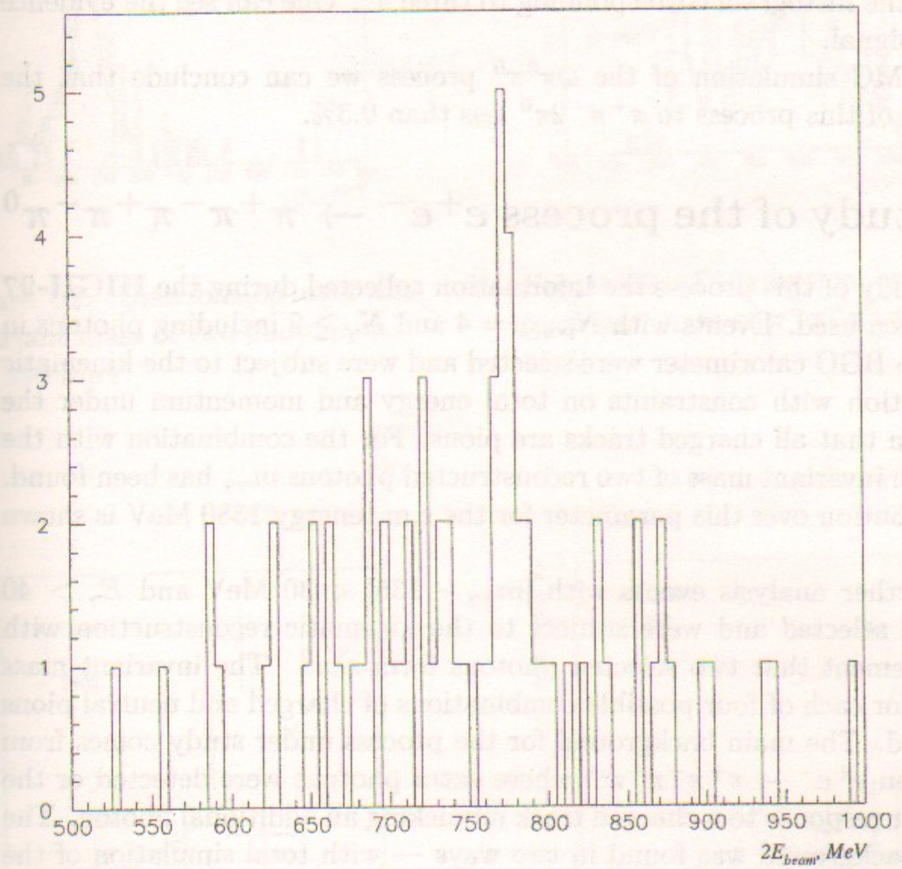

Figure 61: Distribution of $\pi^+\pi^-\pi^0$ invariant mass for $\pi^+\pi^-3\pi^0$ events

tion was the same as for $e^+e^- \to \pi^+\pi^-2\pi^0$ except that the three π^0's were required. To suppress the main background coming from $e^+e^- \to \pi^+\pi^-2\pi^0$, we require that $\chi^2 < 10$.

In the distribution of $M_{inv}(3\pi^0)$ a signal from the process $e^+e^- \to \eta\pi^+\pi^-$ with $\eta \to 3\pi^0$ is clearly seen. In order to suppress this events, we require that $M_{inv}(3\pi^0) > 650$ MeV. Figure 61 shows the distribution of $M_{inv}(\pi^+\pi^-\pi^0)$ for the energy range $1300 < 2 \cdot E_{beam} < 1400$ MeV. Each event gives three entries to the histogram corresponding to three π^0. One can see the evidence for the ω signal.

Using MC simulation of the $\omega\pi^0\pi^0$ process we can conclude that the admixture of this process to $\pi^+\pi^-2\pi^0$ less than 0.3%.

29 Study of the process $e^+e^- \to \pi^+\pi^-\pi^+\pi^-\pi^0$

For the study of this process the information collected during the **HIGH-97** run has been used. Events with $N_{track} = 4$ and $N_\gamma \geq 2$ including photons in the endcap BGO calorimeter were selected and were subject to the kinematic reconstruction with constraints on total energy and momentum under the assumption that all charged tracks are pions. For the combination with the best χ^2 the invariant mass of two reconstructed photons $m_{\gamma\gamma}$ has been found. The distribution over this parameter for the c.m. energy 1380 MeV is shown in Fig. 62.

For further analysis events with $|m_{\gamma\gamma} - 135| < 30$ MeV and $E_\gamma > 40$ MeV were selected and were subject to the kinematic reconstruction with the requirement that two selected photons form a π^0. The invariant mass $m_{\pi^+\pi^-\pi^0}$ for each of four possible combinations of charged and neutral pions was plotted. The main background for the process under study comes from the reaction $e^+e^- \to \pi^+\pi^-\pi^+\pi^-$ where extra photons were detected or the calorimeter response to a charged track mimicking an additional photon. The shape of background was found in two ways — with total simulation of the $e^+e^- \to a_1\pi \to \pi^+\pi^-\pi^+\pi^-$ channel and assuming that events at the energy below 1280 MeV come from a background process only. The shapes of both distributions were found to be in good consistence with one another.

Detection efficiencies as well as the shapes of signal and combinatorial background were found from the total simulation for the processes $e^+e^- \to \eta\pi^+\pi^-$ and $e^+e^- \to \omega\pi^+\pi^-$ with a consequent decay of ω and η into three pions. It was assumed that ω decays into three pions via $\rho\pi$. The detection efficiencies were found to be $(28.0 \pm 0.5)\%$ and $(24.0 \pm 0.5)\%$ for $\omega\pi^+\pi^-$ and $\eta\pi^+\pi^-$ channels respectively independently of the energy. The radiative

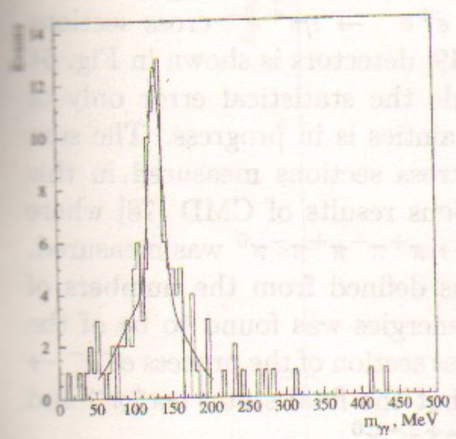

Figure 62: Distribution over the invariant mass of two photons $m_{\gamma\gamma}$ at 1380 MeV

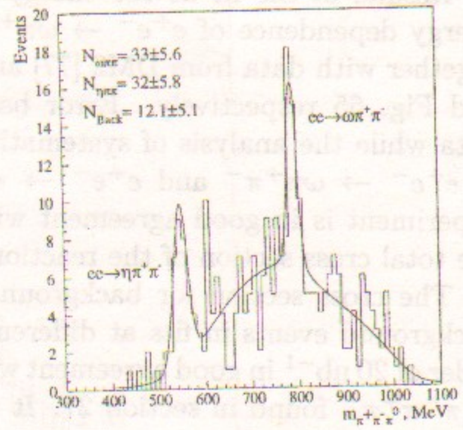

Figure 63: Distribution over the invariant mass of $\pi^+\pi^-\pi^0$ at 1380 MeV

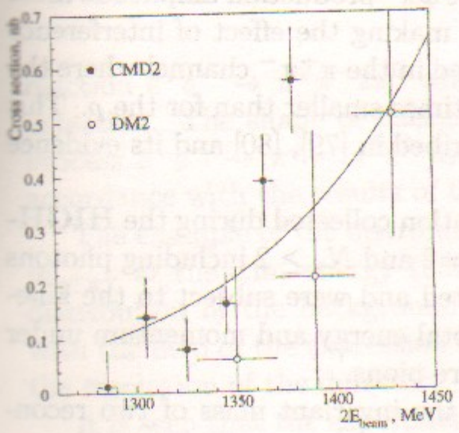

Figure 64: $e^+e^- \to \omega\pi^+\pi^-$ cross section

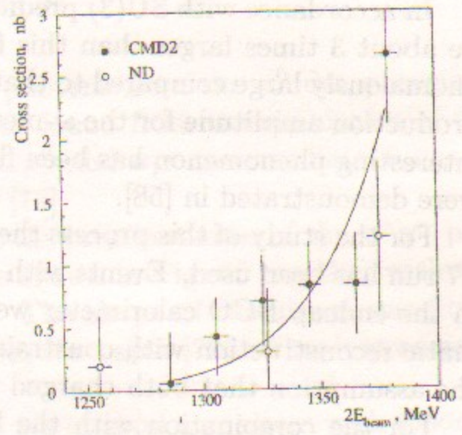

Figure 65: $e^+e^- \to \eta\pi^+\pi^-$ cross section

correction for the processes under study equals 25%.

Results of the fit at the energy 1380 MeV are shown in Fig. 63. The energy dependence of $e^+e^- \to \omega\pi^+\pi^-$ and $e^+e^- \to \eta\pi^+\pi^-$ cross sections together with data from DM2 [77] and ND [49] detectors is shown in Fig. 64 and Fig. 65 respectively. Error bars include the statistical error only of data while the analysis of systematic uncertainties is in progress. The sum of $e^+e^- \to \omega\pi^+\pi^-$ and $e^+e^- \to \eta\pi^+\pi^-$ cross sections measured in this experiment is in good agreement with previous results of CMD [78] where the total cross section of the reaction $e^+e^- \to \pi^+\pi^-\pi^+\pi^-\pi^0$ was measured.

The cross section for background process defined from the numbers of background events in fits at different c.m. energies was found to be of the order of 20 nb^{-1} in good agreement with a cross section of the process $e^+e^- \to \pi^+\pi^-\pi^+\pi^-$ found in section 27. It means that the final states $\omega\pi^+\pi^-$ and $\eta\pi^+\pi^-$ saturates the process $e^+e^- \to \pi^+\pi^-\pi^+\pi^-\pi^0$.

30 Evidence for $\rho - \omega$ interference in the reaction $e^+e^- \to \pi^+\pi^-\pi^0$ above ϕ-meson

The effect of the $\rho-\omega$ interference is usually studied in the reaction $e^+e^- \to \pi^+\pi^-$ (see Section 9). However there exist another interesting possibility to study this effect in the reaction $e^+e^- \to \pi^+\pi^-\pi^0$ above the ϕ-meson.

In accordance with SU(3) predictions the $\omega\pi^0$ production amplitude must be about 3 times larger than this for $\rho^0\pi^0$ making the effect of interference anomalously large compared to that observed in the $\pi^+\pi^-$ channel where the production amplitude for the ω-meson is 3 times smaller than for the ρ. This interesting phenomenon has been first described in [79], [80] and its evidence were demonstrated in [58].

For the study of this process the information collected during the **HIGH-97** run has been used. Events with $N_{track} = 2$ and $N_\gamma \geq 2$ including photons in the endcap BGO calorimeter were selected and were subject to the kinematic reconstruction with constraints on total energy and momentum under the assumption that both charged tracks are pions.

For the combination with the best χ^2 the invariant mass of two reconstructed photons $m_{\gamma\gamma}$ has been found.

For further analysis events with $|m_{\gamma\gamma} - 135| < 20$ MeV, $E_\gamma > 40$ MeV, $0.2 < \psi < 2.8$ rad and $r_{vert} < 0.3$ cm were selected and were subject to the kinematic reconstruction with the requirement that two selected photons form a π^0. The main background for the process under study comes from the

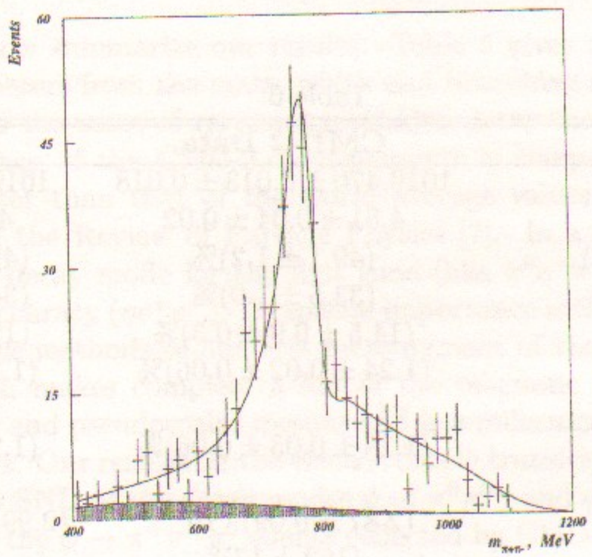

Figure 66: Observation of $\rho - \omega$ interference in the invariant mass spectrum of charged pion pairs in the reaction $e^+e^- \to \pi^+\pi^-\pi^0$ at $1340 \div 1360$ MeV. Fitted histogram - experimental distribution over the $\pi^+\pi^-$ invariant mass; hatched plot - $\pi^+\pi^-$ invariant mass distribution for the background process $e^+e^- \to \pi^+\pi^-\pi^0\pi^0$ included in the whole fit

reaction $e^+e^- \to \pi^+\pi^-2\pi^0$ where two photons from the π^0 decay escaped detection. The shape of background was found from the simulation of the process $e^+e^- \to \pi^+\pi^-\pi^0\pi^0$ assuming $\omega\pi^0$ and $a_1\pi$ intermediate states in accordance with the results of the work [76].

The example of the distribution over the invariant mass of the $\pi^+\pi^-$ pair $m_{\pi^+\pi^-}$ at the c.m. energy 1350 MeV is shown in Fig. 66 together with the distribution of the background events. The shape of the signal was fitted with the help of the expression taken from the paper [79] taking into account the resolution of the detector.

It is seen that the experimental data are in good agreement with theoretical expectations with the $\rho - \omega$ mixing parameter δ close to its value known from other experiments almost, i.e. δ is purely real and equals 3.5 MeV.

Table 6:

	CMD-2 Data	PDG'98
m_ϕ, MeV	$1019.470 \pm 0.013 \pm 0.018$	1019.413 ± 0.008
Γ_ϕ, MeV	$4.51 \pm 0.04 \pm 0.02$	4.43 ± 0.05
$Br(\phi \to K^+K^-)$	$(49.1 \pm 1.2)\%$	$(49.1 \pm 0.8)\%$
$Br(\phi \to K_L K_S)$	$(33.5 \pm 1.0)\%$	$(34.1 \pm 0.6)\%$
$Br(\phi \to 3\pi)$	$(14.5 \pm 0.9 \pm 0.3)\%$	$(15.5 \pm 0.7)\%$
$Br(\phi \to \eta\gamma)$	$(1.24 \pm 0.02 \pm 0.06)\%$	$(1.26 \pm 0.06)\%$
$\eta \to \pi^0\pi^0\pi^0$		
$Br(\phi \to \eta\gamma)$	$(1.18 \pm 0.03 \pm 0.06)\%$	$(1.26 \pm 0.06)\%$
$\eta \to \pi^+\pi^-\pi^0$		
$Br(\phi \to e^+e^-)$	$(2.87 \pm 0.09) \cdot 10^{-4}$	$(2.99 \pm 0.08) \cdot 10^{-4}$
$\delta_{\phi-\omega}$	$(162 \pm 17)^\circ$	
$Br(\phi \to \eta'\gamma)$	$(1.35^{+0.55}_{-0.45} \pm 0.2) \cdot 10^{-4}$	$(1.2^{+0.7}_{-0.5}) \cdot 10^{-4}$
$\eta' \to \pi^+\pi^-\gamma\gamma$		
$Br(\phi \to \eta'\gamma)$	$(0.58 \pm 0.18 \pm 0.15) \cdot 10^{-4}$	$(1.2^{+0.7}_{-0.5}) \cdot 10^{-4}$
$\eta' \to \pi^+\pi^-\pi^+\pi^-\pi^0$		
$\eta' \to \pi^+\pi^-\pi^+\pi^-\gamma$		
$Br(\phi \to \eta e^+e^-)$	$(1.12 \pm 0.17 \pm 0.17) \cdot 10^{-4}$	$(1.3^{+0.8}_{-0.6}) \cdot 10^{-4}$
$\eta \to \gamma\gamma$		
$Br(\phi \to \eta e^+e^-)$	$(1.00 \pm 0.18) \cdot 10^{-4}$	$(1.3^{+0.8}_{-0.6}) \cdot 10^{-4}$
$\eta \to \pi^+\pi^-\pi^0$		
$Br(\phi \to \pi^+\pi^-\gamma)$	$(0.38 \pm 0.16) \cdot 10^{-4}$	$< 3 \cdot 10^{-5}$
$Br(\phi \to \pi^0\pi^0\gamma)$	$(1.08 \pm 0.17 \pm 0.09) \cdot 10^{-4}$	$< 1 \cdot 10^{-3}$
$Br(\phi \to \eta\pi^0\gamma)$	$(0.90 \pm 0.24 \pm 0.10) \cdot 10^{-4}$	$< 2.5 \cdot 10^{-3}$
$Br(\phi \to \pi^0 e^+e^-)$	$(1.29 \pm 0.29 \pm 0.19) \cdot 10^{-5}$	$< 1.2 \cdot 10^{-4}$
$Br(\phi \to \mu^+\mu^-\gamma)$	$(1.3 \pm 0.6) \cdot 10^{-5}$	$(2.3 \pm 1.0) \cdot 10^{-5}$
$Br(\phi \to \rho\gamma)$	$< 3 \cdot 10^{-4}$	$< 7 \cdot 10^{-4}$
$Br(\phi \to \rho\gamma\gamma)$	$< 5 \cdot 10^{-4}$	no data
$Br(\phi \to \eta\pi^+\pi^-)$	$< 3 \cdot 10^{-4}$	no data
$Br(\phi \to \mu^+\mu^-)$	$(2.80 \pm 0.30 \pm 0.46) \cdot 10^{-4}$	$(2.5 \pm 0.4) \cdot 10^{-4}$
$Br(\phi \to \pi^+\pi^-)$	$(1.81 \pm 0.25 \pm 0.19) \cdot 10^{-4}$	$(0.8^{+0.5}_{-0.4}) \cdot 10^{-4}$
$Br(\phi \to \pi^+\pi^-)_{direct}$	$< 0.15 \cdot 10^{-4}$	no data
$Br(\phi \to \pi^+\pi^-\pi^+\pi^-)$	$(0.77 \pm 0.21 \pm 0.20) \cdot 10^{-5}$	$< 8.7 \cdot 10^{-4}$

31 Conclusions

Two tables below summarize our results. Table 6 gives the results on the ϕ-meson parameters from the mass, width and branching ratios of the main decay modes to the rates of rare and forbidden decay modes. One can see that the accuracy of the CMD-2 measurements is comparable or in some cases even better than that of the world average values presented in the 1998 edition of the Review of Particle Physics [7]. In a few cases CMD-2 observed some decay mode for the first time (like $\pi^0 e^+e^-$) or significantly improved the accuracy (ηe^+e^-). Of special importance is the confirmation by two independent methods of our first measurement of the rare decay mode $\phi \to \eta'\gamma$ which makes complete a list of the magnetic dipole transitions between vector and pseudoscalar mesons and is a milestone for the theory of radiative decays. Our results on the electric dipole transitions confirm earlier observations by SND of the decay modes $\phi \to \pi^0\pi^0\gamma$ and $\phi \to \eta\pi^0\gamma$. A large data sample of the $\phi \to \pi^+\pi^-\pi^0$ events collected by CMD-2 allowed a study of the decay dynamics from the Dalitz plot and it was shown that the $\rho\pi$ mechanism dominates over the direct 3π production [12].

Table 7 presents our results on the ρ- and ω-meson parameters. It is noteworthy that the new values of the width and particularly the mass of the ω are significantly different from the previous world average values. A very thorough analysis of the possible systematic uncertainties as well as dedicated runs with the beam energy calibration increase our confidence in these results.

Also listed in Table 7 are results obtained in the ϕ-meson energy range using the tagged kaons and η-mesons. This is a good demonstration of the high potential of future ϕ-factories for high precision studies of the kaon and η-meson properties. Finally, we present the cross section of the kaon regeneration and total inelastic cross section obtained for the first time at a very small momentum of 110 MeV/c, also relevant to CP studies at the ϕ-factories.

Not shown in these tables are the results obtained on multihadronic production above the ϕ-meson - measurements of both possible channels of the four pion production, first evidence for the fact that the interference of $\omega\pi$ and $a_1(1260)\pi$ amplitudes is sufficient for the complete description of both $\pi^+\pi^-\pi^0\pi^0$ and $\pi^+\pi^-\pi^+\pi^-$ channels. For the first time in this energy range we observed both channels of the 5π production and obtained evidence for the $\omega\pi\pi$ mechanism. Observation of three pion production in the energy range above the ϕ indicates that the $\rho - \omega$ interference is important.

Altogether results presented in this work are a very good illustration of

Table 7:

	CMD-2 Data	PDG'98
m_ω, MeV	$782.65 \pm 0.09 \pm 0.10$	781.94 ± 0.12
Γ_ω, MeV	$8.82 \pm 0.18 \pm 0.20$	8.41 ± 0.09
Γ_{ee}, keV	$0.63 \pm 0.01 \pm 0.02$	0.60 ± 0.02
$Br(\omega \to \pi^+\pi^-)$	$(1.3 \pm 0.3)\%$	$(2.21 \pm 0.30)\%$
m_ρ, MeV	$775.28 \pm 0.61 \pm 0.20$	776.0 ± 0.9
Γ_ρ, MeV	$147.7 \pm 1.29 \pm 0.40$	150.5 ± 1.1
Γ_{ee}, keV	$6.93 \pm 0.11 \pm 0.10$	6.77 ± 0.32
$Br(\rho \to e^+e^-)$	$(4.67 \pm 0.15) \cdot 10^{-5}$	$(4.49 \pm 0.22) \cdot 10^{-5}$
$Br(\rho \to \pi^+\pi^-\pi^+\pi^-)$	$< 2 \cdot 10^{-5}$	$< 2 \cdot 10^{-4}$
$Br(K_S \to \pi e \nu)$	$(7.19 \pm 1.35) \cdot 10^{-4}$	$(6.70 \pm 0.07) \cdot 10^{-4}$, recalculation from K_L
$Br(K^+ \to \pi^+\pi^0)$	$(21.69 \pm 0.48 \pm 1.03)\%$	$(21.16 \pm 0.14)\%$
$Br(K^+ \to \pi^0 e^+ \nu)$	$(4.89 \pm 0.17 \pm .17)\%$	$(4.82 \pm 0.06)\%$
$Br(\eta \to e^+e^-\gamma)$	$(7.56 \pm 0.92 \pm 1.13) \cdot 10^{-3}$	$(4.9 \pm 1.1) \cdot 10^{-3}$
$Br(\eta \to \pi^+\pi^-e^+e^-)$	$(3.5 \pm 2.0) \cdot 10^{-4}$	$(13^{+12}_{-8}) \cdot 10^{-4}$
$Br(\eta \to \pi^+\pi^-)$	$< 3 \cdot 10^{-4}$	$< 9 \cdot 10^{-4}$
$Br(\eta \to \pi^0\pi^0)$	$< 5 \cdot 10^{-4}$	no data
σ_{reg}(Be, 110 MeV/c)	$(55.1 \pm 5.9 \pm 5.0)$ mb	no data
σ_{tot}(Be, 110 MeV/c)	$(580 \pm 72 \pm 174)$ mb	no data

the advantages that a general-purpose detector operating at a high luminosity collider has. Analysis is in progress to produce final results with a low systematic uncertainty to meet the original goals of CMD-2, we also expect new data taking runs above the ϕ-meson.

Acknowledgements

The authors are grateful to the staff of VEPP-2M for excellent performance of the collider, to all engineers and technicians who participated in the design, commissioning and operation of CMD-2.

We express our sincere gratitude to our collaborators D.H. Brown, P.B. Cushman, S.K. Dhawan, J.P. Miller, B.L. Roberts and W.A. Worstell for their contribution at the earlier stages of this experiment and constant support.

We acknowledge the contribution to CMD-2 of our colleagues R.Yu. Demina, V.E. Fedorenko, M.Yu. Lelchuk, A.V. Maksimov, V.A. Monich, A.B. Nomerotsky, E.V. Popkov, S.I. Redin, V.P. Savinov, A.E. Sher, M.A. Shubin, V.G. Zavarzin and I.V. Zhuravkov.

Special thanks are due to N.N. Achasov, A.B. Arbuzov, M. Benayoun, V.L. Chernyak, V.P. Druzhinin, V.S. Fadin, V.B. Golubev, V.V. Gubin, V.N. Ivanchenko, I.B. Khriplovich, E.A. Kuraev, L. Montanet, S.I. Serednyakov, G.N. Shestakov, Z.K. Silagadze, A.I. Vainshtein for numerous discussions and constant interest.

This work is supported in part by grants:
RFBR-98-02-1785, Intas 96-0624.

References

[1] S.Eidelman and F.Jegerlehner, Z. Phys. **C67** (1995) 585.

[2] Y.S.Tsai, Phys. Rev. **D4** (1971) 2821.
H.B.Thacker and J.J.Sakurai, Phys. Lett. **B36** (1971) 103.
S.I.Eidelman and V.N.Ivanchenko, Phys. Lett. **B257** (1991) 437.

[3] M.A.Shifman, A.I.Vainshtein, V.I.Zacharov, Nucl. Phys. **B147** (1979) 385.

[4] G.A.Aksenov *et al.*, Preprint Budker INP 85-118, Novosibirsk, 1985.

[5] E.V. Anashkin *et al.*, ICFA Inst. Bull. **5** (1988) 18.

[6] V.V.Anashin *et al.*, Preprint Budker INP 84-114, Novosibirsk, 1984.

[7] C.Caso *et al.*, Eur. Phys. J. **C3** (1998) 1, Review of Particle Physics.

[8] R.R.Akhmetshin *et al.*, Phys. Lett. **B364** (1995) 199.

[9] R.R.Akhmetshin *et al.*, Phys. Lett. **B398** (1997) 423.

[10] R.R.Akhmetshin *et al.*, Phys. Lett. **B415** (1997) 445.

[11] R.R.Akhmetshin *et al.*, Phys. Lett. **B415** (1997) 452.

[12] R.R.Akhmetshin *et al.*, Phys. Lett. **B434** (1998) 426.

[13] P.O'Donnell, Rev. Mod. Phys. **53** (1981) 673.

[14] M.Benayoun *et al.*, hep-ph/9902326.

[15] M.N.Achasov *et al.*, JETP Lett. **68** (1998) 573.

[16] N.N.Achasov and V.N.Ivanchenko, Nucl. Phys. **B315** (1989) 465.

[17] N.N.Achasov and V.V.Gubin, Phys. Rev. **D56** (1997) 4084.

[18] D.Cocolicchio *et al.*, Phys. Lett. **B238** (1990) 417.

[19] P.Franzini, Proc. of the Workshop on Physics and Detectors for DAΦNE, Frascati, April 1991, p.733.

[20] F.E.Close, Proc. of the Workshop on Physics and Detectors for DAΦNE, Frascati, April 1991, p.309;
F.E.Close, N.Isgur, S.Kumano, Nucl. Phys. **389** (1993) 513.

[21] J.L.Rosner, I.Dunietz, J.Hauser, Phys. Rev. **D35** (1987) 2166.

[22] M.N.Achasov *et al.*, Phys. Lett. **B440** (1998) 442.

[23] M.N.Achasov *et al.*, Phys. Lett. **B438** (1998) 441.

[24] L.G.Landsberg, Sov. Phys. Uspekhi **28** (1985) 435.

[25] V.B.Golubev *et al.*, Sov. J. Nucl. Phys. **41** (1985) 756.

[26] V.N.Bayer, Pis'ma v ZETF **17** (1973) 446.

[27] L.M.Barkov *et al.*, Proc. 5th Int.Conf. Instrumentation for Colliding Beam Physics, March 15-21, 1990, Novosibirsk, Russia (World Scientific, 1990, p.480).

[28] V.M.Aulchenko *et al.*, Nucl. Instr. Meth. **A252** (1986) 299.

[29] E.V.Anashkin *et al.*, Nucl. Instr. Meth. **A323** (1992) 178.

[30] V.M.Aulchenko *et al.*, Preprint Budker INP 93-1, Novosibirsk, 1993.

[31] D.N.Grigoriev *et al.*, IEEE Trans. Nuc. Sci., **42** (1995) 505.

[32] V.M.Aulchenko *et al.*, Nucl. Instr. Meth. **A265** (1988) 137.

[33] R.R.Akhmetshin *et al.*, Preprint INP 99-10, Novosibirsk, 1999.

[34] E.A.Kuraev, V.S.Fadin, Sov. J. Nucl. Phys., **41**(1985)466

[35] A.B.Arbuzov, E.A.Kuraev et al., Preprint JHEP 10(1997)001

[36] F.A.Berends, R.Kleiss, Nucl. Phys., **B228**(1983)537

[37] Ya.S.Derbenev, A.M.Kondratenko, S.I.Serednyakov, A.N.Skrinsky, G.M.Tumaikin, Yu.M.Shatunov, Preprint Budker INP 76-64, Novosibirsk, 1976.

[38] V.V. Anashin *et al.*, Preprint Budker INP 84-123, Novosibirsk, 1984.

[39] K.Y.Mikhailov, Master thesis. Novosibirsk, 1998.

[40] R.R. Akhmetshin *et al.*, Preprint Budker INP 95-35, Novosibirsk, 1995.

[41] A.N.Filippov, P.M.Ivanov, I.A.Koop, E.A.Perevedentsev, Yu.M.Shatunov, A.N.Skrinsky, Proceedings on XV^{th} International conference on high energy accelerators. Hamburg, July, 1992.

[42] G. Korn, T. Korn, Mathematical handbook. Moscow, 1977, p. 614. (In Russian).

[43] L.M.Barkov *et al.*, Nucl. Phys. **B256** (1985) 365

[44] R.Barate *et al.*, Z. Phys., **C76** (1997) 15.

[45] A. Lysenko *et al.*, Nucl. Instr. Meth. **A359** (1995) 419.

[46] V.M.Aulchenko *et al.*, Preprint INP 92-28(in Russian), Novosibirsk, 1992.

[47] E.V. Anashkin *et al.*, Nucl. Instr. Meth. **A283** (1989) 752.

[48] V.M. Aulchenko *et al.*, Nucl. Instr. Meth. **A336** (1993) 53.

[49] S.I. Dolinsky *et al.*, Phys. Reports **202** (1991) 99.

[50] L.M. Barkov *et al.*, English Translation of Sov. Phys. ZETF Letters **46** (1987) 164.

[51] R.R. Akhmetshin *et al.*, Preprint Budker INP 98-30, Novosibirsk, 1985.

[52] P. A. Lukin., Study of the $\phi \to K_L K_S$ process. CMD-2 Internal note, 1996.

[53] P. M. Ivanov *et al.*, ZETFP **36** (1982) 91.

[54] R.R. Akhmetshin *et al.*, Proceedings of the 7th International Conference on Hadron Spectroscopy, Upton, NY, 1997, p.778.

[55] N.N.Achasov, V.Gubin and E.P.Solodov, Phys. Rev. **D55** (1997) 2672.

[56] N.N.Achasov and V.Gubin, Phys. Rev. **D57** (1998) 1987.

[57] N.N.Achasov and V.Gubin, Proceedings of the 7th International Conference on Hadron Spectroscopy, Upton, NY, 1997, p.574.

[58] M.N.Achasov *et al.*, Preprint Budker INP 98-65, Novosibirsk, 1998.

[59] E.V. Anashkin *et al.*, Preprint Budker INP 99-1, Novosibirsk, 1999.

[60] R .R. Akhmetshin *et al.*, Preprint Budker INP 95-62, Novosibirsk, 1995.

[61] R. Baldini, A. Michetti, Preprint LNF-96/008 (1996).

[62] G.Barbellini and C.Santoni, CERN-EP/89-8 and CERN-PPE/90-09.

[63] B.Aubert *et al.*, Phys. Lett. **17** (1965) 59.

[64] M.Hashimoto, Phys. Rev. **D54** (1996) 5611.

[65] A. Bramon *et al.*, Phys. Lett. **B317** (1993) 190.

[66] S. I. Eidelman *et al.*, Phys. Lett. **B346** (1995) 186.

[67] R. S. Plant, M. C. Birse Phys. Lett. **B365** (1996) 292.

[68] L. M. Kurdadze *et al.*, JETP Lett. **47** (1988) 512.

[69] B.Bartoli *et al.*, Nuovo Cim. **A70** (1970) 615.

[70] L.M.Kurdadze *et al.*, Phys. Lett. **B42** (1972) 515.

[71] G.Cosme *et al.*, Phys. Lett. **B63** (1976) 349.

[72] A.Cordier *et al.*, Phys. Lett. **B109** (1982) 129.

[73] D.Bisello *et al.*, Preprint LAL-91-64, Orsay, 1991.

[74] V.M.Aulchenko *et al.*, Preprint Budker INP 86-106, Novosibirsk, 1986.

[75] S.I.Eidelman, JETP Lett. **26** (1977) 417.

[76] R.R. Akhmetshin *et al.*, Preprint Budker INP 98-83, Novosibirsk, 1998.

[77] A.Antonelli *et al.*, Z. Phys. **C56** (1992) 15.

[78] L.M.Barkov *et al.*, J. Nucl. Phys. **47** (1988) 393.

[79] N.N.Achasov *et al.*, Sov. J. Nucl. Phys. **23** (1976) 610.

[80] N.N.Achasov *et al.*, Phys. Lett. **B50** (1974) 448.

R.R. Akhmetshin, G.A. Aksenov, E.V. Anashkin, M. Arpagaus, V.M. Aulchenko, B.O. Baibusinov, V.Sh. Banzarov, L.M. Barkov, S.E. Baru, N.S. Bashtovoy, A.E. Bondar, D.V. Bondarev, A.V. Bragin, D.V. Chernyak, A.G. Chertovskikh, A.G. Dvoretsky, S.I. Eidelman, G.V. Fedotovich, N.I. Gabyshev, A.A. Grebeniuk, D.N. Grigoriev, V.W. Hughes, P.M. Ivanov, S.V. Karpov, V.F. Kazanin, B.I. Khazin, I.A. Koop, M.S. Korostelev, P.P. Krokovny, L.M. Kurdadze, A.S. Kuzmin, M. Lechner, I.B. Logashenko, P.A. Lukin, A.P. Lysenko, Yu.I. Merzlyakov, K.Yu. Mikhailov, A.I. Milstein, I.N. Nesterenko, V.S. Okhapkin, A.V. Otboev, E.A. Perevedentsev, A.A. Polunin, A.S. Popov, T.A. Purlatz, N.I. Root, A.A. Ruban, N.M. Ryskulov, A.G. Shamov, Yu.M. Shatunov, A.I. Shekhtman, B.A. Shwartz, V.A. Sidorov, A.N. Skrinsky, V.P. Smakhtin, I.G. Snopkov, E.P. Solodov, P.Yu. Stepanov, A.I. Sukhanov, J.A. Thompson, V.M. Titov, A.A. Valishev, Yu.V. Yudin, S.G. Zverev

Recent results
from CMD-2 detector at VEPP-2M

Budker INP 99-11

Ответственный за выпуск А.М. Кудрявцев
Работа поступила 18.02. 1999 г.

Сдано в набор 19.02.1999 г.
Подписано в печать 19.02.1999 г.
Формат бумаги 60×90 1/16 Объем 7.4 печ.л., 5.9 уч.-изд.л.
Тираж 250 экз. Бесплатно. Заказ N° 11

Обработано на IBM PC и отпечатано на
ротапринте ИЯФ им. Г.И. Будкера СО РАН
Новосибирск, 630090, пр. академика Лаврентьева, 11.